Engineering and Screening of Genetically Encoded FRET Calcium Indicators

Dissertation zur Erlangung des Doktorgrades der Naturwissenschaften
an der Fakultät für Biologie
der Ludwig-Maximilian-Universität München

vorgelegt von

Julia Litzlbauer

München, den 26.08.2014

1. Gutachter: PD Dr. Oliver Griesbeck
2. Gutachter: Prof. Dr. Leibold

Tag der mündlichen Prüfung: 13.4.2015

Table of Contents

Table of Figures

Table of Tables

Abbreviations

AHP	After-hyperpolarization
ATPase	Adenosine 5'-triphosphatase
BAPTA	1,2-bis(o-aminophenoxy)ethane-N,N,N',N'-tetraacetic acid
BCA	Bicinchoninic acid
BFP	Blue fluorescent protein
Bp	Base pair
BSA	Bovine serum albumin
Ca^{2+}	Calcium
CaM	Calmodulin
CCD	Charge-coupled device
CFP	Cyan fluorescent protein
cp	Circularly permutated
DAP	Depolarizing after-potentials
ΔF/F	Change in fluorescence/ (starting) fluorescence
ΔR/R	Change in ratio/ (starting) ratio
DMEM	Dulbecco's Modified Eagle's Medium
DMSO	Dimethylsulfoxid
DNA	Deoxyribonucleic acid
dNTP	Deoxyribonucleotid triphosphate
ECFP	Enhanced cyan fluorescent protein
EYFP	Enhanced yellow fluorescent protein
EDTA	Ethylene diamine tetraacetic acid
EGTA	Ethylene glycol tetraacetic acid
FACS	Fluorescence-activated cell sorting
FCS	Fetal calf serum
FP	Fluorescent protein
FRET	Förster resonance energy transfer
g	Gram
GECI	Genetically encoded calcium indicators
GFP	Green fluorescent protein
HBSS	Hank's Balanced Salt Solution
HEK	Human embryonic kidney cells
IPTG	Isopropyl-beta-D-thiogalactopyranoside
K^+	Potassium
K_d	Dissociation constant
l	Liter
LB	Luria-Bertani broth

M	Molar
M13	Calmodulin binding peptide
MCS	Multiple cloning sites
Mg^{2+}	Magnesium
mKO	Monomeric Kusabira Orange
MOPS	3-(N-morpholino)propanesulfonic acid
mRFP	Monomeric red fluorescent protein
Na^{+}	Sodium
PAGE	Polyacrylamide gel electrophoresis
PBS	Phosphate buffered saline
PCR	Polymerase chain reaction
pH	Reverse logarithmic representation of relative H^{+} concentration
PMSF	Phenylmethylsulfonylfluoride
R	Ratio
ROC	Receptor operated channel
RT	Room temperature
SHM	Somatic hypermutation
SLiCE	Seamless ligation cloning extract
SOC	Store operated channel
TAE	Tris-acetate-EDTA buffer
TnC	Troponin C
VOC	Voltage operated channel
WT	Wildtype
YFP	Yellow fluorescent protein

Daten der vorliegenden Arbeit werden/ wurden in folgenden Publikationen veröffentlicht:

Litzlbauer J, Schifferer M, Ng D, Thestrup T, Griesbeck O: *Large Scale Bacterial Colony Screening of Diversified FRET Biosensors.* (in preparation)

Thestrup T, **Litzlbauer J**, Bartholomäus I, Mues M, Russo L, Dana H, Kovalchuk Y, Liang Y, Kalamakis G, Laukat Y, Becker S, Witte G, Geiger A, Allen T, Rome LC, Chen TW, Kim DS, Garaschuk O, Griesinger C, Griesbeck O (2014): *Optimized ratiometric calcium sensors for functional in vivo imaging of neurons and T lymphocytes.* Nat Methods 11(2):175-82

Abstract

Fluorescent protein sensors have gained great importance in research as they exhibit a number of advantages over synthetic dyes. They can be targeted precisely, large populations of cells can be imaged simultaneously, and they allow for chronic imaging approaches. Many of them however still suffer from comparably low signal changes. Improving fluorescent protein sensors can be tedious and time-consuming. For this reason, great efforts have been made not only to improve existing sensors, but also to develop better strategies to improve them.

In this work, a novel large-scale bacterial based screening assay was established to complement rational design. Sensor expression, stimulation, and screening in bacteria, as well as the handling of large amounts of data created by such a screening assay were optimized.

While the new assay can be adapted for other applications, it is especially well suited for the screening of genetically encoded Ca^{2+} indicators of the basis of FRET (Förster Resonance Energy Transfer). We used the assay to optimize such sensors, utilizing the Ca^{2+} binding protein Troponin C fused between the fluorescent proteins ECFP and cpCitrine. The resulting 'Twitch' sensor series exhibited a large dynamic range of up to 1000% FRET ratio change, great sensitivity and fast kinetics.

In a second approach, we attempted to develop a similar sensor deploying red-shifted fluorescent proteins. To this end, further screening was conducted to optimize the orange fluorescent protein mKOκ for FRET, and a FRET sensor deploying mKOκ. The sensor we developed utilized troponin C and the fluorescent protein Dreiklang (photoswitchable) in addition to mKOκ. It was bright and exhibited a FRET ratio change of approximately 170%.

In summary, the screening procedures presented in this thesis, will facilitate the development of a range of genetically encoded biosensors, and were already employed to develop a number of highly effective Ca^{2+} FRET indicators.

1 Introduction

Fluorescent proteins have revolutionized life science. As passive tags they enabled the visualization of cell structures and the monitoring of intracellular processes. Moreover, they have been deployed in a variety of active biosensors, allowing the investigation of physiological events. Unlike their synthetic counterparts, sensors based on fluorescent proteins are genetically encoded and can therefore be targeted to specific subsets of cells or subcellular compartments. A method of rapidly testing a high number of fluorescent protein sensor variants would facilitate, and greatly accelerate their optimization.

1.1 Fluorescent Proteins

1.1.1 Fluorescence and FRET (Förster Resonance Energy Transfer)

Before addressing fluorescent proteins, sensors design and screening, a few fundamental concepts will be explained. Firstly, fluorescence is the emission of light from an excited molecule. Following the absorption of light, molecules reach an electronically excited state and must emit a photon in order to return to their ground state. This process is depicted in the Jablonski diagram below (**Figure 1**): After the absorption of light, a molecule is excited from its singlet ground electronic state S_0 to a higher vibrational level of the first or second electronic state (S_1 or S_2). Thereafter, most molecules relax immediately to the lowest vibrational level of S_1, a process called internal conversion. Subsequently, molecules can either return to their ground state by emitting a photon, which becomes visible as fluorescence. Alternatively, they can undergo a spin conversion to the first triplet state T_1. Return to the ground state from T_1 is called phosphorescence and typically occurs slowly, and at longer wavelengths (Lakowicz, 2007).

As the diagram shows, the energy of the emission is usually lower than the energy of the absorption, which means that the emitted light has a longer wavelength. This phenomenon was first observed by Sir G.G. Stokes, and is therefore referred to as the Stokes shift (Stokes, 1852). The average time that a molecule remains in an excited state before it returns to the ground state is referred to as the fluorescence lifetime. The number of photons emitted, relative to the number of photons absorbed in a fluorescent protein, is called the quantum yield. Proteins with higher quantum yields exhibit brighter emission. Brightness is also determined by the extinction coefficient, which is essentially the ability of a protein to absorb light at a given wavelength (Lakowicz, 2007).

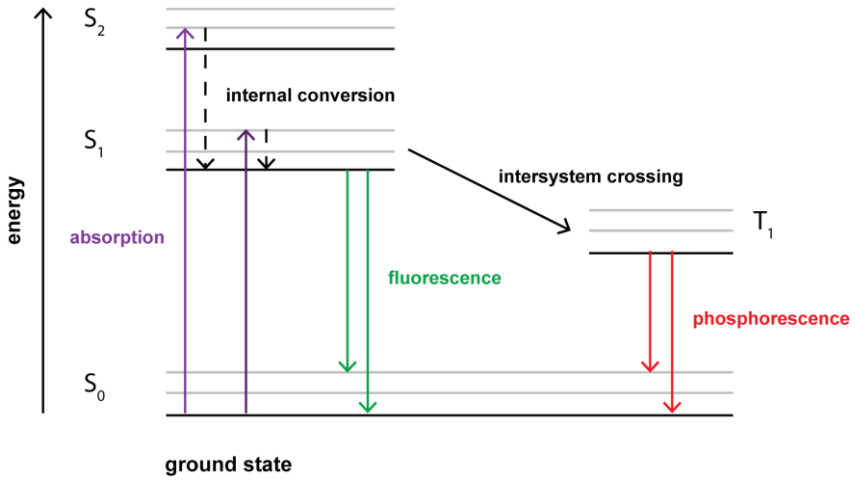

Figure 1: Jablonski Diagram
Illustration of the electronic states of a molecule involved in fluorescence.

FRET stands for Förster (or Fluorescence) Resonance Energy Transfer and was first characterized by Theodor Förster in 1948 (Förster, 1948). It describes the transfer of energy from an excited fluorescent protein, the donor, to another (not necessarily) fluorescent protein, the acceptor. This energy transfer takes place via a dipole-dipole coupling between donor and acceptor (and not through light emitted from the donor being absorbed by the acceptor). FRET can occur if the emission spectrum of the donor overlaps with the excitation spectrum of the acceptor (**Figure 2A**). The extent of energy transfer depends, among other factors, on the extent of this spectral overlap, the distance between donor and acceptor, and their orientation to one another. (Lakowicz, 2007). An example for FRET between two fluorescent proteins is depicted in **Figure 2B**. The occurrence of FRET leads to a decrease in the emission of the excited donor and an increase in the emission of the un-excited acceptor.

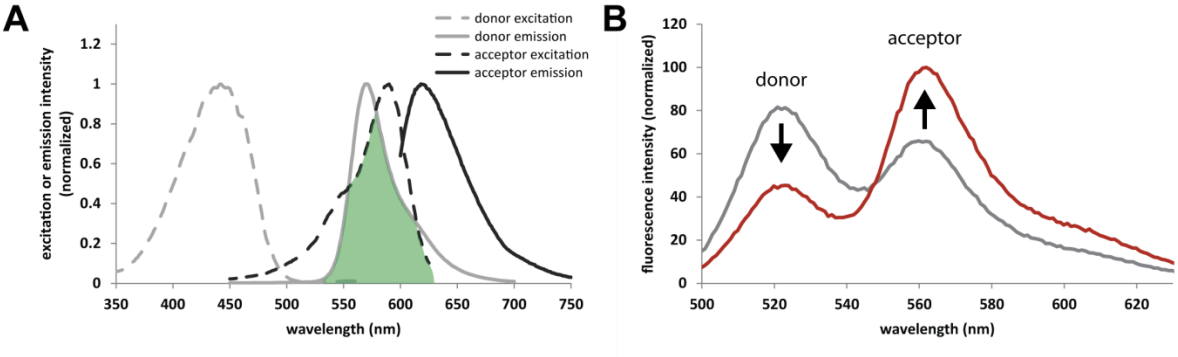

Figure 2: Spectral Overlap of a FRET Pair and an Example of FRET
Excitation (dashed) and emission (solid) spectra of a potential FRET donor and acceptor pair, with the spectral overlap between donor emission and acceptor excitation shaded in green **(A)**. Emission spectra of a FRET sensor, illustrating the decrease in donor emission and the increase in acceptor emission when FRET occurs **(B)**.

1.1.2 Fluorescent Proteins - An Overview

The first fluorescent protein, green fluorescent protein (GFP), was discovered together with the bioluminescent protein Aequorin in the jellyfish *Aequorea victoria* in 1962 (Shimomura et al., 1962). In 1992, GFP was successfully cloned for the first time (Prasher et al., 1992). This represented an important milestone in the history of fluorescent proteins, making them accessible as tools for the first time. The first cloning was quickly followed by the first application of GFP as a marker for gene expression and protein localization in 1994 (Chalfie et al., 1994, S. Wang & Hazelrigg, 1994). A rapid rise in the use of fluorescent proteins as instruments in life science followed. The original GFP has since been modified numerous times to increase its brightness and produce variants in different colors ranging from blue over cyan and green to yellow (e.g.(R. Heim & Tsien, 1996, R. Heim et al., 1994, 1995)).

In addition, more fluorescent proteins ranging in color have been found in other species. In 1999, a number of fluorescent proteins were isolated from various Anthozoa species. Among them was the red emitting protein drFP583, which was later given the commercial name DsRed by Clontech (Matz et al., 1999). This discovery was somewhat surprising given that in contrast to *Aequoria victoria*, Anthozoans don't exhibit any luminescence. Alternative functions of fluorescence in such species have been hypothesized however. As anthozoans depend on the photosynthesis of their algal symbionts, fluorescent proteins could be useful in regulating their light environment. In excess sunlight, they could act photo-protectively through the redirection of light. Under low light conditions, they could absorb light of short

wavelength and transform it into longer wavelengths more suitable for photosynthesis (Salih et al., 2000, Schnitzler et al., 2008).

DsRed, like all red fluorescent proteins discovered to date, had the disadvantage of being an obligate tetramer, which tended to cause problems in experiments. In a tedious screening project, the first red monomer, mRFP, was developed from DsRed, an endeavor which required 33 mutations (R. E. Campbell et al., 2002). An entire collection of monomers based on DsRed was then engineered, which became known as the fruit series, and ranged in color from yellow over orange to red (Shaner et al., 2004).

A very bright orange fluorescent protein was derived from the mushroom coral *Fungia Concinna.* The original tetramer, named Kusabira Orange (KO), could be converted into a monomer utilizing a strategy similar to that used for DsRed (Karasawa et al., 2004). Further improvements led to the brighter and faster maturating versions mKOK (Tsutsui et al., 2008) and mKO2 (Sakaue-Sawano et al., 2008).

Today, fluorescent proteins cover most of the visible spectrum. Many red and far-red fluorescent proteins however, still suffer from reduced brightness, low photostability, slow maturation and a tendency to aggregate, in comparison to the GFP-like variants covering the lower-wavelength regions of the spectrum.

Current endeavors in fluorescent protein development include the further improvement of red, far red and near-infrared fluorescent proteins (e.g. (Chu et al., 2014, Shcherbakova & Verkhusha, 2013). These proteins could be used for multi-parameter imaging in combination with shorter wavelength fluorescent proteins. Moreover, the imaging of red fluorescent proteins offers a number of advantages. Auto-fluorescence of the imaged tissue is lower at higher wavelengths (Monici, 2005). The phototoxicity of the excitation light for the examined organism is also lower (Wiedenmann et al., 2009), and because light scattering is reduced, non-invasive deep tissue imaging can be conducted. Ideal imaging conditions can be found at the optical window of 600 to 1000nm, where the absorbance of hemoglobin and melanin is at its lowest (Lakowicz, 2007).

Another ongoing ambition is the design of large stokes shift fluorescent proteins, which would allow for the construction of FRET pairs with virtually no cross-excitation. Additionally, they could be used for multicolor imaging with only a single excitation wavelength (Kogure et al., 2006, Piatkevich et al., 2010, Shcherbakova et al., 2012, Zapata-Hommer & Griesbeck, 2003).

Furthermore, numerous photoactivatable, photoswitchable and photoconvertible fluorescent proteins have recently been developed (Adam et al., 2014). Among them, the GFP-based Dreiklang proved to be

especially bright, whilst offering the advantage that its photoswitching is reversible (Brakemann et al., 2011).

1.1.3 Fluorescent Proteins – Structure, Chromophore Formation and Structural Rearrangements

Fluorescent proteins have a size of approximately 28 kDa. The structure of GFP was first determined independently by Ormö et al and Yang et al (Ormö et al., 1996, Yang et al., 1997), and all fluorescent proteins known to date exhibit similar characteristics. It is described as a β-barrel, consisting of 11 β-sheets, with dimensions of approximately 25Å x 40Å. The chromophore lies within a helix in the center of the molecule, where it is protected from bulk solvent (**Figure 3**).

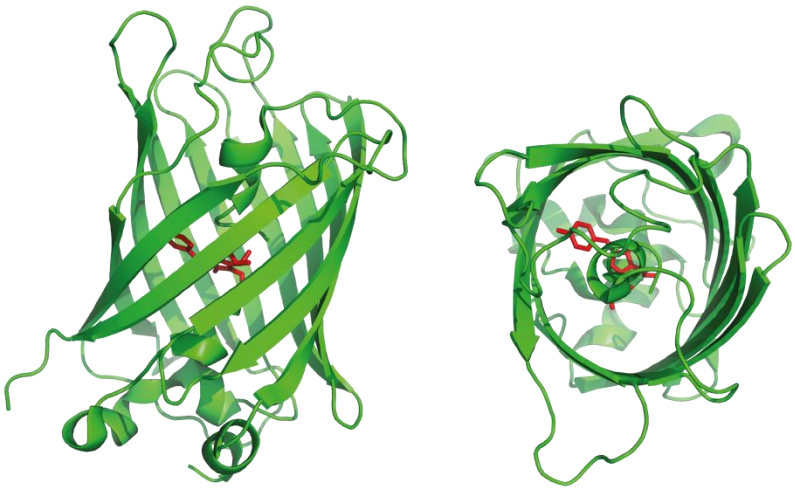

Figure 3: Protein Structure of GFP
GFP protein consisting of 11 β-sheets which build a barrel around the central chromophore, which is depicted in red (PDB file 4KW4).

In GFP, the chromophore consists of an imidazoline ring formed by three amino acids, which can be found in positions 65-67. In the native GFP protein, these 3 amino acids are Ser65-Tyr66-Gly67 (Prasher et al., 1992). It forms autocatalytically and does not require any external cofactors, other than atmospheric oxygen (Reid & Flynn, 1997). The chromophore formation in GFP and GFP-like proteins is thought to be initiated with a neutrophilic attack of the amino nitrogen of glycine at position 67, on the carbonyl carbon of serine at position 65. This reaction forms the imidazoline ring. The carbonyl oxygen of serine is subsequently dehydrated. The newly formed chromophore becomes fluorescent upon oxidation of the a-

b carbon bond of tyrosine at position 66, which extends the conjugation of electron orbitals to include the phenyl ring (**Figure 4**) (Cubitt et al., 1995).

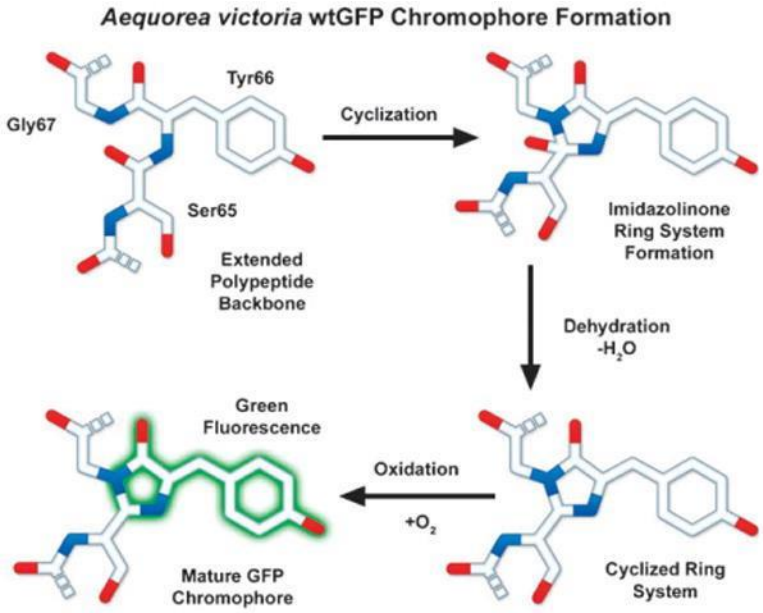

Figure 4: GFP Chromophore Formation
Steps in the formation of the GFP chromophore: The imidazoline ring is formed by a neutrophilic attack of the amino nitrogen of Gly67, on the carbonyl carbon of Ser65, followed by a dehydration of the carbonyl oxygen of Ser65. The a-b carbon bond of Tyr66 is oxidized to conjugate the ring system (reproduced from (Day & Davidson, 2009) with permission of The Royal Society of Chemistry).

In the orange fluorescent mKO, the chromophore is formed by the tripeptide Cys65-Tyr66-Glu67 and consists of three rings (Kikuchi et al., 2008). A recent model depicted in **Figure 5** suggests that the formation of red chromophores occurs via a branched pathway. The process is initiated by a cyclization reaction followed by an oxidation step, generating a colorless intermediate. This intermediate can either turn into a green fluorescent chromophore, or a blue intermediate, which then transforms into a red fluorescent chromophore. Green dead-end products have been observed among a number of red-emitting proteins such as DsRed (Baird et al., 2000). What happens at this branch point depends on a hydroxide moiety, which can be reversibly removed from the intermediate. With the hydroxide moiety attached, water can be removed from the intermediate, producing a green chromophore. With the hydroxide moiety eliminated, the intermediate undergoes further oxidation, producing a blue intermediate. A base-induced elimination of water leads then to the formation of a red chromophore (Pletnev et al., 2010, Strack et al., 2010). For the formation of the third ring of mKO, a subsequent cyclization of the N-acylimine group is necessary. In mKO, the conjugated electron orbital system is less

extended, which is why it emits at a shorter wavelength than its red precursor (Subach & Verkhusha, 2012).

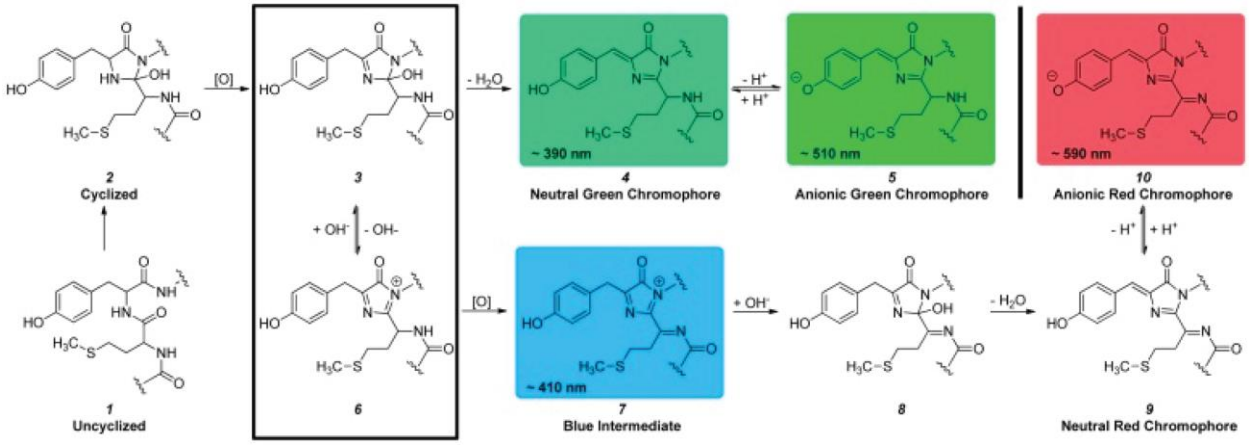

Figure 5: Red Chromophore Formation
The formation of red chromophores via a branched pathway, as proposed by Stack and colleagues (Strack et al., 2010), can result either in a green or a red dead-end product. The branch point is encircled (reproduced from (Moore et al., 2012) with permission).

Fluorescent proteins have the ability to tolerate major rearrangements of their structure, such as a dislocation of their amino- and carboxyl termini (N- and C-termini). In the resulting circularly permutated (cp) protein (**Figure 6**), the original N- and C-termini are connected with a short linker sequence, and the protein is opened at a different site, resulting in a protein with the same three-dimensional structure, but with new N- and C-termini (Baird et al., 1999). The utilization of a cp version of a given protein can change the orientation of the chromophore to a binding partner considerably. The value of cp variants in the development of single fluorophore and FRET sensors will be illustrated in chapter 1.3.1.

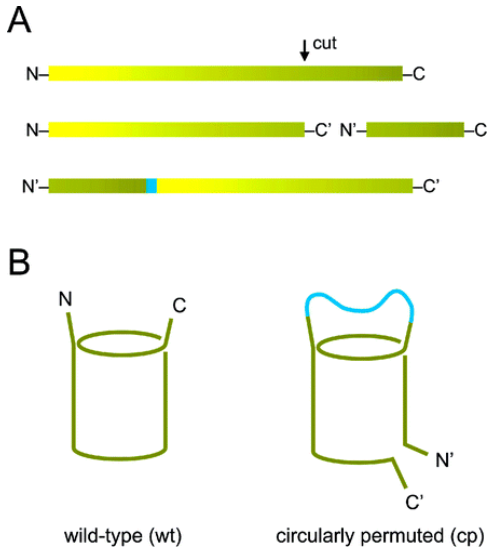

Figure 6: Circular Permutation Scheme
The protein sequence is opened at an alternative site, resulting in new N- and C-termini, whereas the old N- and C-termini become connected by a short linker sequence (blue) and will, as a result, lie somewhere in the middle of the sequence **(A)**. Circularly permutated (cp) fluorescent protein with unchanged structure but new N- and C-termini **(B)** (Reprinted with permission from (Mank & Griesbeck, 2008). Copyright (2008) American Chemical Society.)

1.2 Calcium in Cell Physiology

1.2.1 Calcium Signaling

The interest in calcium indicators is great because calcium (Ca^{2+}) is an intracellular messenger of tremendous importance. Essentially, an elevation of the Ca^{2+} level in a cell triggers the activation of a range of processes. This elevation can differ in speed, amplitude and spatio-temporal organization, giving Ca^{2+} the potential to be involved in the control of diverse biological functions (e.g. fertilization, learning and memory, muscle contraction, cell proliferation and cell death) (Berridge et al., 2000).

Sources of Ca^{2+} for a cell are both internal and external. Internally, Ca^{2+} is stored in the endoplasmic reticulum. It can be released into the cytoplasm of the cell through various channels such as those belonging to the inositol-1,4,5-triphosphate receptor or ryanodine receptor families. The transport back into the endoplasmic reticulum occurs via sarco-endoplasmic reticulum ATPases. The numerous Ca^{2+} channels which allow the entry of external Ca^{2+}, are classified by their mode of activation. Among them are the voltage operated channels (VOCs), the receptor operated channels (ROCs), and the store operated channels (SOCs). The latter are activated when the Ca^{2+} stores within a cell become depleted. Plasma

membrane Ca^{2+}-ATPase pumps and Na^{+}/Ca^{2+} exchangers quickly transport Ca^{2+} out of the cells again, once its signaling function is completed (Berridge et al., 2000).

During the process of Ca^{2+} signaling, the mitochondrion plays an important role. It is able to take up Ca^{2+} rapidly during the development of a signal, and slowly release it back into the cytoplasm afterwards, thereby shaping the Ca^{2+} signal (Berridge et al., 2000). Ca^{2+} binding proteins also help shape the Ca^{2+} signal by binding calcium ions in specific domains and sequestering them, since only free Ca^{2+} is biologically active. Besides, these Ca^{2+} binding proteins participate in numerous cellular functions. A recent review broaching the issue has been written by Yáñez and colleagues (Yáñez et al., 2012). Selected examples will be introduced in chapter 1.2.3.

1.2.2 Calcium Signaling in Neurons

Neurons fire action potentials (rapid changes in their membrane potential) in order to encode and conduct signals. These action potentials are primarily sustained by sodium (Na^{2+}) and potassium (K^{+}) currents across the membrane. Ca^{2+} however, does play an important role in shaping them, and also manipulates the overall firing pattern of a neuron (Bean, 2007).

In an action potential, at least 3 phases can be distinguished: depolarization, repolarization and hyperpolarization (**Figure 7**). An explosive inward current of Na^{+} is responsible for the depolarization phase, and a slower outward current of K^{+} marks the repolarization phase. Ca^{2+} enters the cell via multiple voltage-activated channels, which exhibit comparably slow activation kinetics. For this reason, they are only activated towards the end of the depolarization phase. The incoming Ca^{2+} activates several forms of Ca^{2+}-activated K^{+} channels, which contribute to the repolarization of the neuron, and shape the hyperpolarization phase, or after-hyperpolarization (AHP). In this context, Ca^{2+} contributes to a reduced excitability of the neuron directly following an action potential, by increasing the distance to its firing threshold. Ca^{2+} can however, also have the opposite effect. Its accumulation evokes depolarizing after-potentials (DAP) which make the neuron more excitable by bringing it closer to its threshold (Bean, 2007, Berridge, 1998).

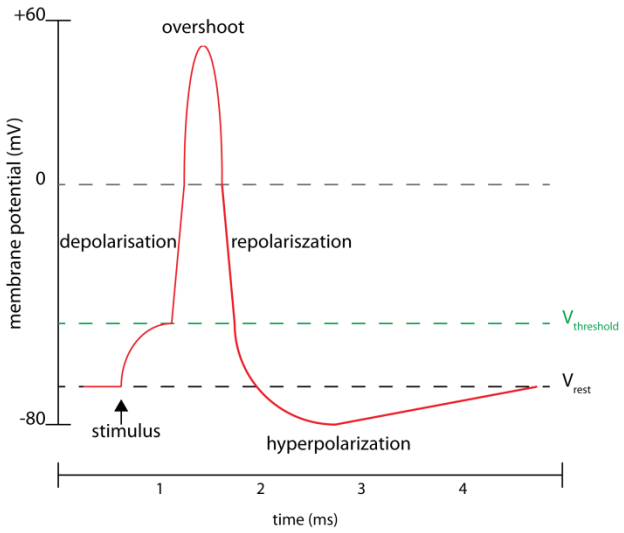

Figure 7: Phases of an Action Potential
An action potential is generated if a stimulus depolarizes the membrane from its resting potential (V_{rest}) above the threshold potential ($V_{threshold}$). Distinct phases of an action potential which can be distinguished as indicated.

In addition to its modulatory role in firing action potentials, Ca^{2+} is associated with the release of neurotransmitters, gene transcription, and synaptic modifications in connection with learning and memory (Berridge, 1998). A disturbance in neuronal calcium signaling plays a role in many neuronal diseases like Migraines, Huntington's disease, Alzheimer's disease and Parkinson's disease (Brini et al., 2014).

1.2.3 Calcium Binding Proteins

Once Ca^{2+} is released into the cytoplasm of a cell, it is only available for a short time before either being transported outside or into the endoplasmic reticulum, or being sequestered by a wide range of Ca^{2+} binding proteins. As previously mentioned, these Ca^{2+} binding proteins can function as a buffer, but they can also trigger diverse cellular functions. In the latter case, the binding of Ca^{2+} induces a conformational change in these proteins, which in turn causes a cellular reaction. Many Ca^{2+} sensors take advantage of the Ca^{2+} induced conformational change in Ca^{2+} binding proteins.

1.2.3.1 EF-Hand Domains

Many Ca^{2+} binding proteins have a common structural Ca^{2+} binding motif, which is called the EF-hand domain. Its name is derived from the way this motif was first described in parvalbumin (Kretsinger & Nockolds, 1973). An EF-hand consists of a loop comprising 12 amino acids, capable of binding Ca^{2+} or Mg^{2+}, flanked by 2 alpha helices (**Figure 8A**). Ca^{2+} is held in place by ligands provided by 6 of the 12 amino acids that form the loop, which are called the coordinating residues. These residues, many of them negatively charged, build a pentagonal bipyramid, housing Ca^{2+} in the middle (**Figure 8B**). They are occupied by the following amino acids: 1(+X), 3(+Y), 5(+Z), 7(-Y), 9(-X) and 12(-Z), with the numbers indicating the position of the amino acid within the loop, and the letter indicating its position in the pyramid. An extensive network of hydrogen bonds between the coordinating residues and the positions in between them stabilizes the close proximity of multiple negative charges within the coordination sphere. EF-hands occur mostly in pairs and influence how one another function. An example of this influence is positive cooperation, where Ca^{2+} binding to one EF-hand facilitates Ca^{2+} binding to the second EF-hand (Gifford et al., 2007, Lewit-Bentley & Réty, 2000).

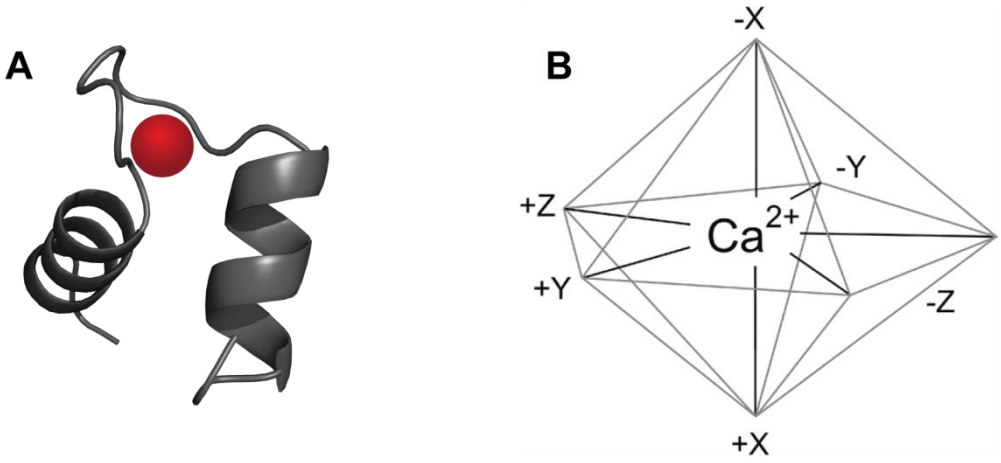

Figure 8: Structure of an EF-Hand and Scheme of its Ca^{2+} Coordination
Helix-loop-helix motif of an EF-hand coordinating one calcium ion (red) in its loop (PDB file NCBI) **(A)**. Scheme of Ca^{2+} coordination in an EF-hand with positions involved in Ca^{2+} coordination indicated (Reprinted with permission from (Mank & Griesbeck, 2008). Copyright (2008) American Chemical Society) **(B)**.

1.2.3.2 Troponin C

Troponin C represents one part of the troponin complex, together with troponin I and troponin T. The troponin complex is found in muscle cells and was discovered and named in 1965 by Ebashi and Kodama (Ebashi & Kodama, 1965). In muscle cells, contraction is initiated by a nerve impulse leading to an increase in Ca^{2+}. Ca^{2+} binds to troponin C, which undergoes a conformational change, causing a rearrangement of the whole troponin complex. This leads to an increased interaction of actin and myosin in the muscle and the formation of cross-bridges, thereby generating the tension necessary for contraction (Ohtsuki, 2007). Troponin C consists of two pairs of EF-hands, which are called the N- and the C-terminal lobe (N- and C-lobe), connected by a long α helix (**Figure 9**). The C-lobe exhibits a very high Ca^{2+} affinity, binds Mg^{2+} competitively, and is under physiological conditions mostly occupied. It is assumed to fulfill a structural function in the troponin complex. The N-lobe has a low Ca^{2+} affinity and is only occupied, when the Ca^{2+} level in the cell rises, which is why it is thought to play a regulatory role (Herzberg & James, 1985, Vassylyev et al., 1998). Its large Ca^{2+} induced conformational change and the range of its Ca^{2+} affinity make troponin C an interesting candidate for use in genetically encoded Ca^{2+} sensors (see chapter 1.3.1). Since it only naturally occurs in muscle cells, it is thought to interfere little with cellular functions in other cell types of cells, which may limit side effects.

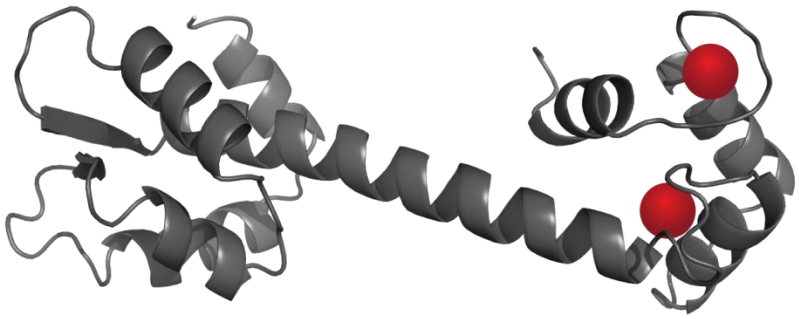

Figure 9: Structure of Troponin C
Troponin C is comprised of two pairs of EF-hands connected by a long α helix. In this scheme, two calcium ions (red) are bound to EF-hands three and four of the C-terminal lobe (PDB file NCBI).

Another popular Ca^{2+} binding protein is the ubiquitous and evolutionary highly conserved calmodulin (Cheung, 1970, Kakiuchi & Yamazaki, 1970). It occurs in all eukaryotic organisms, and is involved in a variety of important cellular processes. Like troponin C, it consists of two pairs of EF-hands, and undergoes a large conformational change upon Ca^{2+} binding (Chin & Means, 2000). Calmodulin has been used as a

Ca^{2+} binding moiety in many genetically encoded sensors (see chapter 1.3.1), but its importance in so many cellular functions introduces the risk of affecting important cell functions.

1.3 Genetically Encoded Calcium Indicators

1.3.1 Single Fluorophore and FRET Indicators

Fluorescent proteins are deployed in a wide range of genetically encoded indicators. The term "genetically encoded" means that these indicators are composed solely of amino acids and can be expressed within an organism of interest *in situ*. Genetically encoded calcium indicators (GECIs) consist of one or more fluorescent proteins, as well as a Ca^{2+} binding moiety. This Ca^{2+} binding moiety is attached to the fluorescent proteins in a way that its binding of Ca^{2+} causes a change in fluorescence. Two kinds of GECIs exist, single fluorophore indicators, and FRET indicators for ratiometric imaging.

The very first fluorescent protein FRET pair created, consisted of the fluorescent proteins BFP and GFP, with a cleavable spacer in between. This was just a proof of principle without an indicator function, but it showed that FRET between different color variants of fluorescent proteins was possible (R. Heim & Tsien, 1996). Soon thereafter, the first FRET sensor was designed. It consisted of the two fluorescent proteins BFP and GFP, as well as a calmodulin binding domain, and exhibited a Ca^{2+} dependent disruption of FRET when calmodulin was bound (Romoser et al., 1997). In the same year, another approach was suggested, which used calmodulin and the calmodulin-binding protein M13 for Ca^{2+} detection, flanked by BFP or CFP as a donor, and GFP or YFP as an acceptor. In the Ca^{2+}-free state, little interaction occurred between the donor and the acceptor. Binding of Ca^{2+} was thought to make calmodulin wrap around M13, which changed the distance and orientation of the two fluorescent and led to an increase of FRET (Miyawaki et al., 1997). This sensor was named Cameleon, and has since undergone considerable improvement, the latest variant being yellow Cameleon-Nano (YC-Nano) (Horikawa et al., 2010).

The aforementioned GECIs were all based on calmodulin and M13 (or other calmodulin binding proteins), yet the fact that those proteins are ubiquitous in all kinds of cells, frequently led to side effects when the sensor proteins disturbed regular cell function (Tallini et al., 2006). In response, an obvious measure seemed to exchange calmodulin with a Ca^{2+} binding protein that was rarer. This protein was found in troponin C, which is only present in muscle cells. Troponin C represented the basis for a new sensor series. This sensor series consisted of ECFP as a donor, the YFP-based Citrine as an acceptor, and troponin C from either humans or chickens provided the Ca^{2+} binding domain. Moreover, the latest additions TN-XL and

TN-XXL incorporated a number of mutations which reduced the affinity of troponin C for Mg^{2+}. In regards to TN-XXL, the affinity for Ca^{2+} was increased by doubling the high affinity C-lobe and removing the lower affinity N-lobe (N. Heim & Griesbeck, 2004, Mank et al., 2006, 2008). Indeed, when the biocompatibility of these troponin C-based sensors was tested in transgenic mice, very few side effects were observed (Direnberger et al., 2012). Further improvement could be achieved however, by reducing the number of Ca^{2+} binding sites in the sensors (from four) to reduce their Ca^{2+} buffering, which was shown to impact cellular Ca^{2+} signaling (Helmchen et al., 1996).

The first single fluorophore indicator was developed in 1999, when Baird and colleagues experimented with rearrangements of the GFP protein. They found that they were not only able to make circular permutations of the protein which were still functional (see chapter 1.1.3), but that GFP tolerated the insertion of entire proteins at certain locations, without losing its function. When calmodulin was inserted into EYFP for example, it was observed that its conformational change (due to Ca^{2+} binding) affected fluorescence by promoting deprotonation of the chromophore. This newly discovered Ca^{2+} indicator was called Camgaroo, as it was yellow in color and "carried" the smaller calmodulin in its "pouch" (Baird et al., 1999).

In an alternative single fluorophore indicator series, the Pericams, a circularly permutated version of EYFP was placed in the middle of the construct, flanked by calmodulin on one side and M13 on the other (Nagai et al., 2001). Simultaneously, a second group used the same design, but chose EGFP as a fluorescent protein instead. The addition of a number of mutations and linkers between EGFP and calmodulin on one side, and M13 on the other side resulted in one of the most popular sensor series to date, namely the GCaMP series (Nakai et al., 2001). The latest members of this series are GCaMP6s, GCaMP6m and GCaMP6f (for slow, medium and fast), which are all quite sensitive and vary in kinetics, with the most sensitive ones exhibiting slower kinetics and vice versa (Chen et al., 2013). A summary of the main types of GECIs is provided in **Figure 10**.

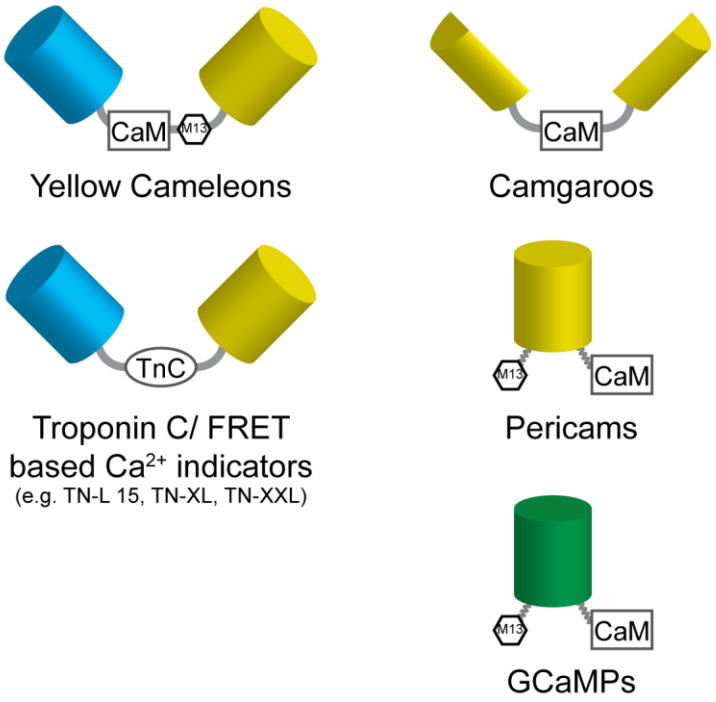

Figure 10: Design Principles of the Main Types of GECIs
Main types of genetically encoded FRET and single fluorophore indicators for Ca^{2+}. Calmodulin (CaM) and the calmodulin-binding protein M13 or troponin C (TnC) are engaged for Ca^{2+} detection.

Current endeavors in the field of GECIs include the development of red-shifted sensors (Akerboom et al., 2013, Zhao et al., 2011), as well as the creation of smaller probes (Tang et al., 2011).

1.3.2 Advantages of Fluorescent Protein Indicators in Comparison to Synthetic Dyes

In addition to fluorescent protein indicators, fluorescent synthetic dyes are powerful tools in visualizing biological events (Terai & Nagano, 2013). Both approaches offer a number of advantages and disadvantages. With a size of around 1 kD, synthetic fluorophores are usually smaller than fluorescent proteins which are approximately 28 kD in size. Synthetic dyes exhibit large signal changes and are bright throughout the visible spectrum, whereas the availability of fluorescent protein sensors at longer wavelengths is still limited. Moreover, organic dyes offer fast kinetics, good selectivity, linear response properties, photostability, and pH resistance. That being said, they also have a number of disadvantages. In contrast to genetically encoded fluorescent proteins, organic dyes require loading, which can be

difficult depending on the animal or tissue of interest. In addition, loading a dye does not allow a discrimination of specific cell types or subcellular structures, whereas genetically encoded indicators can be targeted to a specific subset of cells, or to certain parts of a cell. Furthermore, it is not possible to image chronically with organic dyes, as they will eventually leak out of the cells, whereas genetically encoded sensors are expressed continuously (Kremers et al., 2011, Mank & Griesbeck, 2008).

1.4 Screening of Genetically Encoded Calcium Indicators

1.4.1 Existing Screening Assays – An Overview

Even in the early days of fluorescent proteins, screening has been an important method of modifying and improving a given protein. All those early screens intended to make GFP brighter and change its emission and excitation profile, have been conducted in bacteria. Thousands of mutant GFPs were created via error prone PCR, transformed into bacteria, and subsequently visually screened on agar plates (e.g.(R. Heim & Tsien, 1996, R. Heim et al., 1994)), a technique which remains popular. The range of criteria which can be screened for has, however, increased in the meantime. In addition to brightness and emission profiles, screens have also been conducted to identify longer fluorescence lifetimes (Goedhart et al., 2010) and decreased photobleaching (Ai et al., 2006).

An alternative method, allowing the processing of even higher numbers of protein variants, was devised by Wang and Tsien (L. Wang & Tsien, 2006, L. Wang et al., 2004). They created mutants via somatic hypermutation (SHM, a method used by our immune system to produce antibodies) and subsequently screened them in mammalian cells using fluorescence-activated cell sorting (FACS). Nguyen and Daugherty applied FACS to a pair of fluorescent proteins screening for optimal FRET properties (Nguyen & Daugherty, 2005).

When it comes to the development of a sensor however, the screening process becomes more complicated since one must assess not only one condition, but the dynamics at play when the condition changes. Techniques need to be developed to induce this change and image the sensor in both conditions. For this reason, many attempts to improve existing sensors in the past have been based on rational design (e.g. (Akerboom et al., 2009) (Geiger et al., 2012)). However, even with an abundance of structural information, the consequences of a new mutation, and thus, the properties of a new sensor were often difficult to predict. Hires and colleagues for example, after testing 176 combinations of linkers (which sometimes only differed by one amino acid) inserted into a sensor, described the fitness landscape of

these linkers as 'surprisingly peaked' (Hires et al., 2008). Throughout the years, many different methods have been developed in order to screen sensors.

Tian and colleagues attempted screening in bacterial lysate, which allowed them to screen with high throughput. They observed however, that measurements from this *in vitro* assay only correlated weakly with measurements conducted in cells. Therefore, they designed a lower throughput cell based screening assay, which they used to develop GCaMP3 (Tian et al., 2009). In 2013, the same group went one step further and decided to screen their sensors, which were developed for the application in active neurons, in electrically stimulated rat primary neuronal cultures. This screening assay was even more specialized, diminishing their throughput further, but it allowed them to screen sensors under the exact conditions they were intended for (Chen et al., 2013, Wardill et al., 2013).

Schultz and colleagues also published a cell based screening assay, which was more rapid and versatile. To this end, they designed a library which, although small, exhibited enough variability to suit a variety of sensors. This library was comprised of FRET backbone plasmids, consisting of different combinations of fluorescent proteins and linkers of two to eight amino acids in length. The backbone plasmids could be combined with different kinds of sensing domains, transfected into cells and imaged in a semi-automated microscope. (Piljic et al., 2011).

Komatsu and colleagues, in their approach, decided that sensor libraries and screening were not even necessary, as long as the backbone included a sufficiently long and flexible linker. This rendered the (almost unpredictable) orientation of the fluorescent proteins to one another unimportant, making FRET completely distance dependent. Therefore, sensor improvement would simply require identifying the most suitable sensor domain for a particular substrate (Komatsu et al., 2011).

Campbell and colleagues recently suggested two bacteria-based screening methods. For their first method, they targeted Ca^{2+} indicators to the periplasm of E.coli cells (using a TorA tag) for investigation. Since the bacterial outer membrane is permeable to small molecules and ions, the environmental Ca^{2+} concentration was easier to control there, rather than in the cytoplasm (Zhao et al., 2011). Their second approach involved the use of a dual expression vector containing the sensor (H3K27 for detection of methylation of lysine 27 of histone H3) and its substrate (vSET), under the control of inducible promoters. They manually replicated colonies on two plates; one which induced expression of the sensor but repressed expression of the substrate, and another which induced the expression of both (Ibraheem et al., 2011). Three years later, the same group refined this technique. They grew the colonies on one plate which allowed the expression of the sensor, but not that of its substrate. Substrate expression was

induced on the same plate after the first round of imaging, by spraying the plate with the inducing substrate arabinose, thereby making manual replicate plating redundant (Belal et al., 2014).

1.4.2 *Escherichia coli* (*E.coli*) as a Model for Screening

Escherichia coli (E.coli) was discovered by Theodor Escherich in 1885 (Escherich & KS, 1988) and is a rod-shaped, gram-negative bacterium which belongs to the family of Enterobactericeae. It is well-known both as a harmless inhabitant of the intestinal bacterial microflora in humans as well as many animals, and a highly versatile, and therefore dangerous pathogen (Kaper et al., 2004).
In science and industry, it is referred to as the "workhorse" of molecular biology due to its heavy use in both DNA and recombinant protein production (Chou, 2007, Huang et al., 2012). Moreover, *E.coli* is an extremely popular model (Müller & Grossniklaus, 2010), since it shares many fundamental processes with higher organisms, but is better characterized, cheaper, and easy to handle and propagate. These qualities made *E.coli* attractive for us in our endeavor to develop a screening assay.

1.4.3 *E.coli* Membrane Structure – the Hurdle in Screening

E.coli cells are routinely used to express foreign protein in their cytoplasm. Their cytoplasm is, like in all gram-negative bacteria, surrounded by a cell envelope consisting of an inner and an outer membrane. These two membranes differ highly in their structure and composition, due to their unique functions and the respective environment they face (either the cytoplasm or external environment). The inner membrane is a classic phospholipid bilayer, containing integral proteins, which span the membrane, and lipoproteins, which are anchored in its outer leaflet. The outer membrane functions as a selective barrier which permits the entry of nutrients, whilst preventing the invasion of toxic agents. It thereby enables *E.coli* to inhabit many different, potentially hostile environments. The outer membrane is asymmetrical, with its inner leaflet consisting of phospholipids, and its outer leaflet consisting of lipopolysaccharides. Like the inner membrane, it contains integral proteins that span the membrane, and lipoproteins which are anchored in the inner leaflet. The integral proteins of the outer membrane are often assembled in a β-barrel conformation, forming channels which allow free diffusion of ions and hydrophilic molecules (Nikaido & Vaara, 1985, Ruiz et al., 2006). The space between the two membranes is called the periplasm. It is highly viscous and contains a thin peptidoglycan layer. Furthermore, it comprises a large number of

soluble proteins involved in protein folding, uptake and transport of nutrients, and the detoxification of dangerous substances (Goemans et al., 2013).

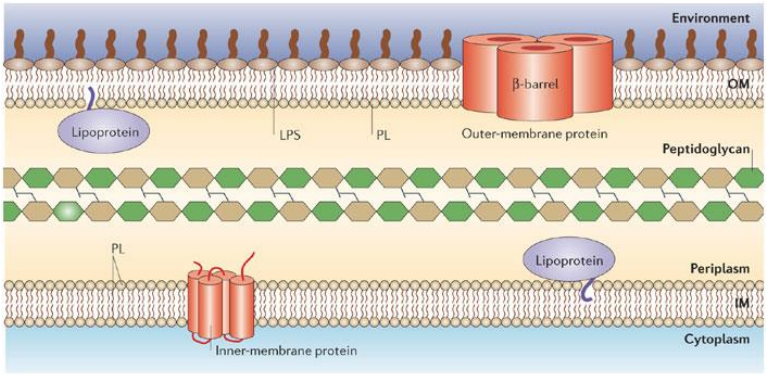

Figure 11: Scheme of the *Escherichia coli* Cell Envelope
The inner membrane (IM) is composed of phospholipids (PL), the outer membrane (OM) consists of phospholipids and lipopolysaccharides (LPS), and the periplasmic space contains a thin peptidoglycan cell wall (Reprinted by permission from Macmillan Publishers Ltd: [Nat Rev Microbiol.] (Ruiz et al., 2006), copyright (2006)).

1.5 Research Objective

Developing genetically encoded indicators can be time-consuming, tedious and repetitive. In rational design, predictions are made on the basis of crystal structures and known mutations, and then each new sensor mutant must be produced, purified and subsequently characterized both *in vitro* and *in vivo*. This lengthy procedure usually requires multiple repetitions, until a sensor finally exhibits all desired features. To make things even more complicated, a crystal structure for each component of the sensor is not always available. Additionally, each sensor as a whole is an artificial protein, assembled from complex proteins which are derived from a range of organisms. This makes it very difficult to predict how the sensor complex will behave as a whole, even if all the individual structures are known. The objective of this study was therefore, to develop a user friendly screening assay which allows the researcher to test an increased quantity of genetically encoded Ca^{2+} sensors in a shorter time span. Ideally, the assay could be applied to screen for qualities such as brightness of the fluorescent proteins, dynamic range of the sensor, Ca^{2+} affinity and kinetics.

Screening on bacterial plates was the method selected, with plates of bacterial colonies expressing different types of sensors in their cytoplasm. Various strategies were employed to penetrate the powerful bacterial membrane and introduce Ca^{2+} into the cells, in order to probe the sensors for their Ca^{2+} response properties.

The newly developed screening method was used to improve a Ca^{2+} sensor series on the basis of FRET, using ECFP as a donor, cpCitrine174 as an acceptor and the C-lobe of troponin C as a minimal Ca^{2+} binding domain. The goal was to produce a sensor with reduced buffering (through the reduction of Ca^{2+} binding sites), higher signal change, higher affinity and faster kinetics, compared to the last sensor of this kind; TN-XXL (Mank et al., 2008). The resulting sensor series was later published as the 'Twitch' series (Thestrup et al., 2014).

Following the 'Twitch' sensor screening, an attempt was made to develop a FRET sensor which exhibited similar qualities, but was shifted further into the red section of the spectrum. Multiple potential donor and acceptor combinations were tested in order to identify the most suitable FRET pair. Eventually, four green fluorescent proteins were chosen as potential donors, and the orange fluorescent protein mKOκ was chosen as an acceptor, since it was considerably brighter than most fluorescent proteins in this spectral range. As mKOκ still exhibited a number of weaknesses as an acceptor, a further round of screening was initiated in parallel to the screening conducted for a red-shifted Ca^{2+} sensor, in order to

develop an improved orange FRET acceptor. The resulting orange fluorescent proteins were characterized in detail.

2 Material and Methods

2.1 Molecular Biology

2.1.1 Polymerase Chain Reaction (PCR)

A polymerase Chain Reaction (PCR) is a standard lab procedure used to amplify a specific piece of DNA. It is a stepwise process involving the denaturation of double-stranded template DNA via heat. The oligonucleotide primers then anneal to their target sequence and become extended by a thermostable DNA polymerase. Repeated cycles of this process lead to an exponential amplification of the template DNA.

For standard PCR reactions Herculase II polymerase was used. This polymerase is based on the *Pfu*-polymerase, which originates from the archeal *Pyrococcus furiosusa*. It exhibits one of the lowest error rates of all DNA polymerases whilst producing high yields with fast cycling times.

All components were added to a PCR reaction tube on ice (**Table 1**). The PCR reaction was carried out in a FlexCycler^2 and began with an initial denaturation step at 95°C to reduce primer dimerization and increase specificity (**Table 2**).

Component	Volume (+ DMSO) [µL]	Volume (- DMSO) [µL]
H_2O	32	37
DMSO	5	-
5x Herculase II buffer	10	10
dNTPs (12.5 mM each)	1	1
template DNA (~100 ng/µL)	0.5	0.5
primers (100 pM)	0.5 each	0.5 each
Herculase II polymerase	0.5	0.5
total volume	50	50

Table 1: PCR Reaction

	Temperature [°C]		Time [mm:ss]
Initial denaturation	95		2:00
Denaturation	95	30 cycles	0:20
Annealing	52-65		0:20
Elongation	72		0:30 per kb
Final Elongation	72		3:00
Pause	4		forever

Table 2: PCR Cycle for Vector DNA Templates ≤ 10 kb

For higher yields, the ratio of template to primer was optimized. The addition of DMSO also had the potential to improve yield by facilitating primer annealing, but could lead to unspecific priming. A decrease of the annealing temperature tended to increase yield, whereas an increase led to more specific priming. The obtained DNA fragments were purified using a QIAquick PCR purification kit or a NucleoSpin®PCR clean-up kit. Both kits utilize the same principle of binding DNA to a silica membrane in the presence of chaotropic salt, and eluting it under low salt conditions.

2.1.2 Error-Prone PCR

Error prone PCR was used to introduce random mutations into a DNA fragment. A JBS Error-Prone kit (Jena Bioscience) was utilized for this purpose. The kit used *Taq* polymerase originally derived from the thermophilic bacterium *Thermus aquaticus* as an enzyme. Since *Taq* does not have a proofreading function, it exhibits an increased error rate of $10^{-4} – 10^{-5}$. In comparison, *Pfu* polymerase, which does have a proof reading function, only exhibits an error rate of approximately $10^{-6} – 10^{-7}$. Furthermore, the kit included an error prone solution with an increased Mg^{2+} concentration and a supplementary of Mn^{2+}, and a mix of dNTPs at an unbalanced ratio. These features further increased the error rate of the PCR reaction. The mutation frequency was controlled by the amount of template DNA and the number of reaction cycles (**Table 3**). The PCR reaction was carried out in a FlexCycler^2 (**Table 4**).

Component	Volume [µL]	Final amount in 50 µL
10 x reaction buffer	5	1 x
dNTP error-prone mix	2	unbalanced ratio of dNTPs
primers	depending on concentration	20-100 pmol
template	depending on concentration	0.2 – 2 ng
***Taq* polymerase**	0.4 - 1	2-5 units
10 x error-prone solution	5	1 x
PCR-grade water	fill up to a total volume of 50	

Table 3: Error-Prone PCR Reaction

	Temperature [°C]		Time [mm:ss]
Initial denaturation	94		2:00
Denaturation	94	20 - 30 cycles	0:30
Annealing	65		0:30
Elongation	72		1:00 per kb
Final Elongation	72		3:00
Pause	4		forever

Table 4: Error-Prone PCR Cycle

2.1.3 Site-Directed Mutagenesis via PCR

Point mutations at specific locations of the template DNA were introduced via site-directed mutagenesis. To this end, sense and anti-sense primers were designed, which flanked the location of interest with approximately 21 bp (7 codons) on either side, but contained the desired nucleotide substitution at the location, instead of the existing amino acid (**Figure 12**).

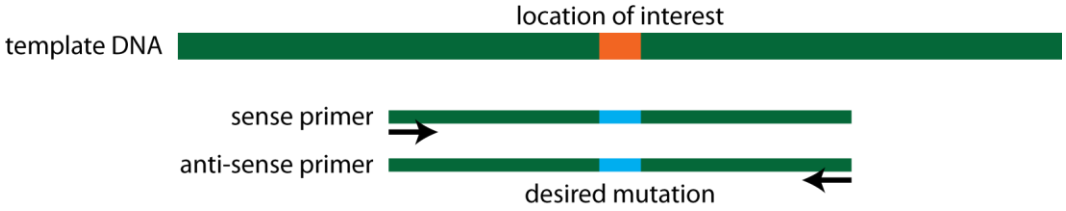

Figure 12: Principle of Site Directed Mutagenesis
A sense and an antisense primer flank the location of interest and contain the desired nucleotide substitution at this location.

If a random mutation at a location of interested was to be introduced, the existing amino acid at this location was substituted with a degenerate codon. The codons NNN and NNB were tested for this purpose (N = A/C/G/T, B = C/G/T). Both codons encoded all 20 amino acids, but while NNN used all 64 codons, NNB only used 48.

In order to ensure the reliability of the PCR process and the subsequent template digestion, a control was carried out along with the mutagenesis reaction, containing all components of the reaction except for the polymerase (**Table 5**, **Table 6**).

Component	Volume mutagenesis [µL]	Volume control reaction [µL]
H_2O	37	37.5
5x Herculase II buffer	10	10
dNTPs (12.5 mM each)	1	1
template DNA (100 ng/µL)	0.5	0.5
primers (10 pM)	0.5 each	0.5 each
Herculase II polymerase	0.5	---
total volume	50	50

Table 5: Site-Directed Mutagenesis Reaction

	Temperature [°C]		Time [mm:ss]
Initial denaturation	95		0:30
Denaturation	95	15 cycles	0:30
Annealing	57		1:00
Elongation	72		6:00
Pause	4		forever

Table 6: Site-Directed Mutagenesis Cycle

Upon completion of the PCR reaction, a DpnI digest was performed to remove template DNA from the PCR reaction (**Table 7**). DpnI is a restriction endonuclease which specifically cuts methylated DNA. The addition of methyl groups to cytosine or adenine is a mechanism bacteria uses to protect itself against foreign DNA (e.g. originating from bacteriophages), by marking its own DNA to distinguish it from intruders'. Since the template DNA was isolated from bacteria it had been methylated, whereas the DNA produced in the PCR reaction had not, and could therefore not be degraded.

The control reaction was further divided into two separate reactions. In the first one, a DpnI digest was performed (negative control), whereas the second one was directly transformed (positive control) (**Table 7**).

Component	Mutagenesis	Positive control	Negative control
PCR product	50 µL	30 µL	20 µL
DpnI	2.5 µL	---	1 µL
incubation	1 hour at 37°C		

Table 7: Site-Directed Mutagenesis - DpnI Digest

5 µl of the DpnI digested mutagenesis product was transformed into chemically competent XL1 blue cells and incubated at 37°C overnight. On the following day, positive control plates were expected to contain numerous colonies comprising the PCR template. Negative control plates were expected to be empty, since all template DNA should have been digested, and no PCR should have taken place.

2.1.4 Restriction Digest of DNA

Prior to ligations using the T4 DNA ligase (from NEB), linearized vector and insert DNA fragments were prepared utilizing restriction enzymes (Pray, 2008) (**Table 8**). Such enzymes cut DNA at their respective restriction recognition sites of typically 6 to 8 base pairs, in most cases leaving behind short overhangs called “sticky ends”, which are compatible with complementary “sticky ends”. Most commonly used plasmid vectors have multiple cloning sites (MCS), with recognition sites for numerous restriction enzymes (**Figure 13**). For the insert DNA, suitable restriction sites are added via PCR by including them in the utilized primers.

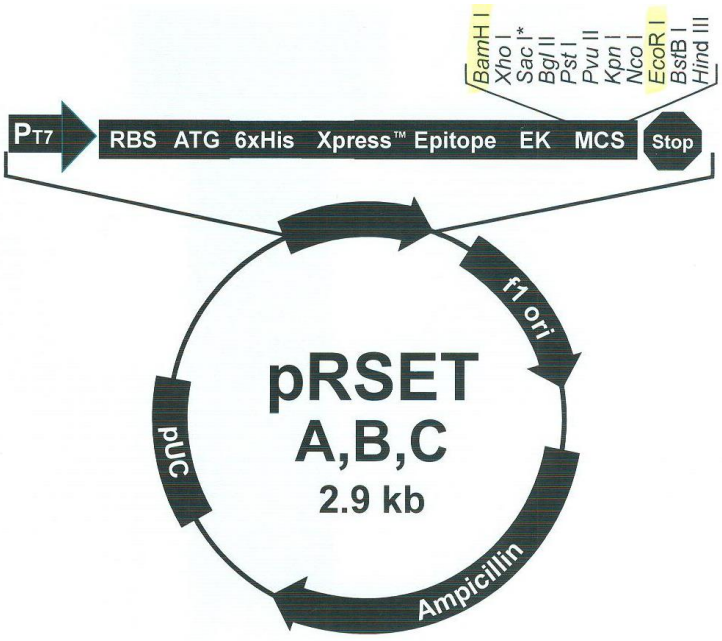

Figure 13: Plasmid Vector pRSETB
The multiple cloning site (MCS) contains recognition sites for numerous restriction enzymes. The restriction sites BamHI and EcoRI, which we predominantly used, are highlighted in yellow.

An analytic restriction digest could be performed after a ligation to confirm its success. In this case, the DNA of a picked clone was purified, a small amount of DNA was digested (**Table 8**), and the presence of vector and insert bands was examined via analytic agarose gel electrophoresis.

The restriction enzymes deployed were BamHI, DpnI, EcoRI, EcoRV, NotI, SacI and SphI (from NEB).

Component	Volume analytic digest [µL]	Volume preparative digest [µL]
H_2O	24.3	32.5
DNA (100-200 ng/ µL)	2	10
enzyme buffer	3	5
BSA (optional)	0.3	0.5
enzyme 1	0.2	1
enzyme 2 (if required)	0.2	1
total volume	30	50

Table 8: Restriction Digest Reaction

Following a restriction digest, agarose gel electrophoresis was used to either extract the desired piece of DNA or to visualize the DNA bands of an analytic digest.

2.1.5 Agarose Gel Electrophoresis

Agarose gel electrophoresis was employed to separate strands of DNA according to their size. This method takes advantage of the negative charge of DNA. When an electric field is applied, the molecules move towards the anode. Short pieces of DNA are able to navigate more quickly through the agarose gel pores.

To prepare 1 % agarose gels, 0.5 g of agarose was added to 50 ml of a 1 x TAE buffer and boiled using a microwave until evenly mixed. In a gel sledge with a suitable comb, 5 µL ethidium bromide was dispensed, before the gel was allowed to polymerize for approximately 20 minutes. Ethidium bromide is a popular stain to detect DNA, exhibiting increased fluorescence under UV light when attached to DNA.
Prior to loading, DNA samples were supplemented with DNA loading buffer (10 x Orange G) to increase the sample density, as well as its visibility. 100 bp or 1 kb DNA ladders (from NEB) were used as DNA standards. Electrophoresis was performed at ~ 100 V for approximately 45 minutes.
DNA bands were visualized under UV light using a Gel Doc™ 2000 Gel Documentation System (from BioRad).

2.1.6 Dephosphorylation of Vector DNA

Prior to ligation, vectors were dephosphorylated with a phosphatase, catalyzing the removal of phosphate groups from their 5’ termini (**Table 9**). Since ligases need these 5’ termini in order to perform ligations, the dephosphorylation impeded self-ligation, thereby reducing the background of empty vector plasmids. Antarctic phosphatase was chosen because it can be heat-inactivated, whereupon vectors can be used without another purification step.

Component	Volume [µL]
DNA (100 – 200 ng/µL)	44
10 x Antarctic phosphatase buffer	5
Antarctic phosphatase	1
Total volume	50
Incubation:	1h at 37°C
Heat inactivation:	15min at 70°C

Table 9: Vector Dephosphorylation

2.1.7 Ligation of DNA Fragments

2.1.7.1 Ligation via Ligase

T4 DNA Ligase was used to catalyze the formation of bonds between DNA fragments (**Table 10**). The complementary sticky ends left behind by most restriction enzymes have an intrinsic tendency to build temporary bonds. These can then be converted into permanent phosphodiester bonds between the 5'phosphate and 3'hydroxyl termini by ligases.

A control ligation was always conducted to estimate the amount of empty vector background, resulting from uncut or self-ligated vector plasmids (**Table 10**).

Component	Ligation Volume [µL]	Control Volume [µL]
vector DNA	total of 4 (vector/insert ratio 1:3 – 1:5)	same amount of vector DNA as in the ligation, but H_2O instead of insert
insert DNA		---
H_2O	13	16
ligase buffer	2	2
T4 DNA ligase	1	1
total volume	20	20
incubation	3 hours at room temperature	

Table 10: DNA Ligation

2.1.7.2 Ligation via SLiCE

SLiCE (Seamless Ligation Cloning Extract) is a rather new, fast and highly efficient cloning method which uses bacterial cell extract to assemble multiple DNA fragments into recombinant DNA molecules in a single reaction (Zhang et al., 2012).

For the production of SLiCE extract, the *E.coli* strain PPY (derived from DH10B) was grown overnight in 5 ml of 2xYT medium, supplemented with suitable antibiotics at 37°C and gently agitated. On the following day, 200 ml of medium containing suitable antibiotics was inoculated using the overnight culture. Cells were grown to an OD_{600} of 5-5.5 at 37°C and under gentle agitation. Thereafter, 1.1 ml of a 36% L-(+)-arabinose solution was added to the culture to induce protein expression. Cells were allowed to grow for another two hours before they were spun down at 5465 x g and 4°C for 10 minutes. The pellet was resuspended in 2.5 ml protein resuspension buffer, supplemented with the protease inhibitors PMSF (4 µM), pepstatin (4 µg/ml) and leupeptin (4 µg/ml). The cell suspension was frozen at -80°C for at least one hour and then fully thawed. Subsequently, approximately 1 mg of lysozyme was added and the suspension was incubated on ice for 30 minutes. RNAse (8 µg/ml) was added, and the cells were ultrasonicated in ice water for 30 minutes. The mix was then centrifuged at 20000 x g and 4°C for 30 minutes, before the pellet was discarded and glycerol was added to the supernatant to a final concentration of 50 %.

The resulting SLiCE extract was incubated at 4°C overnight, then frozen in liquid nitrogen and stored at -80°C.

For the SLiCE reaction, a vector was linearized either via PCR or with the use of restriction enzymes. Inserts were amplified in a PCR reaction, which also provided them with a 20 bp overhang on either side, acting as a homolog to the adjacent DNA fragments (**Figure 14**). PCR products were digested with DpnI to remove template DNA and purified via agarose gel electrophoresis to eliminate background.

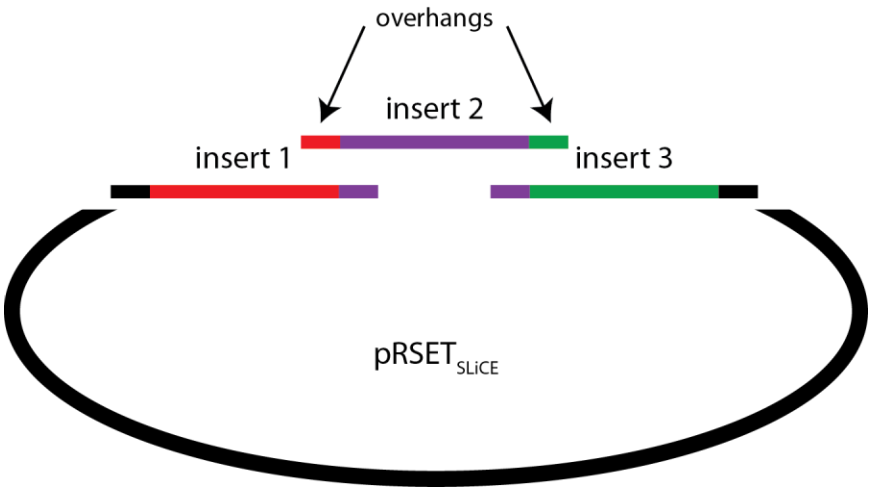

Figure 14: SLiCE Cloning Scheme
Each fragment intended for SLiCE cloning was equipped with short overhangs on either side, which were homolog to the adjacent fragments.

Component	Ligation Volume [µL]
vector DNA	total of 8 (vector/insert ratio 1:3 – 1:5)
insert DNA	
H_2O	
ligase buffer	1
slice extract	1
total volume	10
incubation	15min at 37°C

Table 11: SLiCE Cloning Reaction

After incubation, 1 µL of the SLiCE reaction was transformed into chemical competent XL1 blue cells.

2.1.8 Preparation of Chemically Competent *E.coli* Cells

10 ml of LB medium, supplemented with suitable antibiotics, was inoculated with 1 µL of bacterial cell stock (either XL1 blue or BL21 gold) and incubated overnight at 37°C under gentle agitation. The added antibiotics ensured that only the desired stock, which carried a resistance, grew. On the next day, a 1000 ml Erlenmeyer flask was prepared with 300 – 400 ml of preheated LB medium and 7 ml of the overnight culture. Cells were allowed to grow to an OD_{550} of 0.5 at 37°C under gentle agitation. Afterwards, the cells were incubated on ice for 10 minutes. The cell culture was then divided into 6x50 ml Falcon tubes and

centrifuged for 15 minutes at low speed and 4°C. The supernatant was decanted and the pellets were resuspended in 30 ml of precooled TSS buffer. 7.5 ml of glycerin was added, before the cells were aliquoted into 50 µL portions and immediately frozen in liquid nitrogen. The aliquots were stored at -80°C.

2.1.9 Transformation of Chemically Competent *E.coli* Cells

The *E.coli* strain XL1 blue was used for cloning experiments. It is a common choice for routine cloning and sub-cloning experiments. It has an endonuclease I deficiency (*endA*), which improves the quality of purified DNA by impeding its degradation via unspecific endonucleases in the periplasmic space of *E.coli*. In addition, XL1 blue has a recombination deficiency (*recA*), which means that the inserted plasmid DNA is left unaltered by the cells repair system, improving insert stability. Furthermore, XL1 blue cells have a *hsdR* mutation, preventing the cleavage of cloned DNA by *EcoK* endonucleases, which destroy foreign DNA in *E.coli*.

The *E.coli* strain BL21 gold was used for protein expression. It is most suitable for expression vectors containing the bacteriophage T7 promoter, since the gene encoding T7 RNA polymerase is integrated into the chromosome of BL21. BL21 cells lack the OmpT protease and the Lon protease, which degrades recombinant proteins.

The transformation procedure was identical for both strains. Chemically competent cells were thawed on ice and 1 µL of plasmid DNA was added. In our hands, a DNA concentration of ~ 100 ng/µl proved to be most suitable for BL21 cells, whereas a dilution to ~20 pg/µl was advisable for XL1 cells, which exhibited a higher transformation efficiency. However, these numbers are probably strongly dependent on the way the respective cell stocks are created and treated. Cells were incubated on ice for approximately 20 minutes, and subsequently heat-shocked at 42°C for 45 seconds. Cells were then allowed to recover on ice for 2 minutes. An optional incubation in 0.1 ml of SOC medium at 37°C for 1 hour increased transformation efficiency.
Afterwards, cells could be transferred to LB medium or spread on agar plates containing appropriate antibiotics. Cultures and plates were incubated at 37°C overnight.

2.1.10 DNA Purification and Determination of DNA Concentration

The QIAprep Spin Miniprep Kit was used for standard DNA purification of plasmid DNA (plasmid size ≤ 10 kb) from XL1 blue bacterial cultures. It allowed for purification of up to 20 µg of DNA, which was bound to a silica membrane in the presence of chaotropic salt. After a number of cleaning steps, it was eluted into low-salt buffer or H_2O dd. If higher amounts of DNA were required, the Promega PureYield Plasmid Midiprep Kit was used, which allowed for purification of up to 200 µg of plasmid DNA.

For DNA purification from agarose gels, the QIAquick or NucleoSpin® gel extraction kits were used, which both utilized a silica membrane for DNA binding.

DNA concentration was determined using a NanoDrop 1000 spectrometer, which detected absorbance at 260 nm, with DNA elution buffer or H_2O dd as a blank.

2.2 Protein Biochemistry

2.2.1 Protein Expression

The *E.coli* strain BL21 gold was chosen for protein expression, and pRSETB containing the T7 promoter was utilized as an expression vector. All proteins intended for purification incorporated an N-terminal poly-histidine tag (His-tag) consisting of 6 repeats of the amino acid histidine.
Protein expression was induced either through lactose, or the synthetic lactose analog isopropyl-beta-D-thiogalactopyranoside (IPTG). Both methods initiated the expression of the T7 RNA polymerase, which in turn bound to the T7 promoter and transcribed the coding sequence for the desired protein.
For IPTG induction, BL21 cells, transformed with a plasmid of choice, were grown in 200 ml of LB medium supplemented with suitable antibiotics to an OD_{600} of 0.6 at 37°C under gentle agitation. Protein expression was then induced by the introduction of 0.1 mM IPTG. Cells were allowed to grow for approximately 12-16 hours at room temperature, after which the proteins were purified.
Higher yields of protein could be achieved (via lactose) with an autoinductive LB medium, rendering the need to monitor growth and undertake further steps at appropriate times unnecessary. For autoinduction, BL21 cells were grown in 200 ml of LB medium supplemented with antibiotics, as well as 0.6 % glycerol (v/v), 0.2 % lactose (w/v) and 0.05 % glucose (w/v) (based on (Studier, 2005)) for

approximately 65 hours at room temperature under gentle agitation. Proteins could be purified thereafter. Cells, which were grown in autoinductive LB medium, used glucose as an early energy source. Glucose repressed the induction of T7 RNA polymerase expression by lactose, which meant that all glucose needed to be metabolized before protein production could commence, giving the cells sufficient time to grow. When glucose was depleted, protein expression was induced by lactose. Glycerol, which did not interfere with lactose induction, could be used as a late energy source, supporting continued growth and protein production of the cell culture.

2.2.2 Protein Purification

For protein purification, bacterial cells were harvested at 5465 x g and 4°C for 10 minutes. The supernatant was discarded and the pellet was resuspended in 10 ml of protein resuspension buffer, supplemented with the protease inhibitors PMSF (1 mM), pepstatin (1 µg/ml) and leupeptin (1 µg/ml). The cell suspension was subsequently frozen at -80°C for at least one hour. It was then completely thawed, approximately 1 mg of lysozyme was added and the suspension was incubated on ice for 30 minutes. Lysozyme is a glycoside hydrolase, which degrades bacterial cell walls by catalyzing hydrolysis of 1,4-beta-linkages between N-acetylmuramic acid and n-acetyl-D-glucosamine residues in peptidoglycan.
10 drops of the detergent Triton-X-100 and 10 µg/ml each of DNAse and RNAse were added, and cells were ultrasonicated in ice water for 30 minutes. Cell debris could then be separated from the proteins in solution through an additional centrifugation step at 20000 x g and 4°C for 30 minutes. The pellet was discarded and the supernatant was transferred to a 15 ml Falcon tube and combined with 300 µL of Ni-NTA (nickel-nitrilotriacetic acid) agarose beads. The His-tags contained in all proteins of interest could then form complexes with the nickel ions. Unspecific binding was prevented (via competitive binding) through the presence of 10 mM imidazole (a side chain of histidine). Proteins and beads were incubated at 4°C under gentle agitation for 1 hour. Eventually, the suspension was loaded onto a polypropylene column, which retained the beads, while allowing untagged proteins to pass through. The proteins were washed twice with protein resuspension buffer. Subsequently, they were eluted in 400 µL of protein elution buffer, which contained enough imidazole (250 mM) to out-compete the proteins bound to the Ni-NTA beads, thereby releasing them into the buffer.

2.2.3 Small Scale Protein Purification

If only a small amount of protein was required, cells were pre-cultured in 5 ml of LB medium (supplemented with suitable antibiotics) in 14 ml polystyrene tubes at 37°C under gentle agitation. After approximately 16 hours, 7 ml of medium supplemented with antibiotics and IPTG was added to induce protein production. Cells were allowed to grow for another 8 hours at 37°C, before they were harvested by spinning them down at 5465 x g and 4°C for 10 minutes. Alternatively, cells could be cultured for ~65 hours at room temperature in 8-10 ml of autoinductive LB medium.

The treatment used to break up the cells was identical to the purification protocol outlined in chapter 2.2.2, scaled down to suit a smaller volume. After the second centrifugation step, which separated proteins from cell debris, the supernatant was added to 25 µl of His Mag Sepharose Ni magnetic beads, which were used in place of the Ni-NTA agarose beads to bind the protein. A magnetic rack, which held 24 Eppendorf tubes, retained the proteins in place while buffers were changed with a vacuum pump. The proteins were incubated with the beads for 1 hour at 4°C under gentle agitation. They were then rinsed three times in protein resuspension buffer and eluted in 25 µl protein elution buffer.

2.2.4 Determination of Protein Concentration (Bradford Assay, BCA Assay)

Protein concentration was determined using either the Bradford or the BCA assay, which are both colorimetric assays. In the Bradford assay, Coomassie Brilliant Blue G-250 binds to proteins. This dye exhibits different colors depending on its ionic state. Unbound and under acidic conditions, it predominantly exists in its doubly protonated cationic form and is red in color (A_{max} = 470 nm). When it binds to protein, it is converted into its unprotonated anionic form and turns blue (A_{max} = 595 nm). The shift of absorption from 470 nm to 595 nm can be measured and compared to a known protein standard. In the BCA assay, protein is immersed in an alkaline solution, leading to the reduction of Cu^{2+} to Cu^{1+}. One Cu^{1+} and two molecules of bicinchoninic acid (BCA) can then chelate, resulting in the formation of a purple colored reaction product which can be detected at 562 nm.

BSA (bovine serum albumin) was utilized as a protein standard at known concentrations.

2.2.5 Native PAGE (Polyacrylamide Gel Electrophoresis)

To determine the oligomeric structure of fluorescent proteins, they were compared to known monomers, dimers and tetramers on native PAGE gels, which separated proteins according to their charge to mass ratio, without changing their secondary structure.

The separation gel was prepared (**Table 12**) and sealed with isopropanol, and allowed to polymerize for ~ 30 minutes. Subsequently, the isopropanol was poured out or removed with filter paper and the stacking gel was added on top (**Table 13**). The stacking gel was used to accumulate the proteins, before they entered the separation gel.

Native PAGE – 10 % separation gel	2 gels (10 ml)
H_2O	3.95 ml
30 % acrylamide mix	3.33 ml
1.5M Tris (pH 8.8)	2.5 ml
10 % ammonium persulfate (fresh)	100 µl
TEMED	4 µl

Table 12: Native Gel Separation Gel Reaction

Native PAGE – 5 % stacking gel	2 gels (4 ml)
H_2O	2.72 ml
30 % acrylamide mix	665 µl
1.5M Tris (pH 8.8)	500 µl
10 % ammonium persulfate (fresh)	40 µl
TEMED	4 µl

Table 13: Native Gel Stacking Gel Reaction

Native PAGE running buffer was used, and electrophoresis was conducted at 20 mA and 70 mV for approximately 2 hours.

2.3 Spectroscopy

2.3.1 Excitation, Emission, and Absorbance Spectra of Purified Proteins

Fluorescent spectra were recorded using either a Cary Eclipse fluorescence spectrometer (Varian) or an Infinite M200 PRO plate reader (Tecan). The plate reader allowed for the measurement of up to 96 proteins in parallel and could record absorbance, in addition to excitation and emission.

For the spectrometer, 15 ml of protein was diluted in 1 ml of MOPS buffer (-fluorescence spectroscopy, pH 7.5) and mixed gently in a quartz cuvette to avoid bubbles. The Cary Eclipse scan software was used to record spectra. For the plate reader, 3 µl of protein was diluted in 200 µl of MOPS buffer (-fluorescence spectroscopy, pH 7.5). The plate reader utilized the Tecan i-control™ software.

2.3.2 Determination of Quantum Yield and Excitation Coefficient

The brightness of a fluorescent protein is defined as the product of its quantum yield and its extinction coefficient. It is often indicated as the relative brightness compared to EGFP.

The quantum yield of a protein, which is defined as the ratio of photons absorbed to photons emitted through fluorescence, was determined as follows: A fluorescent protein and a reference fluorophore with a similar excitation profile were diluted in 5 mM Tris (pH 7.5) to an absorbance value at the excitation wavelength of 0.3-1. Absorbance was measured, and both protein and reference were further diluted via serial dilution to 5 concentrations below 0.05. Their absorbance was calculated from the dilution steps, since such low absorbance values cannot be measured reliably. The full emission spectra of all dilutions were then recorded using a step size of 1 nm and constant settings for each measurement. The emission spectra were integrated and the resulting fluorescence intensities of a protein were plotted against the calculated absorbance values. Linear regression was applied to the plots with the intercept set to zero, and the slopes were determined. Using the known quantum yield of the reference fluorophore (Φ_{ST}) and the two slope values (S_{FP} and S_{ST}), the quantum yield of an unknown fluorescent protein (Φ_{FP}) could be calculated using the following formula:

$$\Phi_{FP} = \Phi_{ST}\left(\frac{S_{FP}}{S_{ST}}\right)\left(\frac{R_{FP}^2}{R_{ST}^2}\right)$$

R_{FP} and R_{ST} represent the refractive indexes of the buffers used for the fluorescent protein and the reference respectively.

The extinction coefficient reflects the capability of a fluorescent protein to absorb light at a certain wavelength. To calculate the extinction coefficient, protein concentrations were determined using either the BCA or the Bradford assay. These concentrations were then converted into molar concentrations (C) using the calculated molecular weight of a fluorescent protein, which can be deduced from its sequence (online calculator e.g. http://protcalc.sourceforge.net/, status: 24.6.2014). Absorbance was measured at the excitation maximum and the following formula applied to calculate the extinction coefficient:

$$\varepsilon = \frac{I_A * D}{C * d}$$

I_A represents the absorbance intensity at a given wavelength, D the dilution factor, and d the light's path length through the solution.

2.3.3 Determination of the pK_a of a Protein

To determine the pK_a of a fluorescent protein (indicating its pH stability), a series of 200 mM citrate and borate buffered solutions were prepared, with pH values adjusted in 0.5 pH steps from pH 3 to pH 10 with NaOH and HCl. In a transparent bottom 96 well plate, triplicates of 200 µl of buffer containing 3 µl of protein, were prepared for each pH value and incubated for 10 minutes at room temperature. Subsequently, all emission and absorbance spectra were recorded. To determine the pK_a value, the relative fluorescence values at the protein's emission maximum were plotted against the pH values and a sigmoidal fit was applied.

2.3.4 Determination of the *in vitro* Ratio Change (ΔR) of a Ca^{2+} FRET Indicator

To determine the ratio change (ΔR) of a FRET indicator, the donor was excited at its excitation maximum (or lower in the event of cross-excitation) and an emission spectrum covering both the donor and the acceptor emission was recorded. The sensor was first measured in MOPS buffer (-fluorescence spectroscopy, pH 7.5) which contained EGTA and EDTA to chelate Ca^{2+} ions. To determine the sensors signal change in response to Ca^{2+} and Mg^{2+}, 1 mM Mg^{2+}, 1 mM Ca^{2+} and 10 mM Ca^{2+} were added respectively, and spectra were recorded after each addition.

ΔR upon addition of Mg^{2+} and Ca^{2+} was calculated either manually, or through a Matlab program (written by Christopher Zarboc). The following formula was used:

$$FRET\ ratio\ change = \frac{\Delta R}{R} = \frac{R_{Ca2+saturated} - R_{Ca2+free}}{R_{Ca2+free}}$$

2.3.5 Determination of the Ca^{2+} affinity of a Ca^{2+} FRET Indicator

The Ca^{2+} affinity of a Ca^{2+} indicator was determined using a titration kit based on a method published by Roger Tsien (Tsien & Pozzan, 1989), and a Cary Eclipse fluorescence spectrometer. A Ca^{2+} free solution and a high Ca^{2+} solution (containing 39.8 µM Ca^{2+}) were prepared, both comprising the same amount of protein. Emission spectra for the protein were recorded in the Ca^{2+} free solution and also following successive replacement of Ca^{2+} free solution with high Ca^{2+} solution (titration steps depicted in **Table 14**). K_d values were determined by plotting the $\log_{10}$ values of the [Ca^{2+}] free concentrations in mol/l against the corresponding ΔR values (normalized to ΔR at 39.8 µM Ca^{2+}), and fitting a sigmoidal curve to the plot. Origin 8.1 was used for data analysis.

Step	[Ca^{2+}]free	Volume to replace using a 1 mL sample @ pH = 7.2
# 1	0 µM	---
# 2	0.006 µM	40 µL
# 3	0.013 µM	40 µL
# 4	0.020 µM	40 µL
# 5	0.027 µM	40 µL
# 6	0.035 µM	40 µL
# 7	0.065 µM	112 µL
# 8	0.100 µM	143 µL
# 9	0.225 µM	333 µL
# 10	0.351 µM	250 µL
# 11	0.602 µM	333 µL
# 12	0.853 µM	250 µL
# 13	1.35 µM	333 µL
# 14	1.73 µM	200 µL

Step	$[Ca^{2+}]$free	Volume to replace using a 1 mL sample @ pH = 7.2
# 15	2.85 µM	375 µL
# 16	4.87 µM	400 µL
# 17	7.37 µM	333 µL
# 18	14.9 µM	500 µL
# 19	29.9 µM	500 µL
# 20	39.8 µM	1000 µL

Table 14: Ca^{2+} Titration Steps

2.3.6 Determination of the Kinetics of a Ca^{2+} FRET Indicator (Stopped-Flow Measurement)

The kinetics of an indicator (K_{on} and K_{off}), were measured using an RX2000 rapid mixing stopped-flow unit, in combination with an RX pneumatic drive and a Cary Eclipse fluorescence spectrometer. A Ca^{2+} saturated indicator solution (pH 7.5) and a Ca^{2+} chelating solution (pH 7.5, with BAPTA as a Ca^{2+} chelator) were prepared. Cary Eclipse kinetics software was used to excite the sensor at the donor maximum and alternately record the emission of the donor and the FRET channel at their respective maxima. The saturated buffer and chelating buffer were mixed with an injection pressure of 3.5 bar. Five to six measurements per channel were recorded and their respective means were used to calculate the FRET-donor ratio, which was then plotted. The decay time of a sensor was determined by fitting a single- or double-exponential curve to the ratio curve. Origin 8.1 was used for data analysis.

2.4 Bacterial Plate Screening

2.4.1 Library Generation and Preparation of Screening Plates

DNA libraries of Ca^{2+} FRET indicators were generated via three different strategies:

1. Error prone PCR was used to identify prosperous sites for mutations in fluorescent proteins or indicators.
2. Site-directed mutagenesis was utilized to introduce specific or random mutations at prosperous sites.

3. Random linkers were introduced between fluorescent proteins and Ca^{2+} binding sites to increase the distance between the two chromophores and change their orientation to one-another.

XL1 blue cells were transformed with a DNA library, evenly spread on an agar plate and incubated at 37°C for approximately 16-18 hours. They were then incubated at room temperature for several hours to allow the proteins to further maturate. Libraries of fluorescent proteins were then screened to evaluate time to maturation. Libraries of indicators on the other hand, were stored at 4°C overnight and screened the following day. Ideally, plates consisted of approximately 500 to 800 bacterial colonies, each containing a different type of fluorescent protein or indicator.

It often proved beneficial to blot the colonies on a circular piece of blotting paper (especially when the performance of a sensor was to be evaluated) and screen them on/pick them off the paper directly. For this purpose, the blotting paper (Whatman, 0.34 mm) was soaked in MOPS buffer (-screening, pH 7.5) and carefully pressed against the agar plate, where the colonies readily adhered to it.

Polyethylene spray bottles (Rotert, Germany), with a total volume of 30 ml and a volume per spray of 0.15 +/- 0.05 ml were used to apply solutions to the bacterial colonies. Alternatively, spray guns (JetStream I, K350, HVLP) powered by pressurized air (2 bar) were utilized, with laser pointers attached to facilitate aiming.

2.4.2 Screening of Fluorescent Proteins

Fluorescent proteins were screened in *E.coli* to evaluate time to maturation, brightness, and the degree of cross excitation from potential FRET donors. Plates were screened within 20-24 hours after transformation to identify variants which matured quickly. Increased brightness could be examined using either a Leica M205 FA fluorescence stereomicroscope, or a CoolSNAP ES2 CCD camera with a Lambda LS/30 Stand-Alone Xenon Arc Lamp (Sutter Instrument) and a Lambda 10-2 optical filter changer (Sutter Instrument) which controlled the filter wheel.

A custom python program (written by Christopher Zarbock) was used to process large quantities of colonies and measure their brightness and excitation profile against a reference. This reference was imaged alongside each plate, allowing the program to identify superior variants. The extent of cross excitation from potential donors could be tested by exciting the colonies at the donors' excitation maximum. The program identified colonies, which were less excitable at these wavelengths than the reference.

2.4.3 Screening of Ca^{2+} FRET Indicators

Ca^{2+} FRET indicators were screened in *E.coli* to assess starting ratios (R_0) and ratio changes ($\Delta R/R$). A custom python program (written by David Ng, see appendix 6.1) was used to operate the camera and all accompanying devices, identify the colonies and to record and analyze the data. Maximal emission was recorded for both donor and FRET channel.

At the beginning of each experiment, a baseline of five pictures was recorded in 15 second intervals. The colonies were then sprayed with MOPS buffer (-screening, pH 7.5), containing ionomycin and poly-L-lysine (50 µg/ml each), to penetrate the bacterial cell walls. During a five minute incubation period, 25 pictures were taken in 15 second intervals. Thereafter, MOPS 100 mM Ca^{2+} buffer (-screening, pH 7.5) was applied. In functional sensors, an increase in FRET could then be observed within milliseconds. A further 25 pictures were taken, again in 15 second intervals. Upon completion, the program analyzed the R_0 and $\Delta R/R$ of each sensor, and identified the 10 colonies exhibiting the highest $\Delta R/R$ values. R_0 values were also taken into account, albeit to a lesser extent (see chapters 3.1.6 and 3.1.7). The experimenter was presented with three plots showing the single traces of the best performing colonies, a landscape of all sensors on the plate based on their $\Delta R/R$ and R_0, and a scheme of the plate highlighting the positions of the best performers. These colonies were subsequently picked and cultured for further analysis.

2.5 Cellular Biology

2.5.1 Thawing and Handling of HEK Cells

HEK cells from a stock maintained at -80°C were rapidly thawed in a water bath set to 37°C. They were then transferred to a Falcon tube containing 5 ml of pre-warmed DMEM (Dulbecco's Modified Eagle's Medium), supplemented with 10 % FCS (Fetal calf serum) and 1 % Pen/Strep. Subsequently, cells were spun down at 2000 x g for 5 minutes at 4°C, the supernatant was then discarded and the pellet resolved in 10 ml medium. Cells were cultivated at 37°C with 5 % CO_2.

HEK cells were split at a ratio of 1:10 twice a week. For this purpose, the old medium was removed and cells were carefully rinsed in PBS. They were then incubated in 1 ml of trypsin for three minutes, facilitating their detachment from the surface of the dish. Thereafter, 9 ml of DMEM was added, and clusters of cells were separated from one another by gently pipetting them up and down several times. 1 ml of the cell bearing solution was then added to 9 ml of fresh DMEM in a new dish.

2.5.2 Transfection of Cell Cultures

Genes encoding sensors were subcloned into the vector pcDNA3. HEK cells were transfected via the Ca^{2+} phosphate transfection method, in which Ca^{2+} phosphate precipitates with the DNA. The precipitate then attaches to the cell surface and is subsequently transported into the cell via endocytosis (Graham & Van der Eb, 1973). All substances required heating to 37°C prior to mixing (**Table 15**). The mixture was then incubated at 37°C for 20 minutes, before being added drop-wise to the cells. On the following day, the cell medium was replaced. Thereafter, cells were allowed to recover for at least one hour, before they were imaged.

	Volume per 2ml medium
H_2O	87.6 µl
DNA	1-5 µg
$CaCl_2$	12.4 µl
2x BES (add while vortexing)	100 µl
total volume	200 µl

Table 15: Ca^{2+} Phosphate Transfection

Cells were imaged in Hank's Balanced Salt Solution (HBSS 10x, calcium, magnesium, no phenol red). 0.625 nM of ionomycin was added to induce Ca^{2+} transport into the cells.

2.6 Imaging Setups

2.6.1 Set-up for Bacterial Plate Screening

Bacterial cells were mounted on a movable stage and imaged with a CoolSNAP ES2 CCD camera. A Lambda LS/30 Stand Alone Xenon Arc Lamp (Sutter Instrument) was used as a light source. Light was transmitted through a liquid light guide. Emission and excitation filters, as well as shutters, were controlled by a Lambda 10-2 optical filter changer (Sutter Instrument) (**Figure 15**). A complete list of filters utilized can be found in **Table 16**.

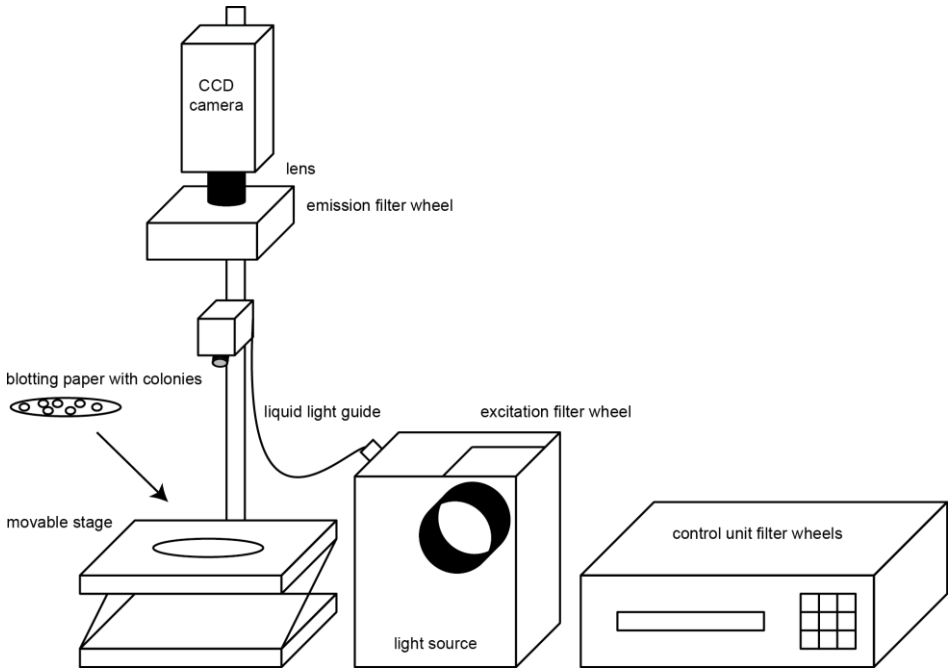

Figure 15: Scheme of the Set-up for Bacterial Plate Screening
Screening set-up consisting of two filter wheels, a CCD camera, a lens and a movable stage for the blotting paper containing the bacteria.

Excitation			
Wheel Position	**Filter (wavelengths in nm)**	**Chroma Ordering**	**Application (examples)**
1	HQ 575/ 50	41043	DsRed, mCherry
2	HQ 546/ 12	41003	mKO2
3	HQ 500/ 20	41028	mCitrine
4	HQ 470/ 40	41017	EGFP
5	D 436/ 40	31044v2	ECFP, Cerulean
6	D 395/ 40	31043	tSapphire

Emission			
Wheel Position	**Filter (wavelengths in nm)**	**Chroma Ordering**	**Application (examples)**
1	HQ 640/ 50	41043	DsRed, mCherry
2	HQ 585/ 40 (blocked from 400 to 500 nm)	41003	mKO2
3	HQ 535/ 30	41028	mCitrine
4	HQ 525/ 50	41017	EGFP
5	D 480/ 40	31044v2	ECFP, Cerulean
6	D 510/ 40	31043	tSapphire

Table 16: Excitation and Emission Filters for Bacterial Plate Screening and HEK Cell Imaging

2.6.2 Imaging Setup for Mammalian Cells

HEK cells were imaged in 35 mm glass bottom dishes with 14 mm microwells and a coverglass thickness of 0.085-0.13, coated with poly-L-lysine. An Axiovert 35 inverted fluorescence microscope (Zeiss) was used in combination with a CoolSNAP ES2 CCD camera (Roper Scientific) and a Fluar 40x/ 1.30 oil objective (Zeiss). A complete list of filters utilized can be found in **Table 16**.

2.7 Material

2.7.1 Instruments

Name	Supplier
Axiovert 35 inverted fluorescence microscope	Zeiss
Cary Eclipse fluorescence spectrometer	Varian
Cary Eclipse software (1.1(132))	Varian
Cell profiler cell image analysis software (v.10415)	Broad Institute
CoolSNAP ES2 CCD camera	Roper Scientific
Fiji	(Schindelin et al., 2012)
FlexCycler^2	Analytic Jena
Gel Doc 2000	BioRad
Heracell 240 CO_2 incubator	Thermo Scientific
Infinite® M200 PRO (3.4.2.0)	Tecan
JetStream I K350 spray gun HVLP	Victor Air Tool Co.Ltd.
Lambda 10-2 optical filter changer	Sutter Instrument
Lambda LS/30 stand-alone xenon arc lamp	Sutter Instrument
Leica M205 FA fluorescence stereomicroscope	Leica Microsystems
MagRack 6 magnetic rack	GE Healthcare
Matlab	MathWorks
Metafluor (7.7.0.0)	Meta Imaging Series
NanoDrop 1000 spectrometer	Thermo Scientific
Origin 8.1 Software (v8.1.34.90)	OriginLab Corporation
Polyethylene spray bottles	Rotert
Python 2.7	Python

Name	Supplier
Quantity One software	BioRad
RX2000 rapid mixing stopped-flow unit	Applied Photophysics
RX pneumatic drive	Applied Photophysics
SIGMA 3K30 centrifuge	SciQuip
RC-5B refrigerated superspeed centrifuge	Sorvall

2.7.2 Consumeables

Name	Supplier
Antarctic phosphatase	New England Biolabs
6 % CL-Nickel ChroMatrix™	Jena Bioscience
DMEM + GlutaMAX™-I	Life Technologies
DNA ladders (100bp, 1kb)	New England Biolabs
Error-Prone Kit	Jena Bioscience
Glass bottom dishes 35mm, 14mm microwell, glass thickness 0.085 - 0.13mm	MatTek Corporation
Hank's Balanced Salt Solution (HBSS), $+Ca^{2+}$, $+, Mg^{2+}$	Life Technologies
Herculase II Fusion Enzyme with dNTP Combo	Agilent Technologies
His Mag Sepharose Ni magnetic beads	GE Healthcare
NucleoSpin®Gel and PCR Clean-up	Machery-Nagel
Pierce™ BCA Protein Assay Kit	Thermo Scientific
Polypropylene Columns	Qiagen
Precision Plus Protein™ Kaleidoscope™	Bio Rad
PureYield™ Plasmid Midiprep System	Promega
QIAquick Gel Extraction Kit	Qiagen
QIAquick PCR Purification Kit	Qiagen
QIAprep Spin Miniprep Kit	Qiagen
Quick Start™ Bradford Protein Assay	Bio Rad
Restriction Enzymes (BamHI, DpnI, EcoRI, EcoRV, NotI, SacI, SphI)	New England Biolabs
T4 DNA ligase	New England Biolabs
Whatman Gel Blotting Papiere, 0.34 mm	Roth

2.7.3 Chemicals

Name	Supplier
Acetic acid (glacial)	Sigma
Acrylamide/ Bis solution 30%	Serva
Agar LB	Invitrogen
Agarose	Biomol
Ammonium persulfate	Bio Rad
Ampicillin sodium salt	Roth
Anhydrotetracycline hydrochloride	Sigma
L-(+)-Arabinose	Sigma
BAPTA	Invitrogen
BES (N,N-Bis-(2-hydroxyethyl)-2-amino-ethanesulfonic acid)	Roth
Boric acid	Merck
Calcium chloride, dihydrate	Sigma
Citric acid	Sigma
DMEM (Dulbecco's Modified Eagle's Medium)	Life Technologie
DMSO (Dimethylsulfoxid)	Roth
Desoxyribonuclease	Sigma
Doxycycline	Clontech
EDTA (Ethylene diamine tetraacetic acid)	Merck
EGTA (Ethylene glycol tetraacetic acid)	Sigma
Ethidium bromide	Roth
Fetal bovine serum	Life Technologies
D-(+)-Glucose	Roth
Glycerine	Roth
Hydrochloric acid	Merck
Imidazole	Merck
Ionomycin	Merck
IPTG (Isopropyl β-D-1-thiogalactopyranoside)	Roth
Kanamycine	Roth
Lactose monohydrate	Roth
LB broth	Invitrogen

Name	Supplier
Leupeptin hydrochloride	Sigma
Lysozyme	Sigma
Magnesium chloride hexahydrate	Merck
Methylglyoxal	Sigma
MOPS	Merck
Orange G	Sigma
Penicillin/ Streptomycin	Life Technology
Pepstatin A	Sigma
PMSF (Phenylmethylsulfonylfluoride)	Sigma
Poly-L-Lysine hydrobromide	Sigma
Potassium chloride	Roth
Potassium dihydrogen phosphate	Merck
Ribonuclease	Sigma
Sodium chloride	Sigma
Sodium hydroxide	VWR BDH Prolabo
Sodium phosphate monobasic	Sigma
Streptomycin	Sigma
TEMED (Tetramethylethylenediamine)	Bio Rad
Trizma base	Sigma
TritonX	Roth
Tetracycline	Fluka
Trypsin	Sigma
Yeast extract	Sigma
2X YT microbial medium	Sigma

2.7.4 Buffers and Solutions

Name	Components
Autoinductive LB medium	LB medium + 0.6 % glycerol (v/v) + 0.2 % lactose (w/v) + 0.05 % glucose (w/v)
BAPTA Ca^{2+} chelating solution (pH 7.5) (stopped flow measurements)	10 mM MOPS 50 mM KCl 20 mM BAPTA
BES buffer (cell transfection)	50 mM BES 280 mM NaCl 1.5 mM Na_2HPO_4
Borate buffer (pH 8.4)	Boric acid KCl
CaEGTA solution (Ca^{2+} titration)	10 mM K_2CaEGTA 1 mM $MgCl_2$ MOPS buffer - Ca^{2+} titrations pH 7.2
Ca^{2+} saturated indicator solution (pH 7.5) (stopped flow measurements)	10 mM MOPS 4 mM $CaCl_2$ 2 mM $MgCl_2$ 50 mM KCl 0.2 – 1 µM indicator
DMEM, 10 % FCS, 1% Pen/Strep	500 ml DMEM 50 ml FCS, heat-inactivated 5 ml Pen/Strep
DNA loading buffer – 10 x Orange G (pH 7.5)	10 mM EDTA 100 mM Tris 50 % glycerol (w/v) 1 % Orange G (w/v)
K_2EGTA solution (Ca^{2+} titration)	10 mM K_2EGTA 1.5549 mM $MgCl_2$ MOPS buffer - Ca^{2+} titrations pH 7.2
LB agar	LB medium + 15 g/l agar + 50 µg/ml ampicillin

Name	Components
LB medium	20 g/l LB
MOPS buffer - Ca^{2+} titrations (pH 7.2)	30 mM MOPS 100 mM KCl
MOPS buffer - fluorescence spectroscopy (pH 7.5)	30 mM MOPS 100 mM KCl 100 µM EDTA 100 µM EGTA
MOPS buffer - screening (pH 7.5)	30 mM MOPS 100 mM KCl
MOPS 100 mM Ca^{2+} buffer -screening (pH 7.5)	+ 100 mM Ca^{2+}
10x Native PAGE running buffer	250 mM Tris base 1.92 M Glycin H_2O to 1L
PBS (pH 7.4)	137 mM NaCl 2.7 mM KCl 10 mM N_2HPO_4 x 2 H_2O 2 mM KH_2PO_4
Poly - L - Lysine	1 mg/ml in borate buffer (pH 8.4)
Protein resuspension buffer (pH 7.8)	20 mM Na_2HPO_4 300 mM NaCl 20 mM imidazol
Protein elution buffer (pH 7.8)	20 mM Na_2HPO_4 300 mM NaCl 250 mM imidazol 10 % Glycerol
50x TAE (pH 8.0)	2 M Trizma Base 57 ml/l acetic acid (glacial) 50 mM ETDA
TSS buffer for competent cells (pH 6.5)	1 % trypton (w/v) 0.5 % yeast extract (w/v) 100 mM NaCl 10 % PEG (w/v) 5 % DMSO (v/v)

Name	Components
	50 mM $MgCl_2$

2.7.5 Plasmids

Name	Supplier
pRSETB	Invitrogen life technologies
pcDNA3	Invitrogen life technologies
pRSFDuet-1	Novagen

2.7.6 Bacterial strains, cell lines

Name	Supplier
XL1 blue	Invitrogen
BL21 gold	Invitrogen
JM109	Promega
PPY	(Zhang et al., 2012)
HEK 293T	ATCC

3 Results

3.1 Establishment of a New Ca^{2+} Sensor Screening Assay

3.1.1 Choice of a Bacterial Strain

The *E.coli* strains BL21 gold, XL1 blue and JM109 were tested for their suitability in the screening assay. BL21 gold is a protein expression strain, and was therefore considered the most logical choice, since XL1 blue and JM109 are more commonly applied in cloning. JM109 was eliminated as an option at an early stage, due to the fact that the cells expressed only a minor amount of protein. Moreover, they seemed to be highly sensitive to any treatment necessary for the screening procedure, apparent from the fact that colonies consistently appeared blurry following experiments, whereas BL21 and XL1 displayed superior robustness.

BL21 exhibited a transformation efficiency which under given conditions, was 5000 times lower than that of XL1. **Figure 16A** shows a plate of BL21 cells transformed with 300 ng of sensor DNA, ultimately resulting in 312 colonies. **Figure 16B** depicts a plate of XL1blue cells transformed with 0.1 ng of the same DNA, resulting this time in 558 colonies. BL21 colonies not only grew faster compared to XL1 colonies, they also reached a greater size, and most notably, exhibited a significantly higher fluorescence intensity (**Figure 16A - C**). Sensors expressed in BL21 did however, produce a comparatively low $\Delta R/R$ in response to Ca^{2+} application. Expressed in XL1 on the other hand, the same sensors exhibited a more distinct Ca^{2+} response (**Figure 16D**). Together with its superior transformation efficiency, this made XL1 blue the most suitable choice for this particular screening assay.

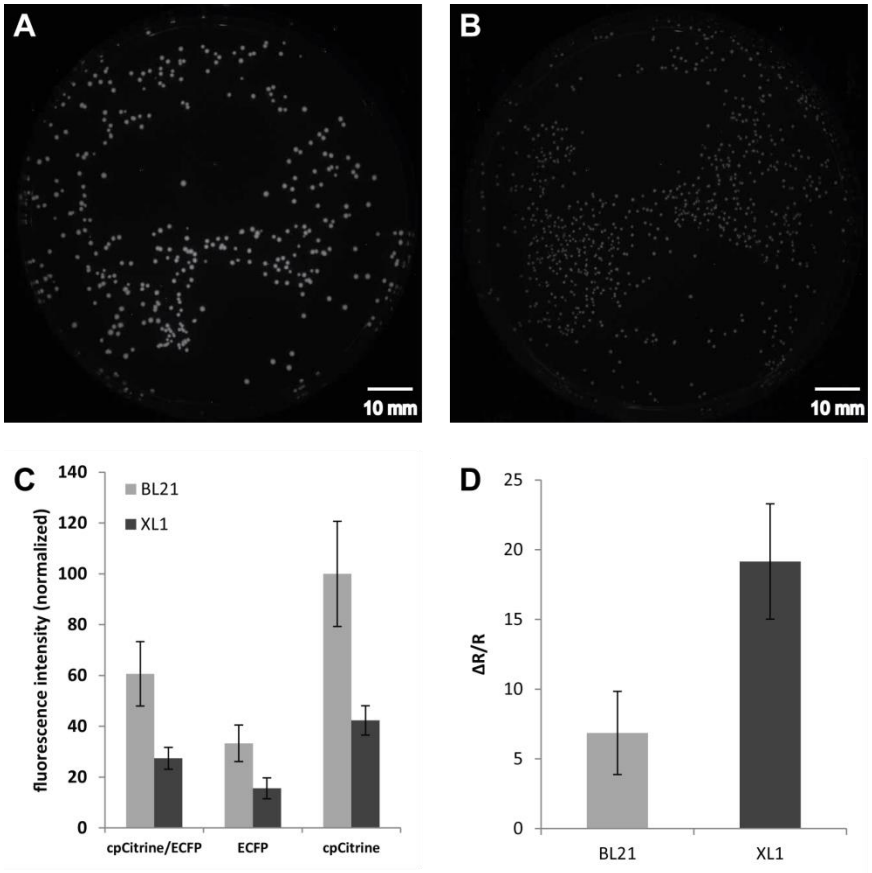

Figure 16: Comparison of Bacterial Strains Considered for Screening
Agar plates containing colonies of BL21 gold **(A)** and XL1 blue cells **(B)** expressing the same sensor, excited under the same conditions (exposure time 4 s, gain 2 x, binning 1). Mean fluorescence intensities of BL21 gold (n = 312) and XL1 blue cells (n = 558), transformed with the FRET sensor TN-XXL (normalized to the mean fluorescence of cpCitrine in BL21). Error bars indicate SD **(C)**. Mean ΔR/R ± SD of BL21 gold (n = 19) and XL1 blue cells (n = 15) transformed with TN-XXL, pre-treated with 50 µg/ml polylysine, 50 µg/ml ionomycin and then sprayed with 100 mM Ca^{2+} **(D)**.

3.1.2 Determination of Optimal Duration for Incubation and Point in Time for Screening

Following transformation, numerous intervals were tested to identify the most suitable duration for incubation and the optimal time to conduct screening. Plates of BL21 cells were transformed with the single fluorophore Ca^{2+} sensor GCaMP3, and incubated at 37°C for 15 to 20 hours, before being imaged. One plate was incubated for 20 hours and then stored at 4°C for one week before it was imaged.
It was observed that colonies continued to become brighter up to 15-17 hours after transformation and remained fairly stable afterwards (depicted as initial sensor brightness F_0 in **Figure 17A**). The change in

fluorescence ΔF/F upon Ca^{2+} application on the other hand, continued to increase for up to 20 hours after transformation (**Figure 17B**), indicating that until then, not all sensors were fully functional. At that point, however, nonresistant satellite colonies began to grow around the main colonies (**Figure 17D**). After one week, the mean F_0 had further increased, but was accompanied by a greater variability between single colonies. The mean ΔF/F value exhibited a decrease, implying that sensors had already started to degrade in the dying bacteria. Furthermore, the shape of the Ca^{2+} response curve over time (**Figure 17C**) had changed from a continuous increase of fluorescence intensity (upon Ca^{2+} application) over several minutes, to a rapid increase, followed immediately by a slow decrease. This could indicate that the bacteria had entered a different growth phase, allowing them to adapt to the incoming Ca^{2+} more quickly. On the basis of these results, it was decided to transfer the plates to room temperature after ~16-18 hours of incubation at 37°C, to suppress the development of satellite colonies. The sensors were allowed to maturate for approximately 5 more hours at room temperature, before the plates were stored at 4°C overnight. Imaging was conducted on the following day when most sensors were anticipated to be fully matured, yet degradation was minimal.

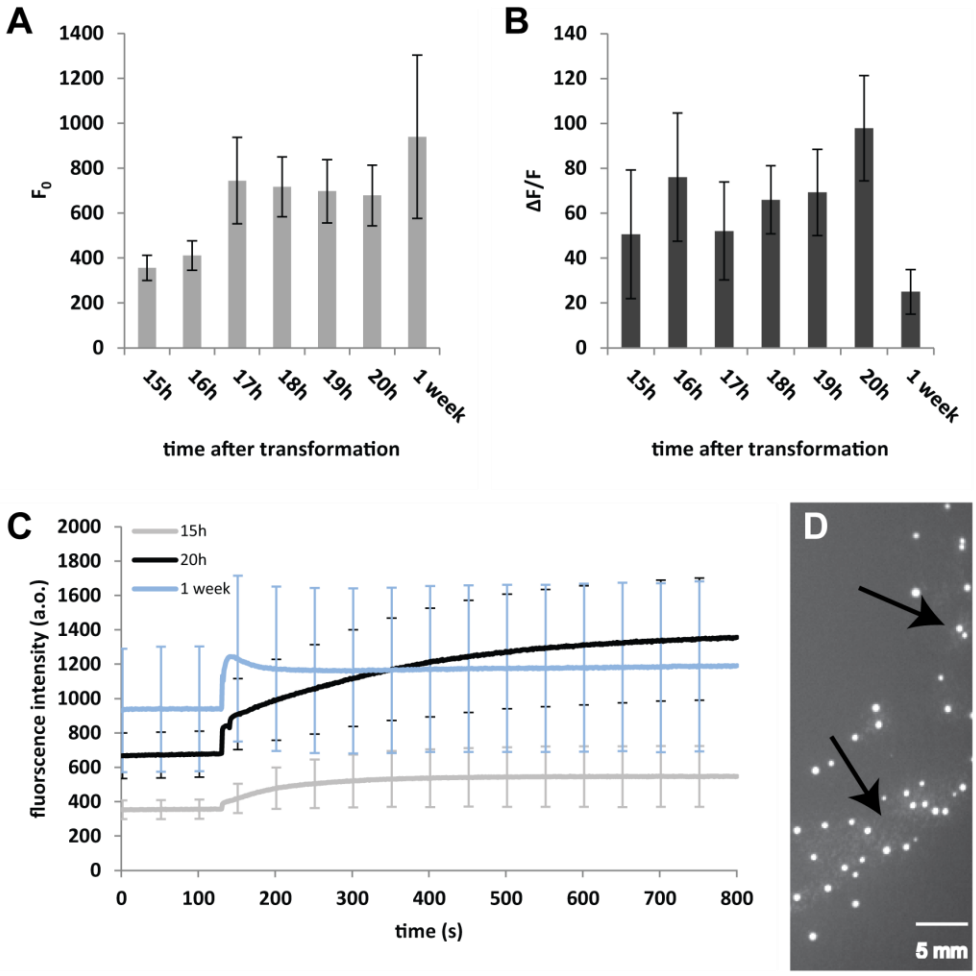

Figure 17: Duration of Incubation and Point in Time for Screening
Starting fluorescence intensities F_0 ± SD (prior to any treatment) **(A)** and fluorescence intensity changes ΔF/F ± SD upon Ca^{2+} application **(B)** at different points in time after transformation of BL21 colonies with the single fluorophore Ca^{2+} sensor GCaMP3. Fluorescence intensities over time for selected points in time after transformation. Error bars indicate SD **(C)**. Satellite colonies around main colonies **(D).** (n_{15h} = 43 colonies, n_{16h} = 151, n_{17h} = 41, n_{18h} = 61, n_{19h} = 99, n_{20h} = 105, n_{1week} = 222)

3.1.3 Background: Screening on Agar Plates and Blotting Paper

The suitability of agar plates and blotting paper for imaging experiments was compared. Firstly, the auto-fluorescence of agar plates and filter paper was measured and it was observed that agar plates exhibited a notably higher auto-fluorescence in all excitation and emission settings tested, namely CFP, YFP and FRET (excitation at the CFP maximum and emission at the YFP maximum) (**Figure 18A**). This however, did not interfere with the measured intensities of the colonies, with R_0 values of TN-XXL measured on both agar plates and blotting paper proving relatively similar (**Figure 18B**). When sprayed with Ca^{2+} however,

colonies blotted onto paper exhibited a significantly larger ΔR/R than those directly measured on plates (**Figure 18C**). This indicated that the Ca^{2+} solution was able to penetrate the colonies more effectively when it was introduced not only from above, but also underneath, since the blotting paper was soaked in solution. In addition, colonies were probably more loosely associated after the blotting process, making them more receptive to the infiltrating solution.

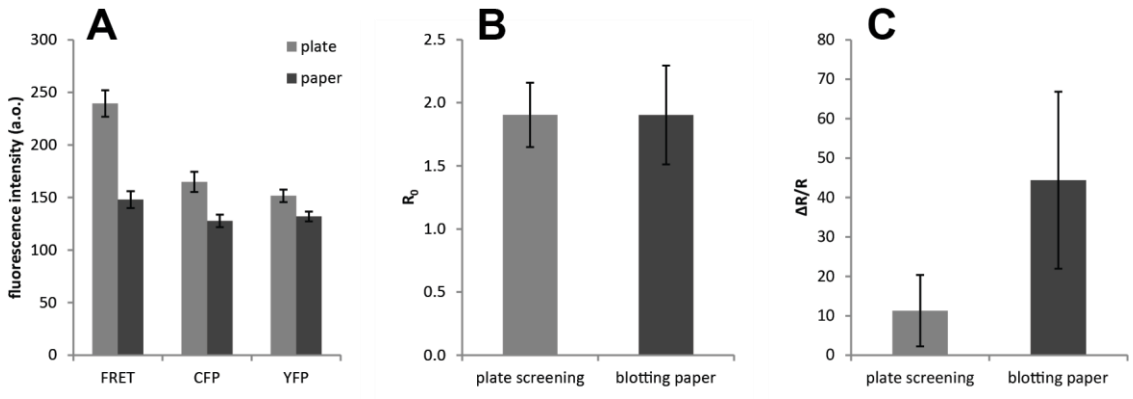

Figure 18: Screening on Agar Plates and Blotting Paper
Autofluorescence of an agar plate and a piece of blotting paper. SD values are displayed **(A)**. Starting ratios R_0 ± SD **(B)** and ratio changes ΔR/R ± SD upon Ca^{2+} application **(C)** of XL1 blue cells transformed with TN-XXL, imaged on an agar plate or on blotting paper. (n_{plate} = 149 colonies, $n_{blotting\ paper}$ = 90 colonies)

3.1.4 Attempts to Increase Ca^{2+} in the Cytoplasm of *E.coli*

3.1.4.1 Application of Extracellular Ca^{2+} (Exclusively)

It was observed that applying Ca^{2+} (e.g. 100 mM) extracellularly onto a plate of BL21 cells transformed with a Ca^{2+} sensor like TN-XXL (**Figure 19A**) or GCaMP3 (**Figure 19B**) induced a small change in the fluorescence of this sensor. This observation indicated that at least some Ca^{2+} was able to overcome the double membrane of the bacterial cells and reach the cytoplasma, where the sensor was expressed, despite *E.coli*'s known ability to control its internal Ca^{2+} levels quite effectively (Gangola & Rosen, 1987). Nevertheless, in a sensor like TN-XXL, with an *in vitro* ratio change of approximately 300-400 %, this change in fluorescence was still barely visible. We assumed that prototype sensors to be screened on bacterial plates in the future, would display an initial ratio change lower than that of TN-XXL. It was therefore concluded that a method was required to introduce more Ca^{2+} into the cytoplasm of *E.coli*.

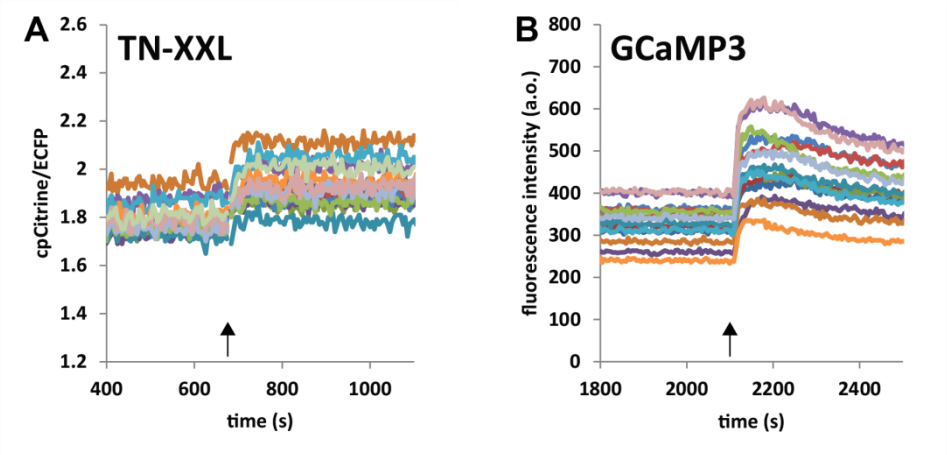

Figure 19: Application of Extracellular Ca^{2+}
Fluorescence intensity traces of individual colonies of BL21 cells transformed with TN-XXL **(A)** or GCaMP3 **(B)**. Arrows indicate at which point in time Ca^{2+} 100 mM was applied.

3.1.4.2 Freeze-thaw Cycles

Freeze-thaw cycles are a common way to break bacterial cell walls. In order to freeze the bacterial cells whilst imaging them, a small amount of liquid nitrogen was carefully poured onto an agar plate of BL21 cells expressing TN-XXL (**Figure 20**). Liquid nitrogen induced a huge and visible increase in FRET, even before the application of Ca^{2+}. Subsequently, the liquid nitrogen caused the likewise frozen agar plate to crack (either immediately or after the application of Ca^{2+}) which led to a dislocation of numerous colonies. The method was therefore abandoned.

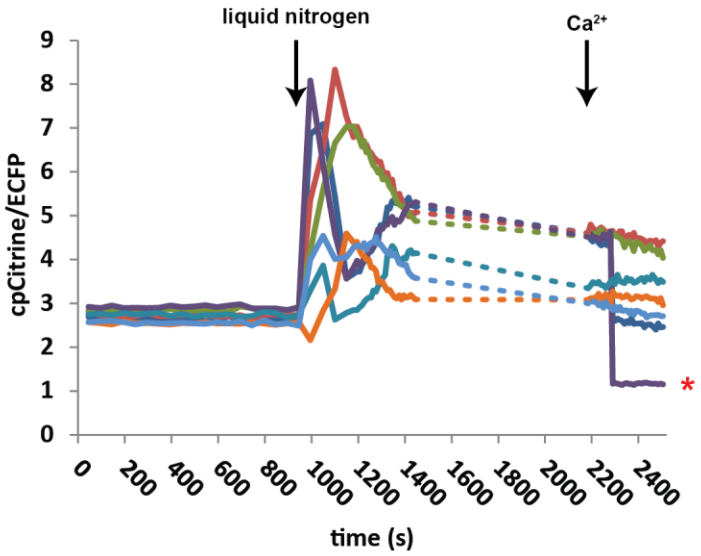

Figure 20: Treatment of *E.coli* Cells with Liquid Nitrogen
Randomly selected fluorescence intensity traces of single BL21 colonies transformed with TN-XXL, reflecting typical responses to liquid nitrogen and subsequent Ca^{2+} application. Dashed lines indicate a short pause in imaging. The red star denotes a dislocated colony.

3.1.4.3 Methylglyoxal

Methylglyoxal is a carbohydrate metabolite believed to induce Ca^{2+} transients in *E.coli* by opening Ca^{2+} channels. Campbell and colleagues tested 0.01 – 100 mM methylglyoxal in combination with 0.1 – 10 mM external Ca^{2+} on *E.coli* cells suspended in Hepes buffer. They determined cytosolic Ca^{2+} levels with aequorin, and observed increases from sub µM levels to up to 14 µM (**Figure 21A**) (A. K. Campbell et al., 2007). In an attempt to replicate this effect, 10 to 100 mM methylglyoxal and 100 mM external Ca^{2+}were applied to plates of *E.coli* cells expressing the Ca^{2+} indicator GCaMP3.

As **Figure 21B** shows, methylglyoxal failed to produce the desired effect in our experiments and actually lead to a rapid decrease in fluorescence intensity of the indicator, instead of the anticipated increase. This implies a decrease in internal Ca^{2+}, which (somewhat counterintuitively) could be attributed to methylglyoxal itself. When Campbell and colleagues investigated the effects of methylglyoxal on *E.coli*, they observed a more rapid decrease in internal Ca^{2+} in the presence of methylglyoxal. They therefore speculated that this metabolite may have activated some form of Ca^{2+} efflux mechanism, in addition to an influx (A. K. Campbell et al., 2007). Moreover, the decrease in GCaMP3 fluorescence intensity could be a sign that not only the intracellular Ca^{2+}, but also the intracellular pH had been altered, since many fluorescent proteins display significant pH sensitivity.

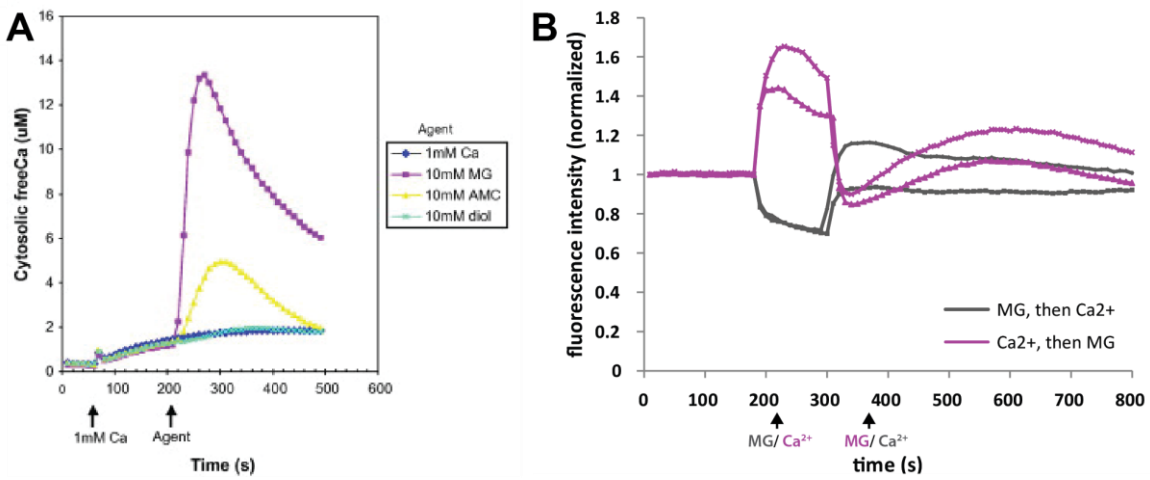

Figure 21: Treatment of *E.coli* Cells with Methylglyoxal
Rise of cytosolic Ca^{2+} following the application of external Ca^{2+} and carbohydrate metabolites, with methylglyoxal (MG) among them (A. K. Campbell et al., 2007) **(A)**. Change in fluorescence intensity of GCaMP3 expressed in the cytosol of BL21 cells, following application of methylglyoxal (10 mM) and Ca^{2+} (100 mM). Values were normalized to the respective initial fluorescence intensity **(B)**. The arrows underneath both charts indicate which substance was applied and at which point in time.

3.1.4.4 Ionomycin

Considering the outer membrane of *E.coli* is permeable to ions (Nikaido & Vaara, 1985), the ionophore ionomycin was tested as a means to transport Ca^{2+} across the inner membrane (Gangola & Rosen, 1987), which was thought to be the actual barrier. In initial tests however, ionomycin had little impact on intracellular Ca^{2+} levels, indicated by the fact that the increase in fluorescence intensity of GCaMP3 was not higher in the presence of ionomycin (**Figure 22**). It was concluded that ionomycin must have failed to cross the outer membrane and reach its point of action. Obviously, a method had to be established to make the outer membrane more permeable.

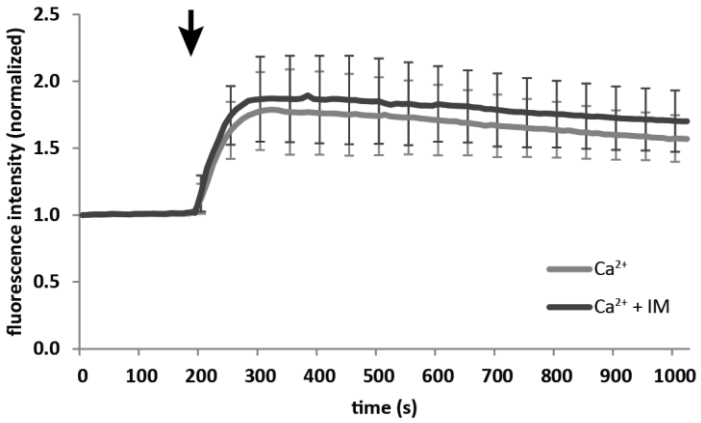

Figure 22: Treatment of *E.coli* Cells with Ionomycin
Fluorescence intensity of GCaMP3 expressed in BL21 cells. The light line represents colonies treated with 100 mM Ca^{2+}, the dark line represents colonies treated with a combination of 100 mM Ca^{2+} and 10 µM ionomycin (IM). The arrow indicates at which point the substances were applied. Values were normalized to the respective initial fluorescence intensity. (n=4 colonies each)

3.1.4.5 Ionomycin + EDTA/ Polylysine

Polycations were shown to increase the permeability of the outer membrane of gram-negative bacteria (Katsu et al., 1984). EDTA was observed to have the same effect (Leive, 1965). BL21 cells expressing a Ca^{2+} indicator were therefore treated either with polylysine or EDTA in combination of ionomycin, prior to Ca^{2+} application. The aim was to have EDTA or polylysine render the outer bacterial membrane more permeable and allow ionomycin to reach the inner bacterial membrane. It could then transport Ca^{2+} across the membrane into the cytoplasm, where the sensor was expressed (**Figure 23**).

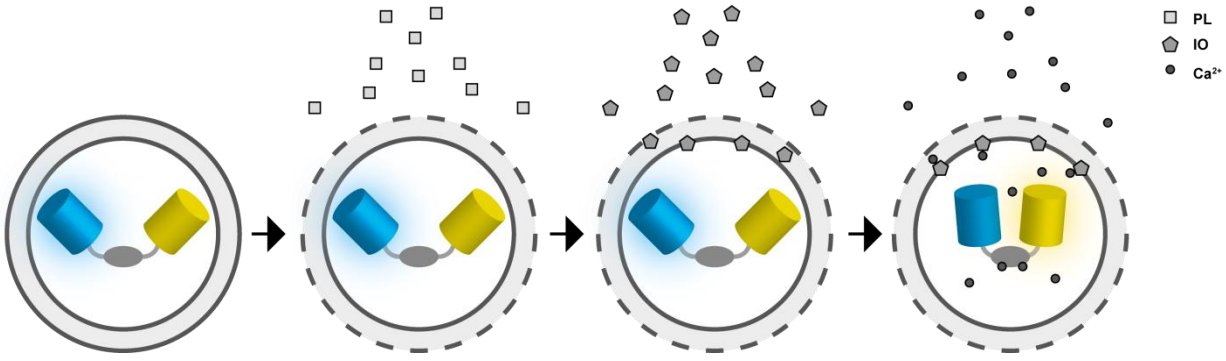

Figure 23: Presumed Cooperation between Polylysine, Ionomycin, and Ca^{2+}
Bacterial cell expressing a genetically encoded Ca^{2+} FRET sensor in its cytoplasm. Polylysine (PL) is thought to make the outer membrane more permeable to ionomycin (IO), which can then transport Ca^{2+} across the inner membrane.

The few experiments carried out with EDTA could not be quantified because the colonies on all plates tested were adversely affected by the treatment, becoming either blurry or being washed off altogether. Whether or not this was caused by EDTA itself was not investigated.

When cells were treated with polylysine and ionomycin prior to Ca^{2+} application, the intracellularly expressed Ca^{2+} sensors showed a higher change in fluorescence compared to cells which were exposed exclusively to Ca^{2+}. This observation was made for both single fluorophore and FRET sensors (**Figure 24A-D**) indicating that with this particular pretreatment, more Ca^{2+} was able to reach the cytoplasm. **Figure 24A** and **C** also reveal that the mere application of polylysine and ionomycin could also lead to a minor increase in fluorescence. A possible explanation for this phenomenon is that Ca^{2+} had accumulated in the periplasm of *E.coli* cells (Jones et al., 2002), and entered the cytoplasm the moment ionomycin came into effect.

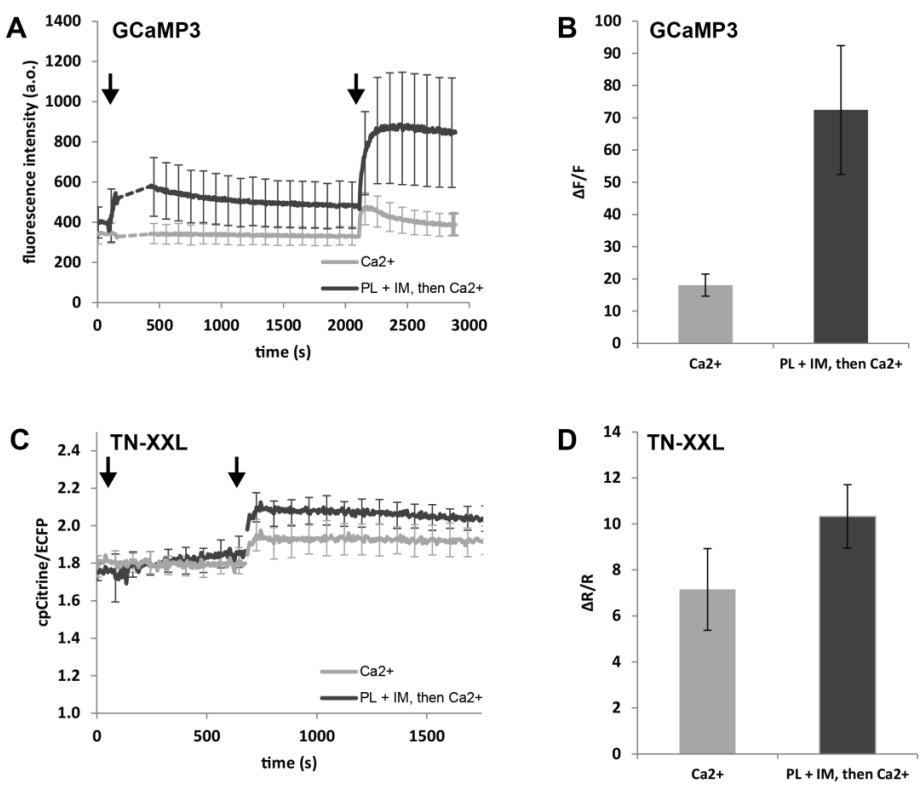

Figure 24: Treatment of *E.coli* Cells with Polylysine and Ionomycin
Average fluorescence intensity of GCaMP3 **(A)** and TN-XXL **(C)** expressed in BL21 cells, which were either subjected exclusively to 100 mM Ca^{2+}, or previously treated with 50 µg/ml polylysine (PL) and 10 µM ionomycin (IM). Arrows indicate the time at which PL + IM (only for dark traces) and Ca^{2+} (for all traces) were applied. Mean ΔF/F of GCaMP3 **(B)** and ΔR/R of TN-XXL **(D)** of pretreated and non-pretreated cells. Error bars reflect SD. $n_{GCaMP3,\ Ca2+} = 14$, $n_{GCaMP3,\ PL+IM,\ then\ Ca2+} = 21$, $n_{TN\text{-}XXL,\ Ca2+} = 15$, $n_{TN\text{-}XXL,\ PL+IM,\ then\ Ca2+} = 15$.

3.1.5 Determination of Suitable Concentrations

3.1.5.1 Polylysine and Ionomycin Concentrations

Various concentrations of polylysine and ionomycin were tested for their ability to penetrate the outer and inner membranes of *E.coli* cells. To this end, one substance was kept at a constant concentration, while the concentration of the second substance was varied. The same experiment was undertaken using both TN-XXL (**Figure 25A**, **B**) and GCaMP3 (**Figure 25C, D**). The dashed grey lines represent the immediate signal change following pretreatment with polylysine and ionomycin (light grey), and the total signal change following the application of polylysine, ionomycin and Ca^{2+} (dark grey). The black lines show the signal change attributed solely to Ca^{2+} application (total signal change minus pretreatment signal change). As can be seen in **Figure 25A** and **C**, a manipulation of the polylysine concentration had little impact on the brightness/FRET of the sensors upon Ca^{2+} application. Following treatment with ≤ 100 µg/ml of polylysine however, an immediate increase in brightness or FRET was observed. Katsu and colleagues (Katsu et al., 1984) observed that polycations such as polylysine replaced divalent cations (including Ca^{2+}) in the outer membrane, thereby setting them free. Accordingly, a possible explanation may be that higher concentrations of polylysine set more Ca^{2+} free, inducing a premature signal change in the sensors before Ca^{2+} was applied externally. Since this is pure speculation however, a concentration of 50 µg/ml of polylysine was selected for future experiments, to avoid the occurrence of this phenomenon. **Figure 25B** and **D** show that an increase from 10 µM ionomycin used in previous experiments (see chapters 3.1.4.4 and 3.1.4.5) to 50 µM, resulted in a much higher signal change following Ca^{2+} application, whereas a further increase to 100 µM had no such effect. Therefore, 50 µM ionomycin was chosen as the optimal concentration and subsequently used in further experiments.

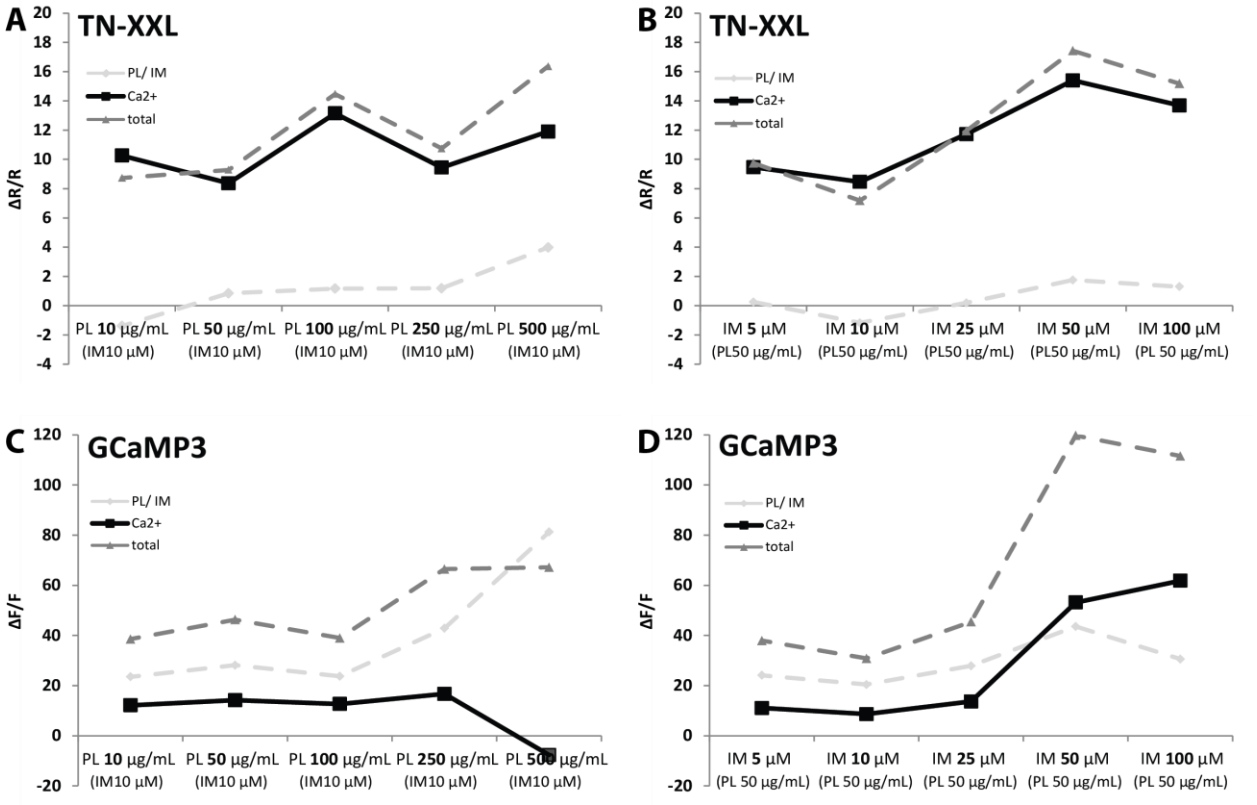

Figure 25: Determination of Suitable Polylysine and Ionomycin Concentrations
ΔR/R of TN-XXL **(A)**, **(B)** and ΔF/F of GCaMP3 **(C)**, **(D)** expressed in BL21 cells treated with different concentrations of polylysine (PL) **(A)**, **(C)** and ionomycin (IM) **(B)**, **(D)** and 100 mM Ca^{2+}. The dashed lines represent immediate reactions to the polylysine and ionomycin pretreatment (light grey) and the total signal changes following the application of polylysine, ionomycin and Ca^{2+} (dark grey), whereas the black lines show the changes attributed solely to Ca^{2+} application (total signal change minus pretreatment signal change). (n = 2 colonies per sensor and concentration)

3.1.5.2 Extracellular Ca^{2+} Concentration

Similarly, a number of Ca^{2+} concentrations were tested for their potential to induce the highest possible signal change in the intracellularly expressed sensors, whilst avoiding side effects. Four concentrations ranging from 1 mM to 1 M were tested on a FRET sensor expressed in XL1 blue cells. As **Figure 26A** shows, ΔR/R increased as a result of rising Ca^{2+} concentrations.

To ensure that the observed ΔR/R values actually reflected an increase of FRET, the single wavelength recordings of the sensor were examined, namely FRET (cpCitrine emission at ECFP excitation), ECFP and cpCitrine (directly excited). The anticipated result was an increase in FRET (since photons were transferred from the excited ECFP to the non-excited cpCitrine), a decrease in ECFP, and that cpCitrine remained

unchanged when directly excited. At 1 M Ca^{2+} (**Figure 26C**) however, a considerable increase in cpCitrine brightness was observed, distorting the FRET signal. Because this change in cpCitrine brightness could not be attributed to FRET, it is likely that such high concentrations of Ca^{2+} caused a drastic change in intracellular pH, thereby increasing the brightness of the pH sensitive cpCitrine. As this effect did not occur with 100 mM Ca^{2+} (**Figure 26B**), yet induced ratio changes remained high, this concentration was chosen for future experiments.

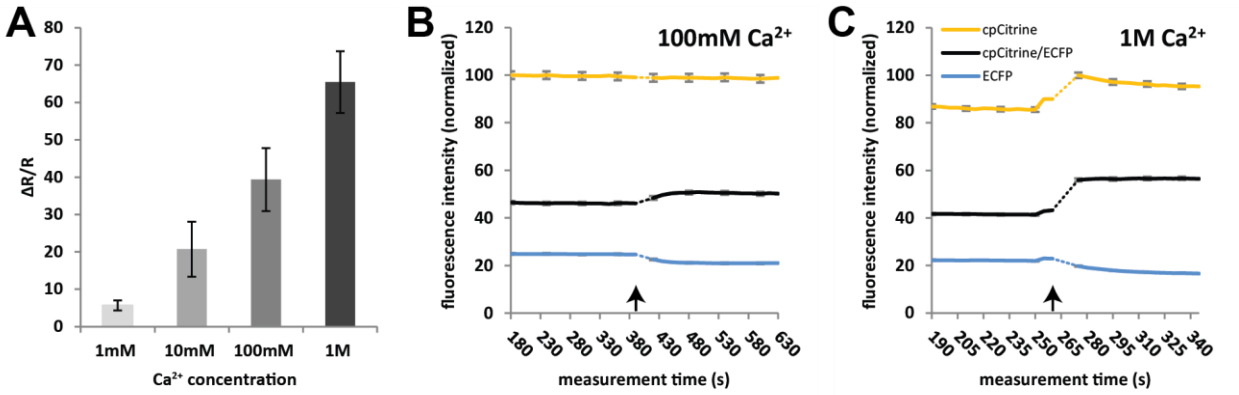

Figure 26: Determination of a Suitable Extracellular Ca^{2+} Concentration
ΔR/R ± SD of a FRET sensor expressed in XL1 blue cells, induced by different concentrations of applied Ca^{2+} (n = 6 colonies per concentration) **(A)**. Single wavelength recordings of colonies of XL1 blue cells transformed with TN-XXL. Arrows indicate the point at which bacterial plates were sprayed with 100 mM Ca^{2+} (n = 197 colonies) **(B)** and 1 M Ca^{2+} (n = 222 colonies) **(C)**. SE values are displayed in gray. Values in (B) and (C) are depicted relative to the maximum of cpCitrine. All cells were treated with polylysine and ionomycin prior to the experiment.

3.1.6 Selection Criteria

In our bacterial based screening assay for new FRET sensors, we were interested in two characteristics; high ΔR/R, and low R_0 (in theory allowing for higher signal changes). For the first three rounds of screening, sensors were grouped into three categories: Lowest R_0, highest ΔR/R and sensors ranking high in both categories (**Figure 27**). Up to 10 candidates per plate were picked for each category. The screening criteria were later changed however, because the sensors exhibiting the lowest R_0 mostly turned out to be either non-functional (e.g. containing a stop-codon) or imaging artefacts. In addition, many sensors which ranked relatively high in both categories were found to have rather average properties overall. As a result, it was decided to screen for high ΔR/R, with R_0 values only taken into account to a lesser extent.

A Matlab program (developed with, and written by Elisabeth Hopp and Christopher Zarbock) was used to analyze the data gained from the first few rounds of screening.

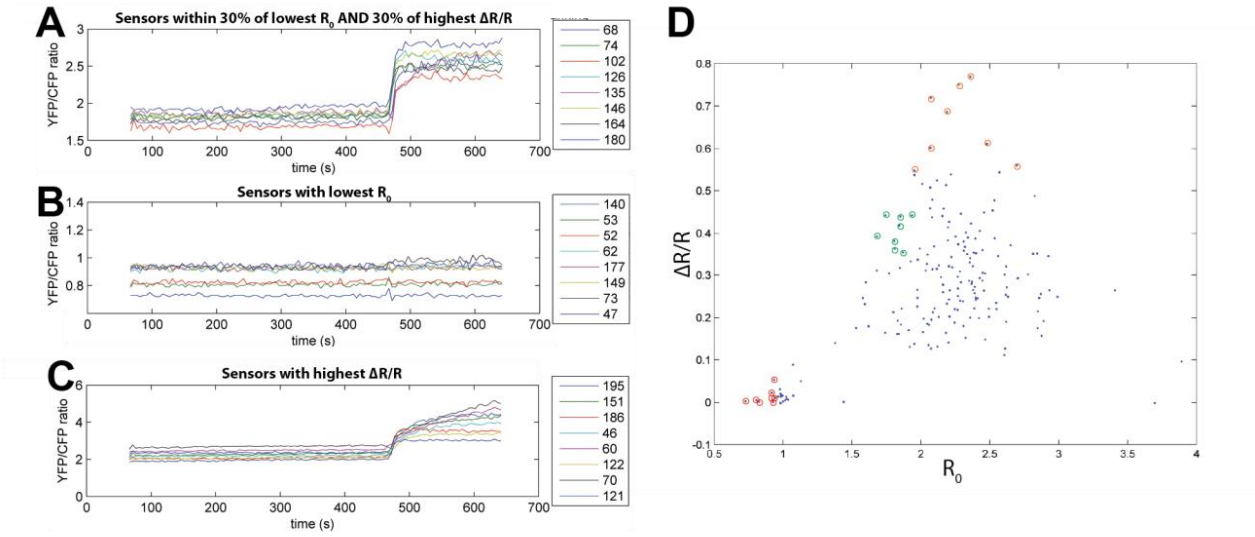

Figure 27: Typical Plots of an Early Screening Experiment
FRET ratio over time of the best performers in the three categories screened for **(A-C)**. Landscape of all colonies on a plate according to their R_0 and $\Delta R/R$, with the best performers in each category highlighted (red – lowest R_0, orange – highest $\Delta R/R$, and green – ranking high in both categories) **(D)**.

3.1.7 Streamlining and Data Management

A Python program (planned with, and written by David Ng, see appendix 6.1) was used in order to streamline and simplify the entire screening process and manage the huge amounts of data created by screening up to 100 bacterial plates per week.

The program controlled the camera, filter wheels and shutters. It guided the user through the screening process step by step, prompting certain actions (e.g. the application of a solution) at the appropriate times. It was able to identify the approximately 700-800 colonies on a plate, and recorded 35 datapoints over time in two different wavelengths for each one. $\Delta R/R$ values for each colony were calculated and a desired number of colonies expressing the best sensor variants were identified. In order to give the $\Delta R/R$ value of a colony more weight as a factor than its R_0 value, $\Delta R/R$ was divided by $R_0^{0.5}$. The user was then presented three plots: A landscape of all sensor variants on the plate according to their R_0 and $\Delta R/R$, with the best performers highlighted (**Figure 28A**), the individual FRET ratio traces over time of the best variants (**Figure 28B**), and a scheme of the plate depicting all colonies, with the positions of the best

performers indicated (**Figure 28C**). The scheme could then be used to identify them on the plate and pick them for further analysis.

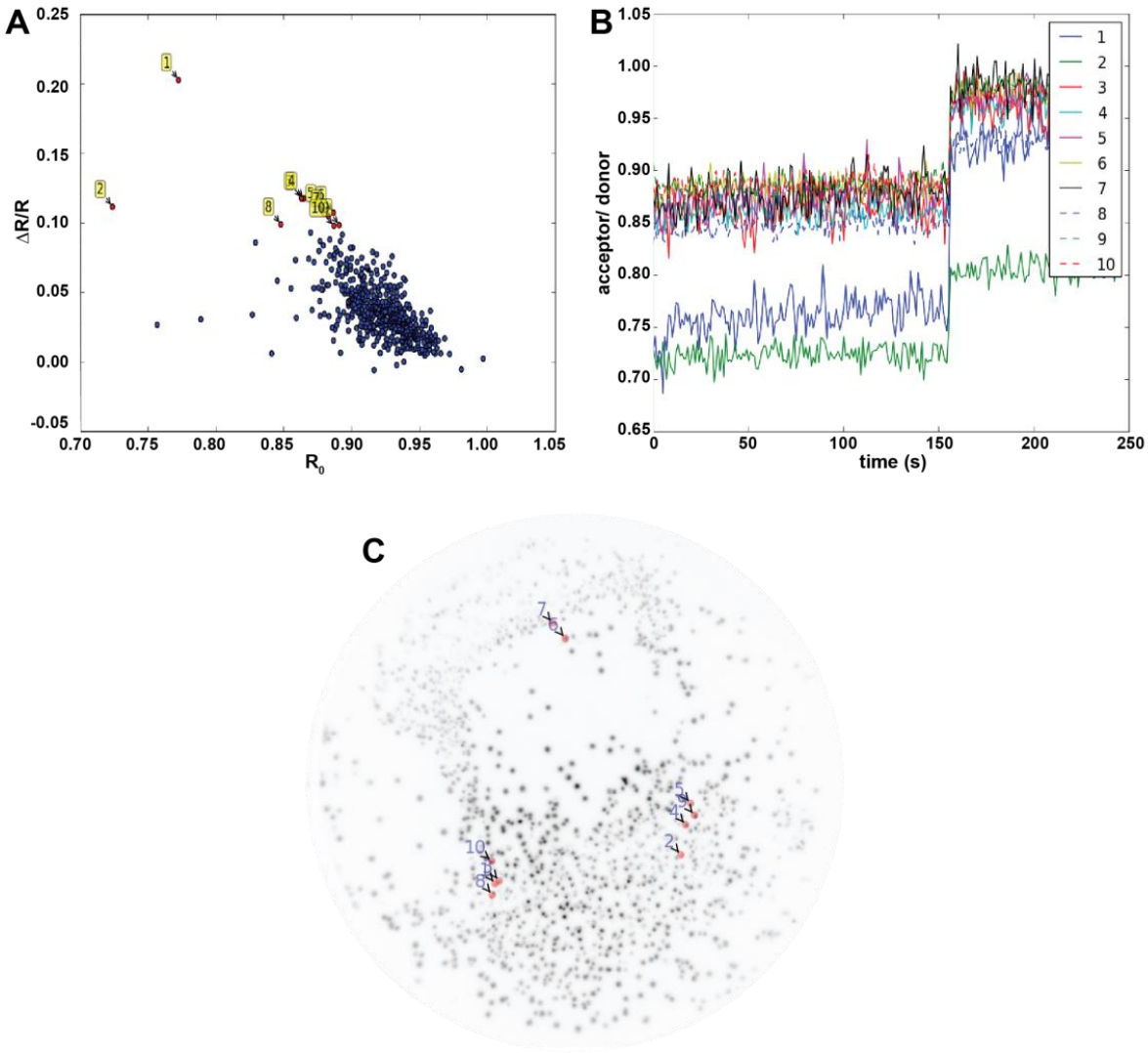

Figure 28: Typical Plots of a Streamlined Screening Experiment
Example of a data set produced for one plate of XL1 blue cells expressing a Ca^{2+} FRET sensor: Landscape of all bacterial colonies screened, according to their R_0 and ΔR/R induced by external application of 100mM Ca^{2+}. The top ten performers are highlighted in red with a yellow tag indicating their ranking **(A)**. Individual FRET traces of the best performers on the plate ranked from 1 to 10 **(B)**. Picture of all colonies on the plate, with the positions of the best performers denoted **(C)**.

3.1.8 Assessment of the Reliability of the Screening Assay

3.1.8.1 Reproducibility

One fluorophore and two sensors were chosen to verify the reproducibility of our screening assay:

- ECFP (no Ca^{2+} binding site and therefore no Ca^{2+} response) as a minimum signal
- TN-XXL with an *in vitro* ΔR/R of 300 – 400 % as a medium signal
- Twitch-3 with an *in vitro* ΔR/R of approximately 700 % as a maximum signal

All were imaged individually on bacterial plates in three experiments per day on three separate days. R_0 and ΔR/R following pretreatment with polylysine and ionomycin (50 µg/ml each) and the application of 100 mM Ca^{2+}, were examined to determine their variability. As **Figure 29A** shows, R_0 values remained consistent from experiment to experiment and from day to day. ΔR/R values on the other hand exhibited considerably more variation (**Figure 29B**), particularly on the first day, when a large fraction of the high signal data points overlapped with the medium signal data points. On days two and three on the other hand, the two signals could mostly be distinguished from one another. Upon analysis of the plot, a shift in most data sets became obvious, with colonies bearing a lower index number (1-x) exhibiting a lower ΔR/R. Since this number was allocated to a colony according to its position on the plate, the position–response correlation was further investigated by plotting all colonies from an experiment into a bubble plot, indicating their position on the plate as well as their ΔR/R, reflected in the size of their data point. As **Figure 29D** shows, there was a clear correlation between the ΔR/R of a colony and its position on the plate. This finding suggested that the plates had not been sprayed evenly, either with polylysine and ionomycin or with Ca^{2+}, leading to sensors in certain regions of the plates receiving less Ca^{2+}, resulting ultimately in a sub-maximal signal change. It was therefore concluded that the technique utilized to apply solutions, required refinement in order to eliminate human error. Bubble plots were also created for the R_0 values (**Figure 29C**) and YFP intensities (**Figure 29E**) of all colonies on a given plate. R_0 values exhibited no abnormalities, whereas the YFP intensity plot revealed slight inconsistences in illumination towards the edges of the plate.

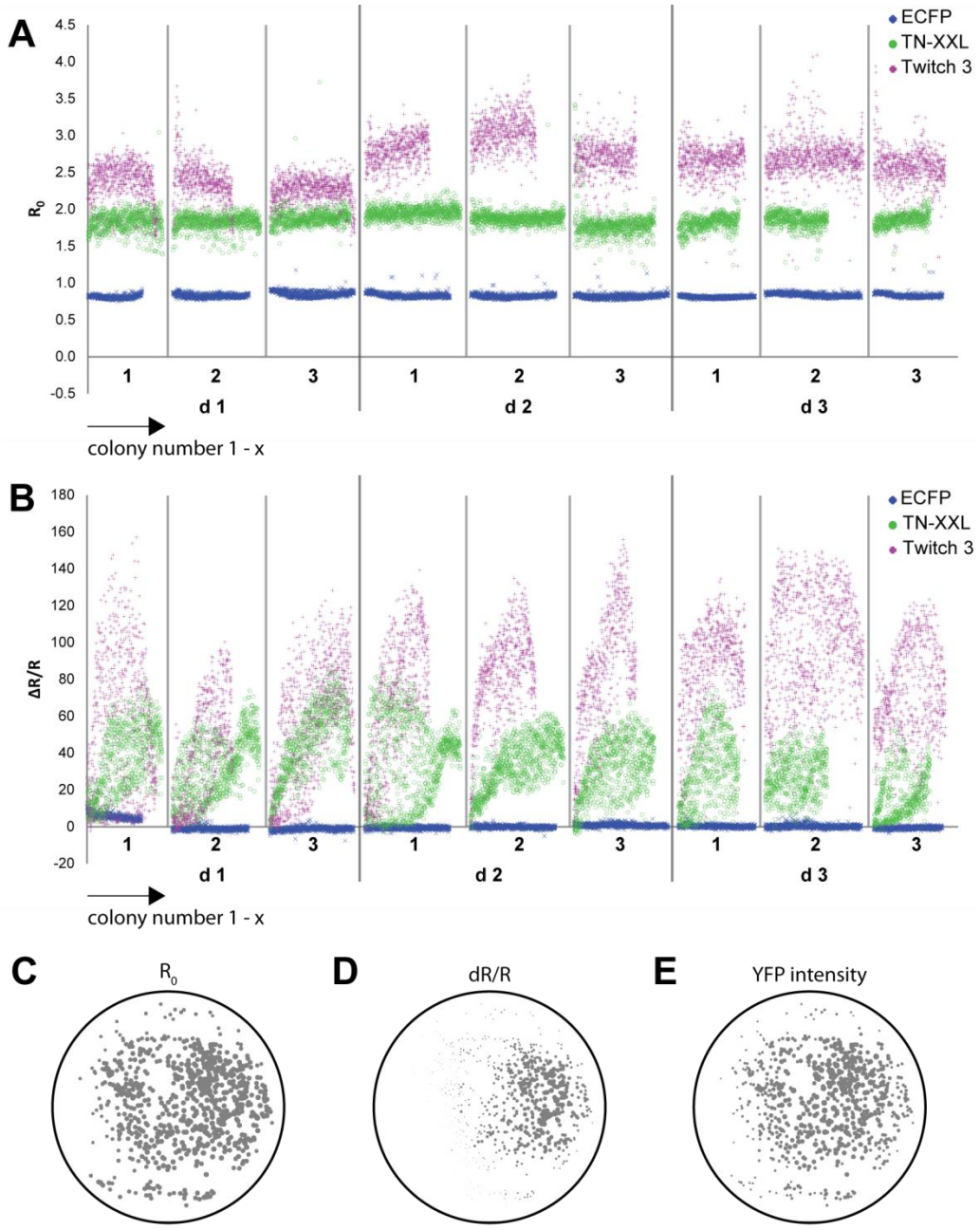

Figure 29: Reproducibility of the Screening Assay
R_0 **(A)** and ΔR/R values following pretreatment with polylysine and ionomycin and application of Ca^{2+} **(B)** of all colonies on a plate, expressing either ECFP or a FRET sensor. Colonies were plotted according to the index number assigned to them (dependent on their position on the plate). ECFP and two different FRET sensors were tested in 3 experiments per day (1 - 3) on 3 separate days (d1 - d3). Bubble plots of R_0 values **(C)**, ΔR/R values **(D)** and YFP intensity **(E)** of each colony correlated with their position on the plate. The experiment depicted (C-E) is experiment 1, of day 1, conducted with the sensor Twitch-3.

To improve the method in which solutions were applied to bacterial plates, the previously used spray bottles were replaced by spray guns (JetStream I, K350, HVLP) contributing to a more consistent spray

pattern with a larger radius. The larger radius simplified the application process in that the experimenter could then simply aim at the middle of the plate from a height of approximately 30 to 40 cm, instead of moving the spray nozzle around in an attempt to achieve optimal coverage. A laser pointer was attached to the gun to facilitate aiming (**Figure 30A**). The experiment depicted in **Figure 29** was repeated and a more regular response pattern of Twitch-3 (**Figure 30B**) confirmed that the spray gun applied the solutions more evenly. Nevertheless, a higher concentration of the solution in the center, and a decline towards the edges was unavoidable due to the design of the valve. However, as this spray pattern was predictable and reproducible, it could be taken into account in the analysis of future experiments.

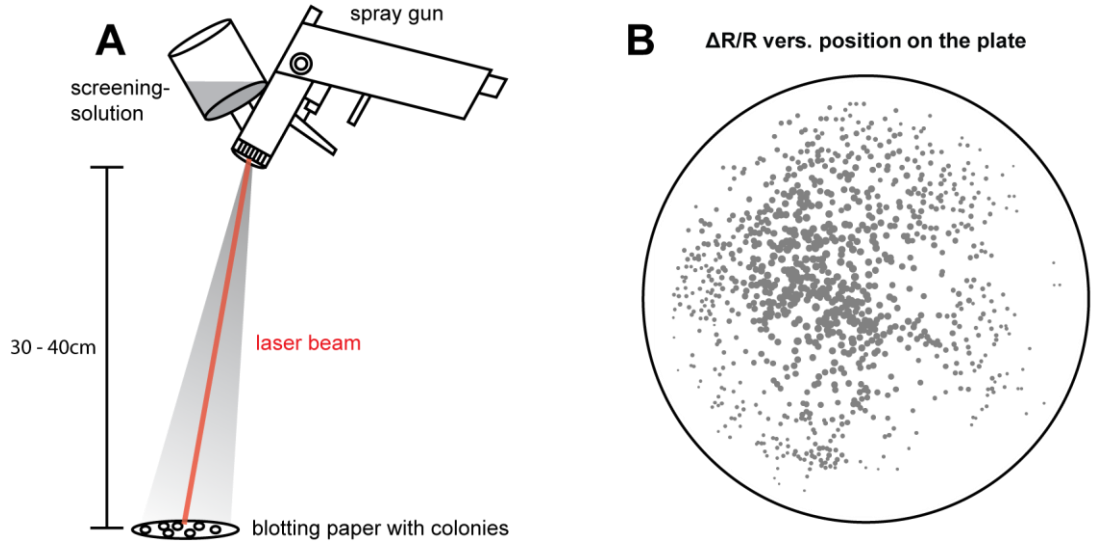

Figure 30: Improved Application of Solutions
Application of solutions using a spray gun, including a laser pointer to facilitate aiming **(A)**. Bubble plot of an experiment using the spray gun, carried out with Twitch-3. The position of each colony on the plate is indicated and its ΔR/R is reflected in the bubble size **(B)**.

3.1.8.2 Bacterial Plate Screening versus in vitro Data

For a second control experiment, a plate of XL1 cells expressing a random library of various FRET sensors was screened and analyzed (**Figure 31A**). Subsequently, 192 colonies (one in three) were picked, their sensor DNA extracted and each sensor expressed and purified for *in vitro* analysis. Measurements of the 192 sensor variants on the plate were correlated with the corresponding *in vitro* measurements. As **Figure 31B** depicts, R_0 values correlated quite well among measurements obtained in *E.coli* and *in vitro*, with a correlation coefficient (Pearson) of 0.61. For the ΔR/R values on the other hand, the correlation of

bacterial and *in vitro* data was weak, with a correlation coefficient (Pearson) of 0.3 (**Figure 31C**). That being said, the plot also revealed that in order to extract 4 out of 5 of the best performers *in vitro*, one would have had to pick 15 colonies, constituting ~8 % of the 192 colonies analyzed, which still would have been a considerable improvement.

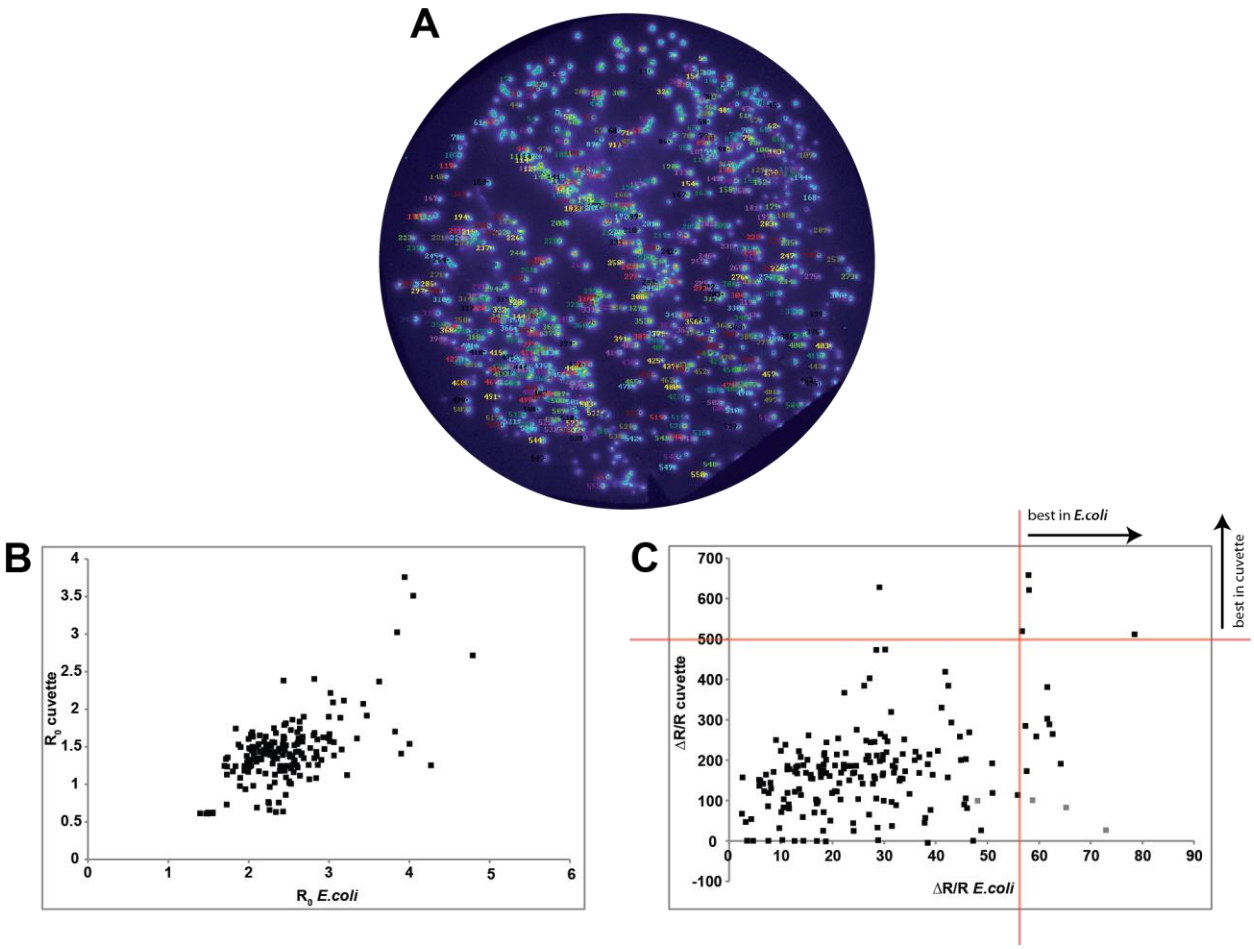

Figure 31: Bacterial Plate Screening Data Correlated with *in vitro* Data
Plate of XL1 blue cells expressing a random library of FRET sensors, which was tested and analyzed. One out of three colonies (resulting in 192 colonies) was picked and the sensor it expressed was probed *in vitro* **(A).** Correlation of the data obtained from *E.coli* colonies and *in vitro* regarding R_0 **(B)** and ΔR/R **(C)** of 192 FRET sensors.

Nevertheless, we wanted to investigate the source of these discrepancies between *E.coli* and *in vitro* data. It seemed plausible that a sensor would be underestimated in *E.coli* due to under- /overexpression, inconsistent illumination and uneven application of solutions (see chapter 3.1.8.1). That so many sensors appeared to be *over*estimated by the plate screening on the other hand, was rather surprising. We

decided to express a number of these sensors (marked in grey in **Figure 32C**) in HEK cells to see if the cellular environment would again permit the function that the sensors seemed to have lost *in vitro*. Indeed, all sensors expressed showed explicit Ca^{2+} responses when 0.625 nM ionomycin was applied to the Ca^{2+}-containing HBSS used for imaging (**Figure 32A-B**). The published sensors TN-XXL and Twitch-2B were imaged, along with the four new sensors to estimate the extent of their FRET response. All four exhibited responses which, while lower than those of our recently published Twitch-2B, were distinctively higher than those of the previously developed TN-XXL (**Figure 32C-D**). In summary, these experiments support the hypothesis that some sensors require a cellular environment to maintain functionality.

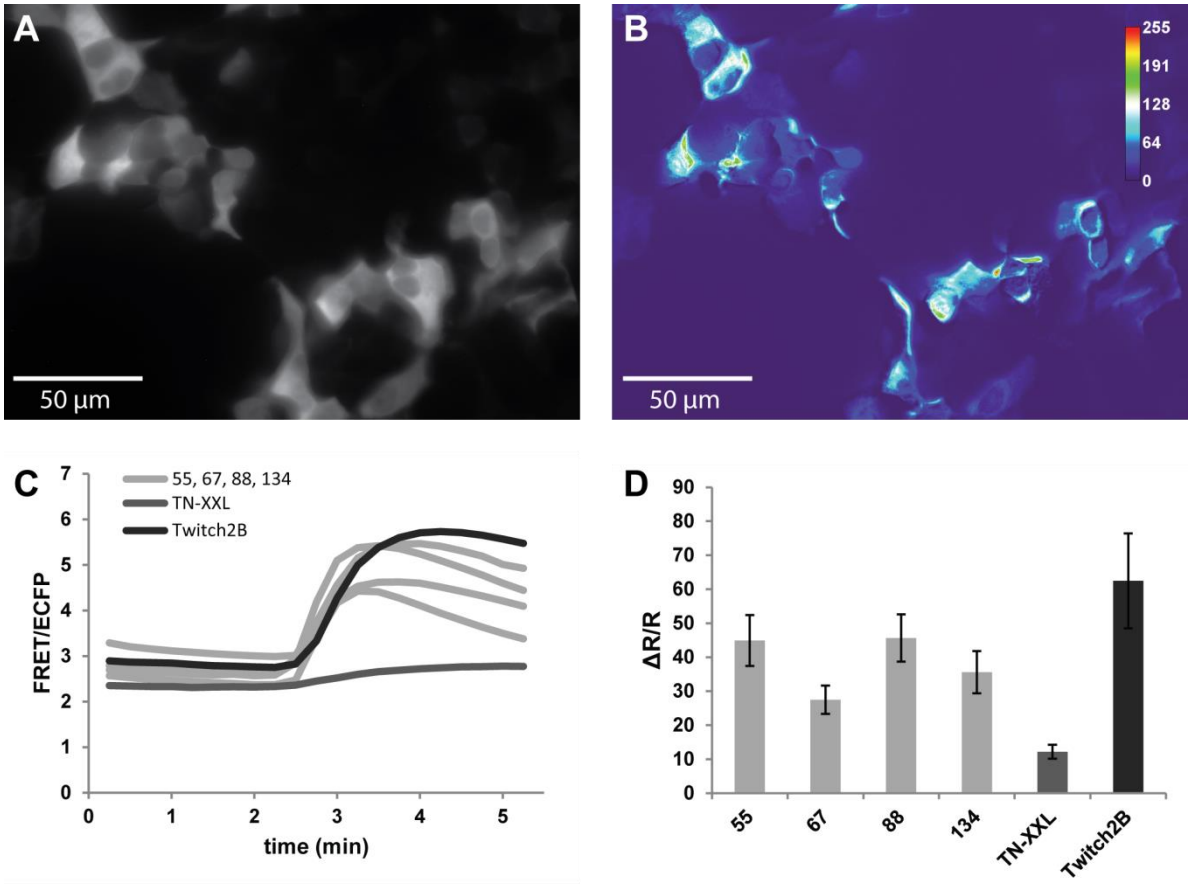

Figure 32: Imaging of *in vitro* Non-functional Sensors in HEK Cells
HEK cells transformed with a Ca^{2+} FRET sensor which was non-functional *in vitro* (exposure time 2500 ms, gain 2 x, binning 1) **(A)**. Subtraction of an image prior to treatment with 0.625 nM ionomycin, from an image after the treatment, showing the FRET increase **(B)**. FRET intensity traces over time for the four sensors which were non-responsive *in vitro* (called 55, 67, 88, 134), in direct comparison to the published sensors TN-XXL and Twitch-2B **(C)**. Mean ΔR/R values ± SE of the same sensors. n_{55} = 36 cells, n_{67} = 44 cells, n_{88} = 43 cells, n_{134} = 33 cells, $n_{TN\text{-}XXL}$ = 35 cells, $n_{Twitch\text{-}2B}$ = 20 cells **(D)**.

3.2 Screening for Improved 'Twitch' Ca^{2+} Indicator Variants

Our newly developed Ca^{2+} screening assay was used to identify improved Ca^{2+} FRET sensors from DNA libraries, thereby contributing to the evolution of the 'Twitch' sensor series. The first member of the 'Twitch' sensor series, Twitch-1, was engineered by Thomas Thestrup. It consisted of the C-terminal domain of troponin C (two Ca^{2+} binding sites) originating from the toadfish; *Opsanus tau*, sandwiched between two fluorescent proteins (ECFP and cpCitrine174) with a flanking proline on either side. In addition, it contained a number of mutations restricting the undesirable Mg^{2+} affinity of the C-lobe (N15D, D17N, N51D, D53N, (Mank et al., 2006)), and another beneficial mutation (M65V), found previously by chance.

This prototype was subjected to a large functional screening in bacterial cells, followed by refined screening steps *in vitro*, and eventually in rat hippocampal neurons (the latter being conducted exclusively by Thomas Thestrup). Some data presented in this chapter was published in Nature Methods (Thestrup et al., 2014).

3.2.1 Creation of a Sensor Library

Two approaches were adopted to create extensive libraries of 'Twitch' sensor variants:

1. **Introduction of random linkers**: FRET heavily depends on the distance between the two fluorescent proteins and their orientation to one another. Random linkers were therefore introduced between the donor and troponin C on one side, and the acceptor and troponin C on the other side, in order to force them further apart and manipulate their orientation (**Figure 33A**).
2. **Mutation of "hotspots" within troponin C**: Prosperous locations within troponin C (selected by Thomas Thestrup) were mutated to change the affinity and kinetics of the sensor, as well is its overall conformation (**Figure 33B**). Some of these hotspots represented locations believed to support the structure of troponin C (**Figure 33C**). The amino acids at such sites stretched from one α helix of troponin C to a second α helix or section of the protein, presumably granting it stability. It was concluded that mutating these particular sites would have a significant impact on the structure and function of troponin C.

   Other hotspots were chosen based on their proximity to the coordinating residues of troponin C, which control the binding of Ca^{2+} in the loop region (**Figure 33D - E**). While mutating the

coordinating residues themselves, was suspected to disable the Ca^{2+} binding function altogether, it was assumed that mutating the positions in between those residues would tune the Ca^{2+} affinity and kinetics of troponin C.

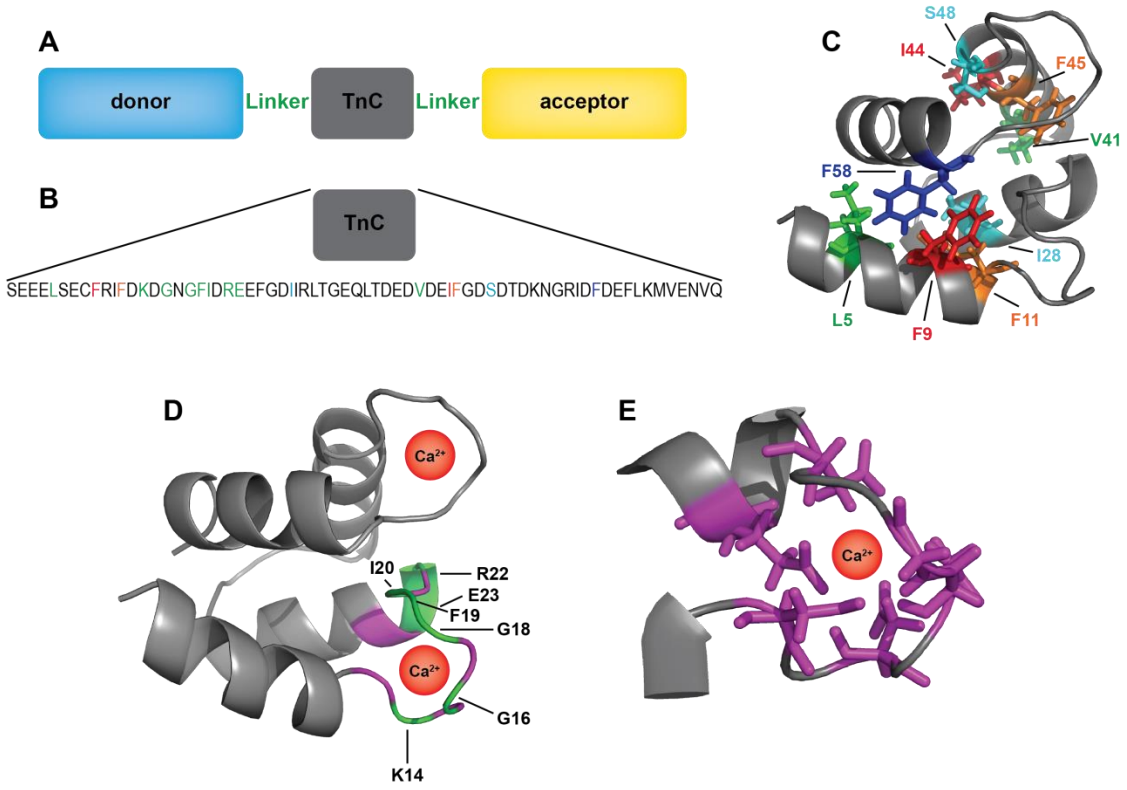

Figure 33: 'Twitch' Indicator Library
Scheme of the general 'Twitch' sensor family structure, with positions of introduced random linkers indicated **(A)**. Sequence of the C lobe of troponin C (TnC); mutated hotspots are highlighted in color **(B)**. Structure of the C lobe of troponin C; positions mutated in order to change the stability of the protein are highlighted in color **(C)**. Troponin C with coordinating residues highlighted in magenta and mutated spots highlighted in green **(D)**. Close-up of the loop region of EF-hand 3; coordinating residues are highlighted in magenta **(E)**.

3.2.2 Bacterial Plate Screening of 'Twitch' Sensor Libraries

3.2.2.1 1st Round of Screening: Random Linkers

In order to further improve the newly developed Ca^{2+} FRET sensor, Twitch-1, additional random linkers with a length of between one and four amino acids were introduced to flank troponin C (**Figure 34**). The diversification of up to 8 amino acid positions, which then had the potential to become one of 20 amino acids (or a stop codon), together with the 16 possible combinations of linker lengths, resulted in a huge library of 4.17E+10 sensor variants. Testing each variant was obviously impossible. Nevertheless, we assumed that numerous linker combinations would prove successful and that covering a small fraction of the library with our screening would therefore be sufficient.

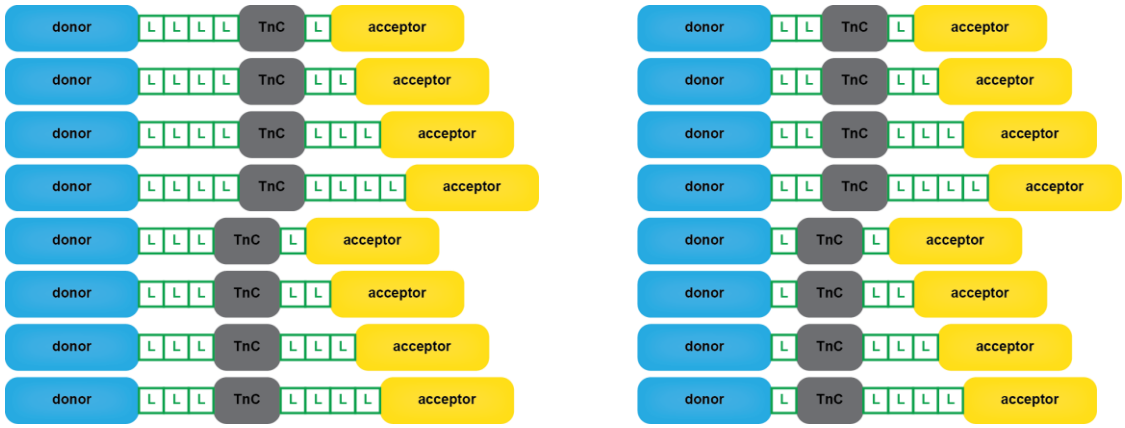

Figure 34: Twitch-1 Linker Library
Linkers were introduced to flank troponin C. All possible combinations of linker lengths (one to four amino acids) are depicted.

Altogether, we screened approximately 100 000 sensor variants on plates of XL-1 blue cells. One plate contained approximately 700-900 colonies, each expressing its own unique sensor. As previously explained, colonies were imaged on blotting paper, treated with ionomycin and polylysine (50µg/ml each) as well as 100mM Ca^{2+}, and their R_0 and $\Delta R/R$ were assessed.

1.142 promising variants were picked, purified on a small scale, and tested *in vitro*. Out of these variants, 1.078 (~94 %) displayed a R_0, and 67 variants (~6 %) displayed a $\Delta R/R$, which was better than that of the original sensor, Twitch-1. 63 variants (~6 %) had both a higher R_0 and a lower $\Delta R/R$ than the template, thereby failing to meet any of the screening criteria. In addition, 115 variants (~10 %) exhibited $\Delta R/R$ values of below 10 %, which was considered non-functional (**Figure 35**).

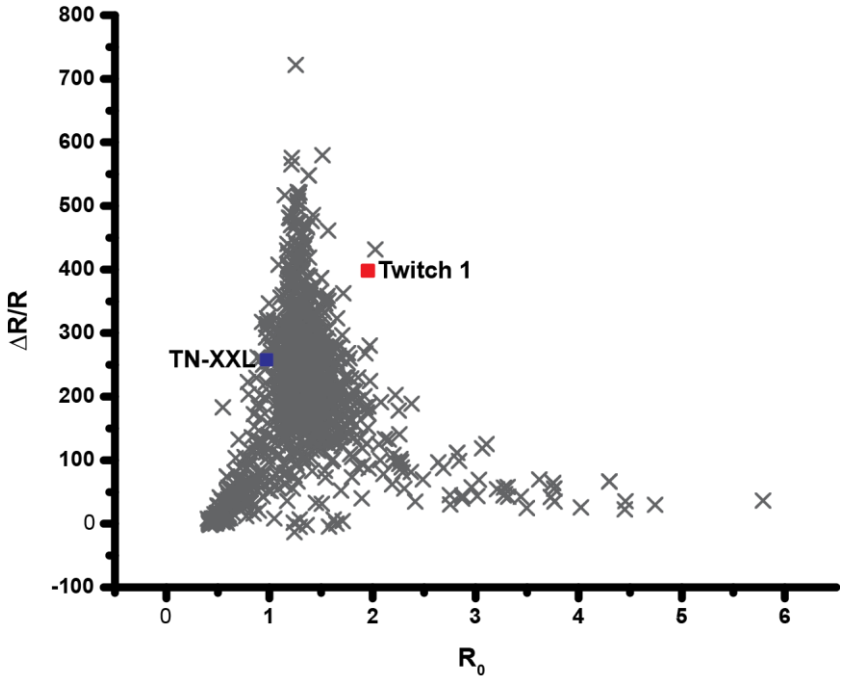

Figure 35: First Round of 'Twitch' Screening: Random Linkers
Plot of all sensor variants picked and measured *in vitro* during the first round of screening (n = 1.142). The parental sensor Twitch-1 and our previously published sensor TN-XXL are displayed as a reference.

Some of the best sensors identified through linker screening were subsequently sequenced (**Table 17**), revealing several patterns. Although there were exceptions, most successful linkers were rather short, consisting of only one or two amino acids. The linker attached to the C-terminal end of troponin C had a slight tendency to be longer than its N-terminal counterpart. Aspartic acid was found remarkably often at the N-terminal end, implying that our library was either strongly biased towards certain amino acids, or that this particular amino acid proved extremely beneficial at this position. Note that the first proline of the C-terminal linker was encoded in its corresponding primer and therefore, does not necessarily reflect a beneficial mutation.

Screening Name	Linker 1 (N-terminal)	Linker 2 (C-terminal)	ΔR/R (%) Ca^{2+}	R_0	dR/R (%) Mg^{2+}	Ca^{2+} Affinity (nM)
xN2.1 119	**D**	**PAL**	704	1.26	25	91
2N1 390	**DA**	**PIY**	622	1.29	67	
B2 150	**D**	**PG**	496	1.27	13	438
D_2 32	**D**	**PQ**	497	1.31	14	452
D_1 371	**D**	**PA**	485	1.30	14	428
C2 450	**D**	**PA**	480	1.33	17	431
2N1 86	**DS**	**PTL**	467	1.27	16	238
B2 139	**E**	**PV**	464	1.39	18	363
E2 497	**D**	**PM**	463	1.57	27	316
B2 225	**D**	**PS**	452	1.30	23	483
B_1 132	**G**	**PAIP**	444	1.15	15	295
2N1 322	**EG**	**PLT**	443	1.24	17	
B_1 117	**D**	**PS**	437	1.32	12	465
2.2 758	**EE**	**PSP**	425	1.39	31	163
4N1.1 460	**SELL**	**PLPLS**	410	1.43	34	86
E2 122	**D**	**PLET**	404	1.18	13	394
C2 47	**E**	**PD**	403	1.19	9	673

Table 17: Successful Linker Combinations
List of some of the best sensors identified in the linker screening including their linkers and properties (note that the first proline in linker 2 was encoded in its corresponding primer).

To investigate bias in our library (produced with the degenerate codon NNN), 40 sensors were randomly chosen and sequenced, and the occurrence of each amino acid was quantified (**Table 18**). A disequilibrium was indeed identified in our library, with a tendency for amino acids with multiple codons, or shorter amino acids, to occur more frequently, as expected. That being said, the overrepresented aspartic acid in our improved sensors, did not emerge particularly often, supporting the assumption that it was indeed an advantageous mutation.

F	L	Y	C	W	P	H	Q	I	M	T	N	K	S	R	V	A	D	E	G	Stop
3	14	3	8	1	20	3	16	9	6	9	4	4	23	5	22	11	12	21	24	3

Table 18: Occurrence of Amino Acids with the Codon NNN
Occurrence of individual amino acids in random linkers, produced with the degenerate codon NNN (encoding all 20 amino acids and the stop codon).

3.2.2.2 2nd Round of Screening: Point Mutations

Twitch-1 and three promising mutants found in the initial linker screening (**Figure 36**) were subsequently selected to serve as templates for a second library, which was generated utilizing site directed mutagenesis.

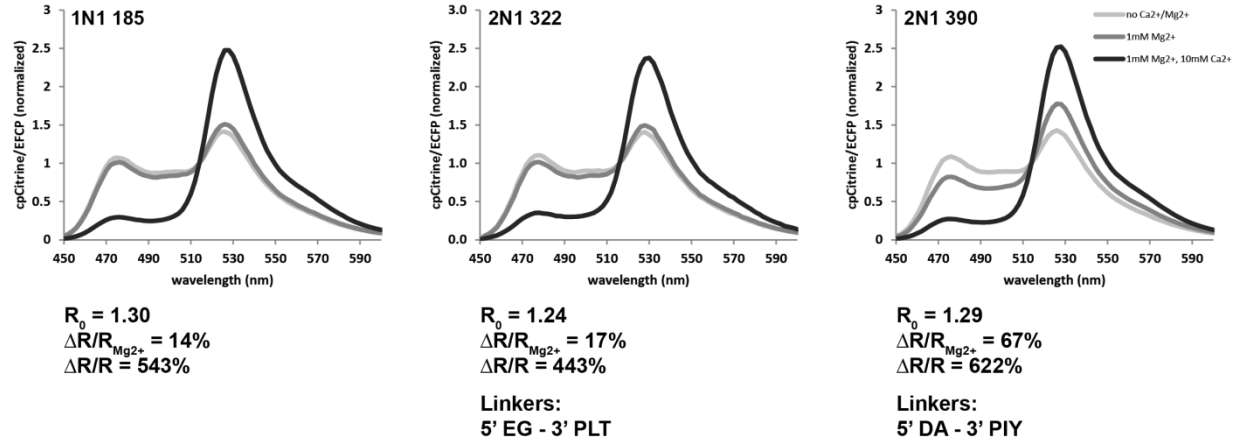

Figure 36: Sensors from the Linker Screening Used as Templates for the Second Round
Emission spectra and overview of characteristics for three promising sensors identified in the initial linker screening, chosen as templates for the second library. Values were normalized to the isosbestic point.

Locations were mutated and screened individually, which reduced the number of potential mutants in this library. Four templates were mutated at 16 locations, which could transform into one of 20 amino acids or a stop codon, producing a total of 1.344 possibilities. Per template and mutation, two to three plates each containing approximately 800 colonies were screened, allowing us to assess the majority of the library.

1.076 promising candidates were picked, purified and tested *in vitro* (**Figure 37**). 542 sensors (~50%) exhibited lower R_0 values, and 154 (~14%) exhibited higher ΔR/R values than all templates. 70 variants (~7%) had higher R_0 values and lower ΔR/R values than all templates, and therefore failed to meet the screening criteria. Only 38 mutants (~ 4%) produced ΔR/R values below 10% and were therefore considered non-functional.

Two of the most successful sensors discovered in this round of screening were later named Twitch-2 and Twitch-3 (**Table 20**). They had mutations in positions K14 and V41 respectively. Other positions facilitating considerable improvements were G16, G18, F19, R22 and F58 (**Table 19**).

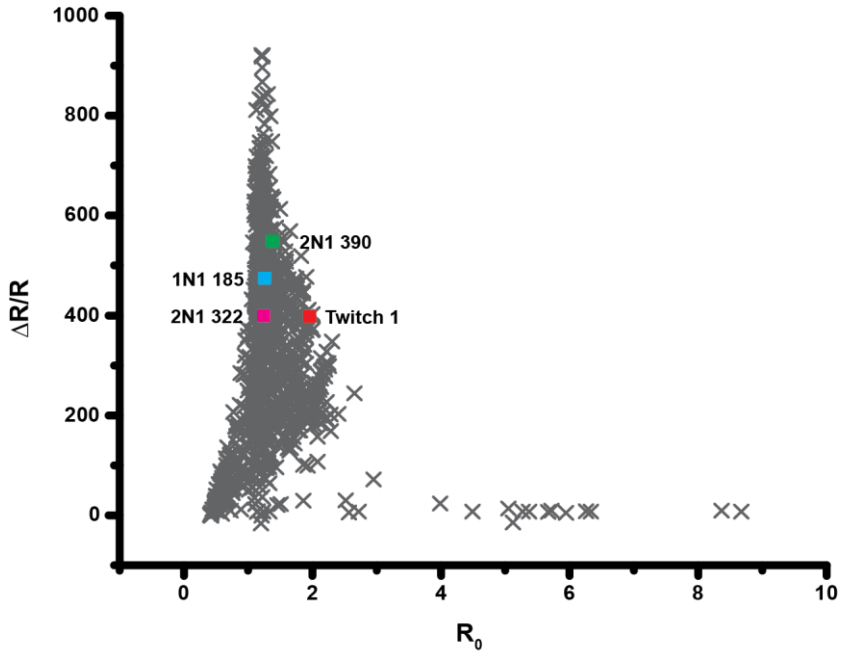

Figure 37: Second Round of 'Twitch' Screening: Point Mutations
Plot of all sensor variants picked in the second round of screening and measured *in vitro* (n = 1.076). The four parental sensors are displayed as a reference.

Name	R_0	ΔR/R (%) Ca^{2+}	Mutation
390 K14x2 161	1.21	922	K14W
390 K14x2 106	1.22	921	K14F
390 K14x2 115	1.22	831	K14N
390 K14x2 159	1.18	746	K14G
390 G16x2 43	1.18	735	G16F
390 G16x1 158	1.34	656	G16R
390 G16x2 209	1.24	656	G16T
390 G16x2 117	1.23	651	G16M
390 G18x2 78	1.23	685	G18Q
390 G18x1 65	1.16	670	G18E
390 G18x2 128	1.21	661	G18N
390 F19x2 25	1.20	735	F19M
390 F19x2 44	1.28	719	F19L
390 F19x2 39	1.20	692	F19A
390 f19x1 94	1.12	685	F19E
390 f19x1 29	1.22	651	F19H
390 R22x2 80	1.22	714	R22P
390 R22x2 109	1.17	694	R22F
390 R22x2 112	1.18	693	R22S
390 R22x2 89	1.14	678	R22T

Name	R_0	ΔR/R (%) Ca^{2+}	Mutation
390 V41x2 26	1.13	811	V41P
390 f58x1 19	1.12	683	F58T

Table 19: Beneficial Point Mutations
List of point mutations giving rise to some of the highest ΔR/R values. According to this list, mutations in the locations K14, G16, G18, F19, R22, V41 and F58 seemed to have especially high impact.

3.2.2.3 3rd Round of Screening: Extended Linkers and New Donor

The best sensor identified in the second round of screening, Twitch-2, featured a two amino acid linker on the N-terminal, and a three amino acid linker on the C-terminal side of troponin C, as well as the additional mutation K14F within EF-hand 3 (**Figure 38A**). In this sensor, the donor ECFP was substituted with the brighter cyan fluorescent protein Cerulean3 (**Figure 38B**). Even though Cerulean3 was based on ECFP, containing only a number of minor mutations, it altered the fluorescent output of the sensor significantly, leading to a loss of Ca^{2+}-induced FRET change of almost 50%. Therefore, a second linker screening on Cer3-Twitch-2 was conducted to restore the high FRET change. To this end, up to three amino acids were attached to either side of the Twitch-2 Ca^{2+} binding site.

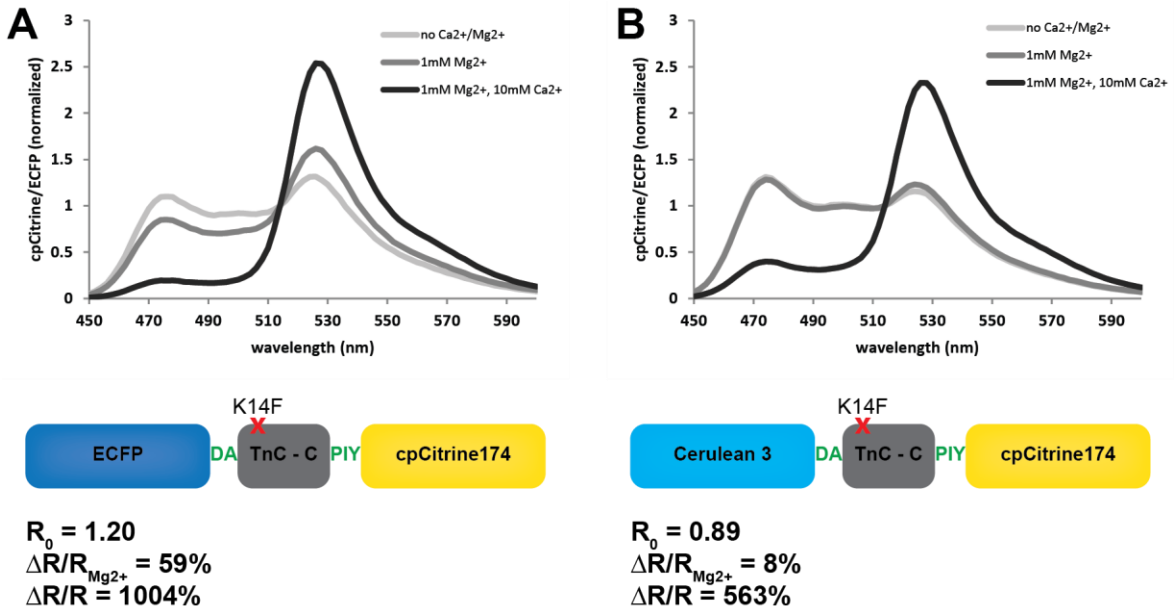

Figure 38: Substitution of ECFP with Cerulean 3 in Sensor Twitch-2
Emission spectra, schemata, and FRET values of Twitch-2 **(A)** and Twitch-2 with donor ECFP replaced by Cerulean3 to form Cer3-Twitch-2 **(B)**. Values were normalized to the isosbestic point.

In the third round of screening, approximately 30 000 variants were screened, and 520 promising candidates were examined *in vitro*. 156 (~31%) had a lower R_0, and 19 (~4%) had a higher ΔR/R response than the parental Cer3-Twitch-2. 37 (7%) were considered non-functional with a ratio change of less than 10% (**Figure 39**). The best sensor in this round of screening, containing two additional amino acids at its N-, and one additional amino acid at its C-terminal end, was later named Twitch-2B (**Table 20**).

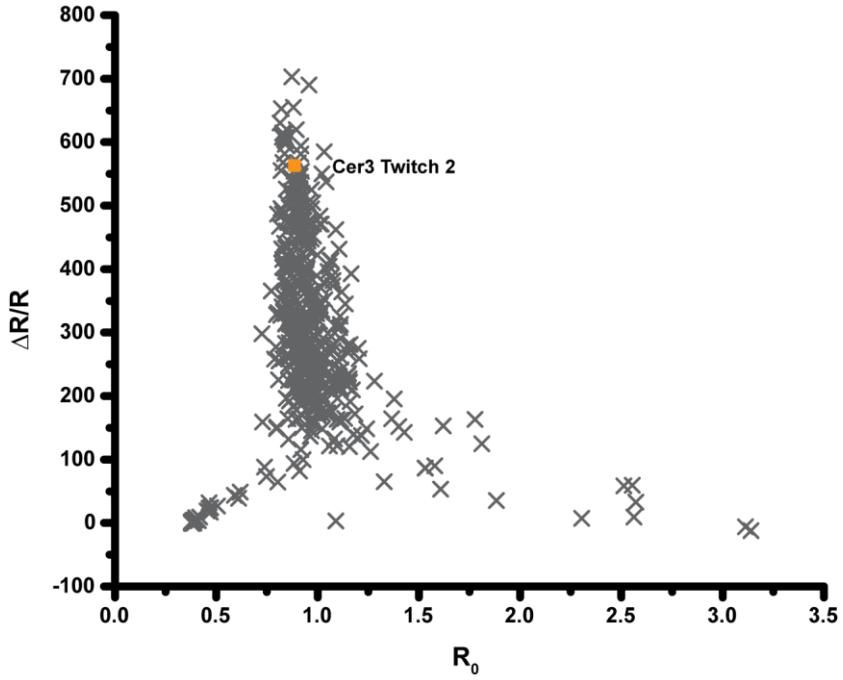

Figure 39: Third Round of 'Twitch' Screening: Extended Random Linkers
Plot of all sensor variants picked in the third round of screening and measured *in vitro* (n = 502). The parental sensor Cer3-Twitch-2 (with Cerulean in favor of ECFP as a donor) is displayed as a reference.

3.2.3 Follow-up Screening Steps

Since bacterial plate screening (whilst quick) proved to be a rather unrefined method, and only facilitated screening for two properties (R_0 and ΔR/R values), follow up steps were necessary to further characterize the sensors.

As previously mentioned, all sensors selected during the plate screening were subsequently purified on a small scale, which allowed for the handling of up to 48 proteins at a time. The disadvantage however, was that traces of contaminating Ca^{2+} lead to slight deviations in measurements, compared to proteins which underwent a more thorough purification. Nevertheless, the measurement of small scale proteins was

reliable enough to refine the estimations regarding R_0 and ΔR/R, gained through bacterial screening. Moreover, sensors were probed for an undesirable affinity for Mg^{2+}.

Sensors which looked promising in the small scale purification were subsequently purified more thoroughly and in larger batches. Their R_0 and ΔR/R were re-measured, to confirm the previous results. Furthermore, the sensors' Ca^{2+} affinity was determined in Ca^{2+} titrations, and their kinetics were obtained by conducting stopped-flow measurements. The best sensors were eventually transfected into mammalian cells to verify that the qualities found in bacteria and *in vitro*, could also be provided in the cell setting they were designed for (**Figure 40**).

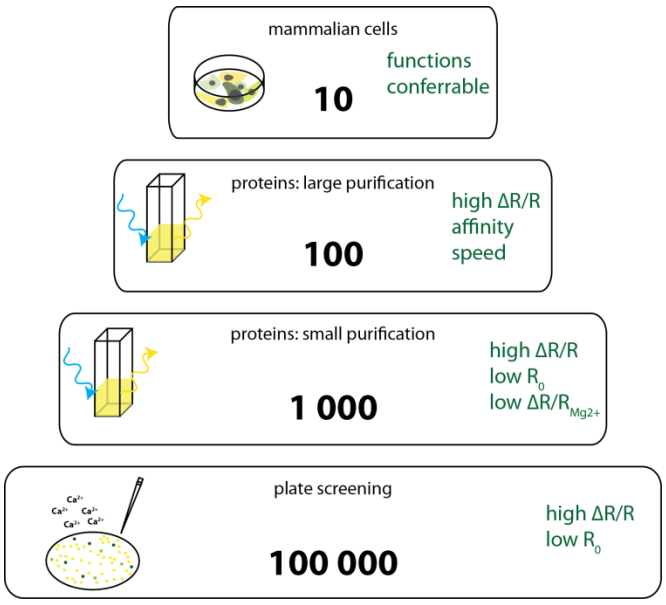

Figure 40: Follow-up Screening Steps (the "Screening Pipeline")
Screening pipeline indicating the individual steps, the number of sensor variants that was typically dealt with, and the properties which could be screened for.

3.2.3.1 Spectroscopy - Data Management

Despite the bacterial plate screening considerably reducing the number of variants to be further investigated, several thousand different sensors were still purified and tested *in vitro.* Consequently, all corresponding data files required analysis, in order to determine R_0 and ΔR/R values. To simplify and accelerate this process, a program (planned with, and written by Christopher Zarbock, see appendix 6.2) was used which automatically analyzed entire folders of spectroscopic data and created plots for each

sensor, comprising all relevant data. Furthermore, a landscape of all sensors tested was generated to facilitate the identification of promising variants (**Figure 41**).

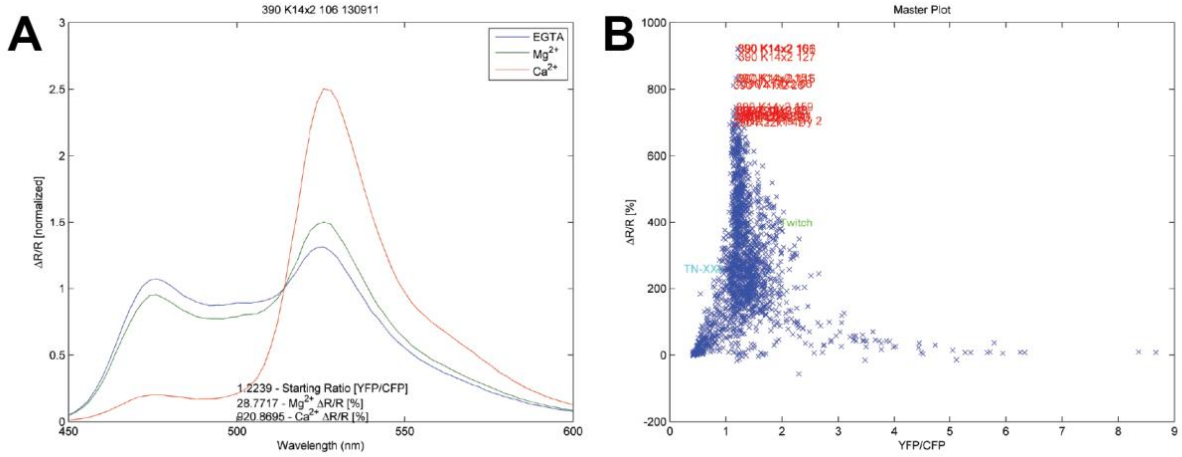

Figure 41: Example of a Data Set Generated by Matlab
Plot of a measured protein comprising all calculated data **(A)**. Landscape of all sensors tested, with sensors exhibiting specific characteristics (in this case ΔR/R values ≥ 700 %) indicated by a name tag **(B)**.

3.2.3.2 Refined Screening: Ca^{2+} Affinity and Kinetics

A drawback of the bacterial plate screening was that it only identified sensors with high signal changes, neglecting entirely other vital characteristics of a sensor, for example its Ca^{2+} affinity and kinetics. Such characteristics however, were considered when designing the library. By setting the criteria for the plate screening less stringently, we were able to yield a diverse pool of sensors in terms of secondary properties, which could subsequently be evaluated in the refined screening steps *in vitro* and in cells.

Figure 42 illustrates the diversity of our library. Using the example of Ca^{2+} affinity, it depicts the parental sensor Twitch-1 and five additional sensors. These sensors were chosen from bacterial plates for their high signal changes, but exhibited a wide range of Ca^{2+} affinities, making them applicable to a diverse range of cell environments.

Table 20 summarizes the properties of those members of the 'Twitch' series, optimized via screening, again covering a range of qualities for different experimental conditions.

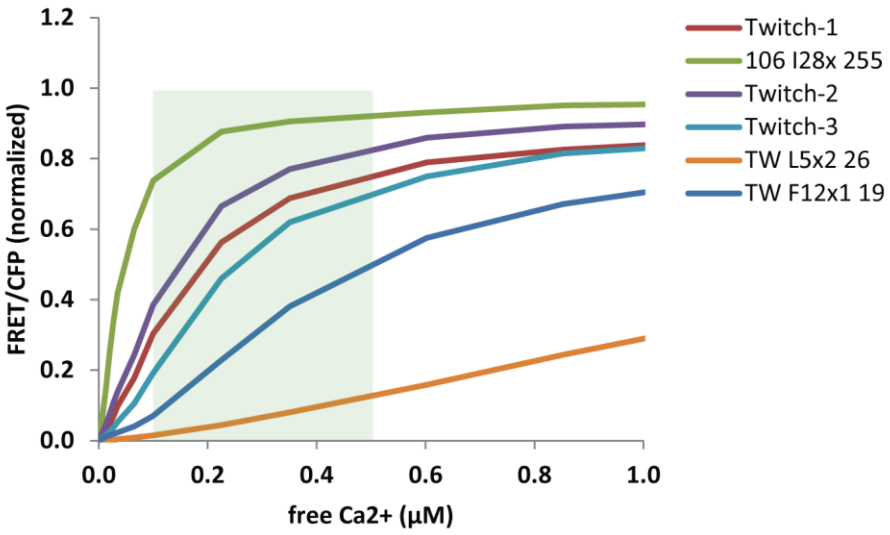

Figure 42: Diversity of Ca^{2+} Affinity Properties in Selected Sensors
Parental sensor Twitch-1 and a selection of sensors identified via screening, which exhibited a wide range of Ca^{2+} affinity properties, with the region most relevant for physiological experiments shaded in blue.

Name	**FRET pair**	**Mutations**	**Linkers**	**YFP/CFP (R_0)**	**ΔR/R (%)**	**Kd (nM)**	**Decay time (s)**	**Maximum ΔR/R @ 160FPs**	**R_0**	**Decay time (s) 10AP**
Twitch-1	ECFP cpCit174	M65V	P, P	1.95	400	250	0.80	80	2.08	1.50
Twitch-2	ECFP cpCit174	K14F, M65V	DA, PIY	1.20	1000	150	2.80	209	1.21	1.81
Twitch-2B	Cer3 cpVenus^{CD}	K14F, M65V	VADA, PIYP	0.80	800	200	5.10	104	1.53	2.11
Twitch-2C	mTurquoise2 cpCit174	K14F, M65V	VADA, PIYP	0.80	700	450	2.60	-	-	-
Twitch-3	*ECFP* cpCit174	V41P, M65V	DA, PLA	1.30	700	250	1.50	321	1.30	2.05
Twitch-3B	ECFP cpVenus^{CD}	V41P, M65V	DA, PLA	1.15	900	150	2.98	185	1.53	2.55

Table 20: Properties of Twitch Sensors 1-3
Summary of properties of those members of the 'Twitch' series, which were improved via screening (modified from (Thestrup et al., 2014)).

3.3 Improvements to mKOκ

3.3.1 Creation of Circularly Permutated Variants of mKOκ

Circular permutations of the fluorescent protein mKOκ were produced by Anselm Geiger. He randomly introduced transposons, which are mobile DNA sequences with the ability to change their relative positions within host DNA (Goryshin & Reznikoff, 1998). Using this method, he was able to identify sites within the protein which could tolerate permutation and the insertion of foreign (e.g. sensor) DNA. Most circularly permutated (cp) variants of mKOκ created in this manner however, lost most of their fluorescence in the process. Moreover, they exhibited slower maturation compared to the original mKOκ (referred to as mKOκ-WT in the following). Out of the three variants with the highest remaining fluorescence intensity (**Figure 43B**), two were chosen for further development. Their new openings were located in a loop opposing the former N- and C- termini (**Figure 43A**), namely at positions 47 (met) and 51 (gly). This was intriguing, as using them in a FRET sensor in place of KO2-WT, would result in a drastic re-orientation of the chromophore, potentially impacting its FRET efficiency. Regarding brightness, cp mKOκ–47 retained ~65 % of the fluorescence intensity of mKOκ-WT, and cp mKOκ–51 still retained ~11 % (**Figure 43C**).

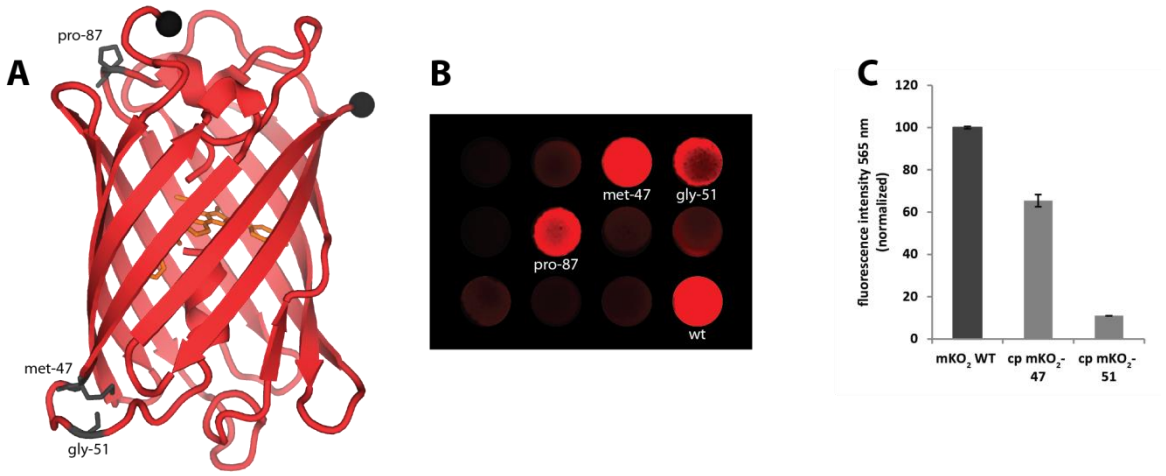

Figure 43: Structure and Relative Brightness of mKOκ and cp mKOκ Variants
Protein structure of mKOκ-WT, with the original N- and C-terminus indicated with black balls, and sites used to create cp mKOκ-47 and cp mKOκ-51 labelled in grey **(A)**. Brightness of mKOκ-WT and cp variants expressed in *E.coli* **(B)**. Fluorescence intensity of cp mKOκ-47 and cp mKOκ-51, relative to the intensity of mKO–WT (excitation 551 nm, emission 565 nm) **(C)**.

3.3.2 Bacterial Plate Screening of mKOκ

3.3.3 Screening Round 1 – mKOκ

DNA libraries of mKOκ mutants were created via error-prone PCR using the templates mKOκ-WT, cp mKOκ-47 and cp mKOκ-51. The resulting DNA fragments were sub-cloned into pRSETB via standard ligation with T4 ligase. Fluorescent proteins expressed in XL1 blue cells were screened on bacterial plates. The three criteria screened for were fast maturation, increased brightness and reduced excitability at 488 nm. The latter criterion was chosen due to the intention to use mKOκ as an acceptor in a FRET sensor. In combination with a green or yellow fluorescent protein as a donor, the long "shoulder" in the excitation spectrum of mKOκ, depicted in **Figure 44**, would lead to cross excitation.

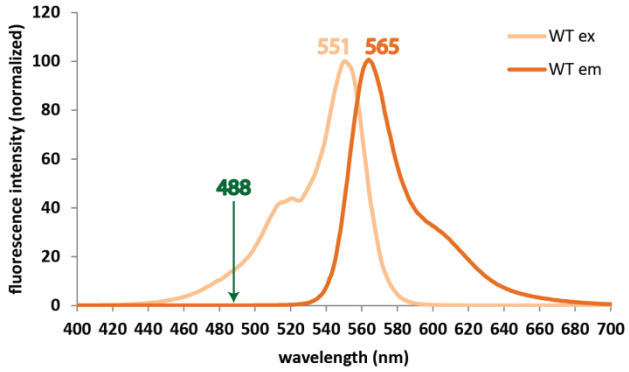

Figure 44: Excitation and Emission Spectra of mKOκ
Excitation and emission spectra of mKOκ normalized to their respective maxima. The undesirable "shoulder" in the excitation spectrum is indicated.

Maturation speed of a variant was assessed by conducting the first screening approximately 20-24 hours after transformation using a M205 FA fluorescence stereomicroscope (Leica). Both cp mKOκ-47 and cp mKOκ-51 only became fluorescent after a minimum of 48 hours, so every mutant that gained fluorescence within 24 hours represented a considerable improvement. A second screening was usually carried out approximately 48 hours after transformation to identify mutants, which matured slowly, but exhibited increased brightness. Some mutants were even bright enough to be manually detected using a stereo microscope.

To discern subtle increases in brightness (especially over the bright parental mKOκ-WT) and reduced excitability at 488 (an attribute difficult to identify), a CoolSNAP ES2 CCD camera was used with an LS/30 stand-alone xenon arc lamp (Lambda) and a 10-2 optical filter changer (Lambda). The following filters

were utilized for excitation: HQ 470 (40), HQ 500 (20) and HQ 546 (12), and for emission: HQ 535 (30) and HQ 585 (40).

A Python screening program was planned, and written by Christopher Zarbock, which compared each mutant to a sample of control colonies expressing mKOκ-WT screened along with each plate. Prior to an experiment, the experimenter marked the region in which control colonies were located. Three pictures were taken of the plate at different excitation and emission wavelengths. The first picture was taken at an excitation of 500 nm and an emission of 535 nm (**Figure 45A**), since almost all colonies are detectable at these wavelengths. A second picture was taken at an excitation of 546 nm and an emission of 585 nm (**Figure 45B**), and a third at an excitation of 470nm and an emission of 585 nm (**Figure 45C**). The former established the brightness and the latter probed for excitability at 488 nm.

Finally, the program compared the data collected for each colony to the mKOκ-WT colonies and identified those mutants, which exhibited higher performance.

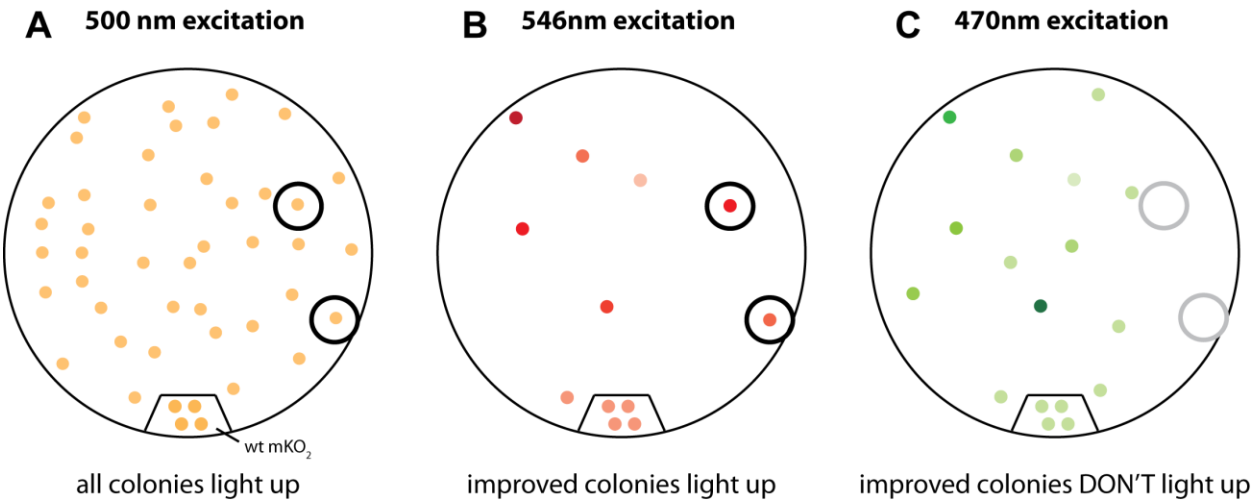

Figure 45: Principle of mKOκ Screening
Most colonies could be detected when imaged at ex 500 nm/em 535 nm **(A)**. Improved brightness of a protein could be determined at ex 546 nm/em 585 nm **(B)**. The undesirable excitability of a protein at 488 nm was tested at ex 470 nm/em 585 nm **(C)**.

A total of approximately 200 plates containing 100-400 colonies each were screened. Slightly more than 100 colonies were picked and their fluorescent proteins purified and tested *in vitro*.

Among the first locations within mKOκ found to have a considerable impact on the brightness of the protein were D141, H172 and G196. Site directed mutagenesis was attempted to find the most suitable amino acids at these locations, but a screening of the resulting library failed to yield any interesting results.

3.3.4 Screening Round 2 - mKOκ in a FRET Sensor

Since the ultimate aim was to use an improved version of mKOκ in a FRET sensor, a second round of screening was conducted with a library of cp mKOκ variants, mutated via error prone PCR and cloned into a vector containing a donor and a Ca^{2+} binding domain (**Figure 46**). Clover was used as a donor and troponin C of the sensor Twitch-3 was used as a Ca^{2+} binding domain. Cloning was achieved through SLiCE.

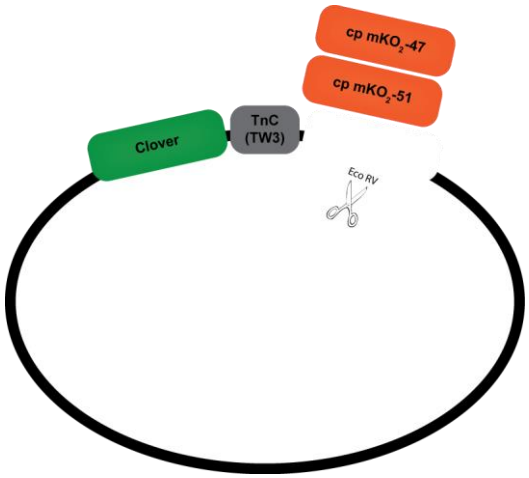

Figure 46: Cloning Strategy for mKOκ Screening Round 2
Scheme of the construct used for the second round of mKOκ screening: A vector containing Clover as a donor, and troponin C (TnC) of Twitch-3 as a Ca^{2+} binding protein, was linearized at a previously introduced EcoRV restriction site. Mutated mKOκ variants were cloned into the position of the acceptor.

Approximately 60 plates containing 500 colonies each (note the higher efficiency of SLiCE cloning compared to standard ligations using T4 ligase in chapter 3.3.3) were screened. 58 mutants were picked and characterized *in vitro*.

3.3.5 Summary of Promising Mutations

Table 21 contains a summary of all mutations identified in improved versions of mKOκ, cp mKOκ-47 and cp mKOκ-51 throughout the screening, merged into one sequence named “mut” (for “mutant mKOκ”). The resulting sequence is depicted in alignment with the parental mKOκ-WT, as well as its progenitors, including the original Kusabira Orange (KO). In addition, the cyan protein MiCy (derived from a stony coral (Karasawa et al., 2004)) is displayed, as it was found to share a surprising number of mutations with our newly discovered proteins in areas which to our knowledge, have not been investigated before (indicated in magenta).

Unique mutations, occurring only once throughout the screening, are indicated in yellow. Since most variants contained multiple mutations, we could only speculate as to which of them were responsible for the improvement. Mutations identified in more than one successful variant (making it more likely that they were beneficial) are indicated in magenta. The two mutations highlighted in turquoise only occurred once, but in a very bright variant which exhibited fast maturation. Since this variant did not bear any additional mutations, at least one of them had to be responsible for these characteristics.

The comparison of the “mut” sequence with mKO, mKOκ and mKO2 revealed that most prosperous sites identified in our screening had not been considered in any of the Kusabira Orange variants. Moreover, none of them were located at/near sites important for the maintenance of the monomeric structure of the protein (indicated in blue). One mutation however, was found at position G196, one of the locations known to influence protein aggregation (indicated in green), therefore potentially triggering its onset.

KO	MVSVIKPEMKMKYFMDGSVNGHEFTVEGEGTGKPYEGHQEMTLRVTMAKGGPMPFSFDLVSHTFCYGHRP
mKO	MVSVIKPEMKMRYYMDGSVNGHEFTIEGEGTGRPYEGHQEMTLRVTMAKGGPMPFAFDLVSHVFCYGHRP
mKOκ	MVSVIKPEMKMRYYMDGSVNGHEFTIEGEGTGRPYEGHQEMTLRVTMAEGGPMPFAFDLVSHVFCYGHRV
mKO2	MVSVIKPEMKMRYYMDGSVNGHEFTIEGEGTGRPYEGHQEMTLRVTMAEGGPMPFAFDLVSHVFCYGHRV
mut	TMSVIIPEMKTRYYMDGSVNGHEFTIAGEGIGRPYEGHQEMTLRVTMAEGGPMPFAFDLVSHVFCYGHRV
MiCy	---GIAQEMRTKYRMEGSVNGHEFTIEGVGTGNPYEGKQMSELVIIKSKGKPLPFSFDILSTAFQYGNRC
KO	FTKYPEEIPDYFKQAFPEGLSWERSLQFEDGGFAAVSAHISLRGNCFEHKSKFVGVNFPADGPVMQNQSS
mKO	FTKYPEEIPDYFKQAFPEGLSWERSLEFEDGGSASVSAHISLRGNTFYHKSKFTGVNFPADGPIMQNQSV
mKOκ	FTKYPEEIPDYFKQAFPEGLSWERSLEFEDGGSASVSAHISLRGNTFYHKSKFTGVNFPADGPIMQNQSV
mKO2	FTKYPEEIPDYFKQAFPEGLSWERSLEFEDGGSASVSAHISLRGNTFYHKSKFTGVNFPADGPIMQNQSV
mut	FTKYPEEIPDYFKQAFPEGLSWERSLVFEDGGSASVSAHISLRGNTFYHISKFTGVNLPADGPIMQNQSV
MiCy	FTKYPADMPDYFKQAFPDGMSYERSFLFEDGGVATASWSIRLEGNCFIHNSIYHGVNFPADGPVMKKQTI
KO	DWEPSTEKITTCDGVLKGDVTMFLKLAGGGNHKCQFKTTYKAAKKILKMPQSHFIGHRLVRKTEGNITEL
mKO	DWEPSTEKITASDGVLKGDVTMYLKLEGGGNHKCQFKTTYKAAKKILKMPGSHYISHRLVRKTEGNITEL
mKOκ	DWEPSTEKITASDGVLKGDVTMYLKLEGGGNHKCQFKTTYKAAKEILEMPGDHYIGHRLVRKTEGNITEQ
mKO2	DWEPSTEKITASDGVLKGDVTMYLKLEGGGNHKCQMKTTYKAAKEILEMPGDHYIGHRLVRKTEGNITEQ
mut	GWEPSTEIITASDGILKGDVTMYLNLGRGGYLRCQFKTTYKAAKDILEMPGDHYIDHRLIRKTVGNITVL
MiCy	GWDKSFEKMSVAKEVLRGDVTQFLLLEGGGYQRCRFHSTYKTEKPV-AMPPSHVVEHQIVRTDLGQTAKG
KO	VEDAVAHC
mKO	VEDAVAHS
mKOκ	VEDAVAHS
mKO2	VEDAVAHS
mut	VEDAVARHSTGGMDELYKGGTGGS
MyCy	FKVKLEEHAEAHVNPLKVK

Table 21: Summary of Potentially Beneficial Mutations Identified in mKOκ
Alignment of a merged sequence of all potentially beneficial mutations discovered in improved mKOκ variants (named "mut" for mutant mKOκ), with mKOκ-WT and all its progenitors, as well as the cyan protein MyCy. Color code: red – folding mutations, blue – mutations necessary for disruption of the dimer, green – inhibition of aggregation, grey – mKOκ/mKO2 mutations (faster maturation), orange – additional mKO2 mutation, yellow – new mutations found only once, magenta – new mutations appearing several times, turquoise – new mutations found only once, but in a significantly improved mutant

3.3.1 Combination of Promising Mutations

Insights gained from the screening were used to design a variant of cp mKOκ-51 combining the most prosperous mutations. The following nine mutations were chosen:

- D141G, N171Y, H172L, K173R, G196D and E209V, as they were discovered in a number of succesful variants, supporting the assumption that they were instrumental in their improvement.
- T31I and K120I, as they were the only two mutations identified in a very bright mutant with fast maturation, and finally;
- M11T, as this mutation was thought to decrease the second excitation peak of mKOκ, the importance of which will be discussed in chapter 3.3.2.3.

The resulting variant will be referred to as cp mKO3 in the following.

3.3.2 Characterization of mKOκ-based New Fluorescent Proteins

Guidelines suggested by Ai and colleagues (Ai et al., 2014) were used to characterize the new versions of mKOκ. To this end, full absorbance, excitation and emission spectra were recorded and quantum yield, extinction coefficient, pH dependence, as well as oligomeric structure were determined.

3.3.2.1 Emission and Excitation

Full excitation and emission spectra were recorded using a Cary Eclipse Fluorescence Spectrometer (Varian), set to a data interval of 1 nm and an excitation and emission slit width of 5 nm. Emission spectra were recorded at an excitation of 551 nm, and excitation spectra were recorded at an emission of 565 nm. An overlay of the spectra revealed no significant shifts, indicating that the emission and excitation profiles of these new mKOκ variants had not been altered (**Figure 47**). In the shoulder of the excitation spectrum (depicted in **Figure 44**), which we intended to eliminate, a slight variation was detected at approximately 500 nm. An overlay with mKOκ-WT did reveal however, that none of the mutants exhibited a decreased excitability in this region, and some actually displayed a minor increase.

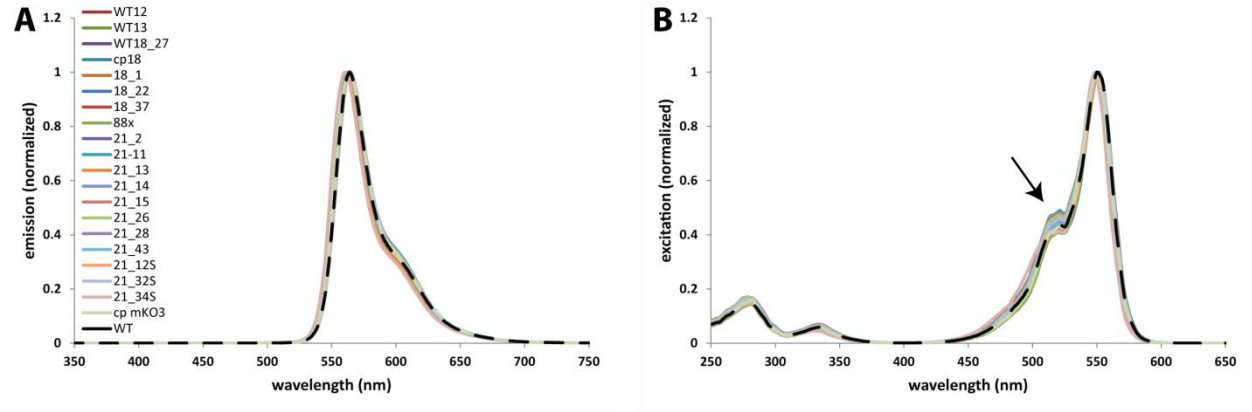

Figure 47: Excitation and Emission Spectra of New mKOκ Variants
Overlay of emission spectra (excitation at 551 nm) **(A)** and excitation spectra (emission at 565 nm) **(B)** of new mKOκ variants in comparison to the original mKOκ-WT which is plotted as a broken black line. The undesirable "shoulder" in the excitation spectrum, which we attempted to decrease, is marked with an arrow. Spectra were normalized to their respective maxima.

One mutant however, to be referred to as WT-7, which had appeared especially bright in the screening, exhibited excitation and emission spectra entirely different from the parental mKOκ-WT. With an excitation maximum at 500 nm and an emission maximum at 508 nm, this mutant had actually turned green (**Figure 48**).

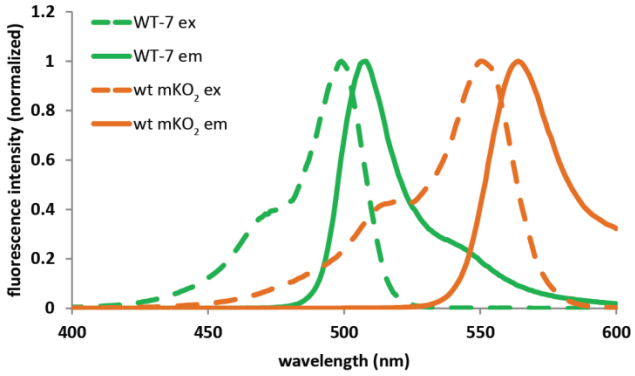

Figure 48: Excitation and Emission Spectra of mKOκ-WT and WT-7
Excitation (broken line) and emission (solid line) spectra of the green mutant WT-7 and the orange parental mKOκ-WT. Spectra were normalized to their respective maxima.

3.3.2.2 Absorbance

Absorbance spectra were measured using an Infinite® M200 PRO plate reader (Tecan). As with the previous measurements, most of the spectra resembled one another, with only minor variations in height and width of the aforementioned shoulder at around 500 nm (**Figure 49**).

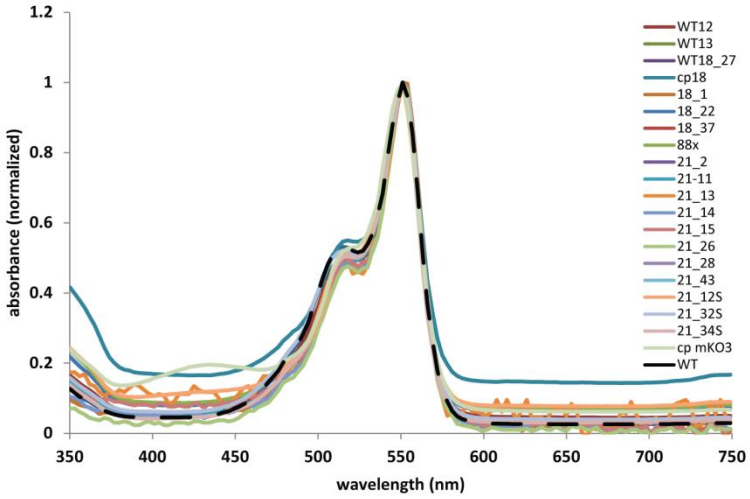

Figure 49: Absorbance Spectra of New mKOκ Variants
Overlay of absorbance spectra of new mKOκ variants and comparison to parental mKOκ-WT, plotted as a broken black line. Spectra were normalized to their respective maxima.

Two absorbance spectra however, differed entirely from the others, namely those of the previously mentioned green WT-7, and a mutant to be referred to as 21S-34. The latter exhibited two equally high peaks; the expected mKOκ peak at 551 nm and an additional peak at 500 nm. The second peak was almost identical to that of WT-7, making 21S-34 a perfect intermediate between the green and the orange version or state of mKOκ (**Figure 50**).

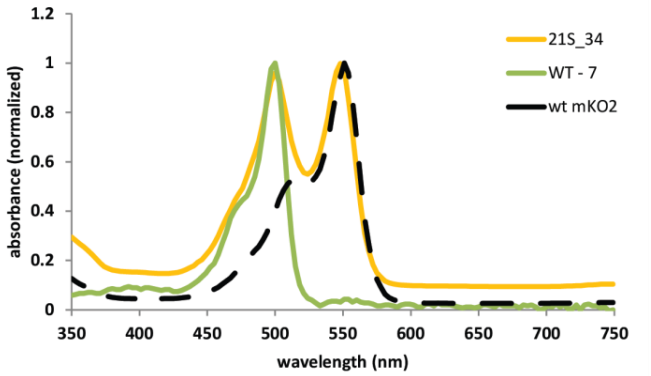

Figure 50: Absorbance Spectra of mKOκ-WT, WT-7, and 21S_34
Absorbance spectra of new mKOκ variants WT-7 and 21S_34 in comparison to the parental mKOκ-WT, plotted as a broken black line. Spectra were normalized to their respective maxima.

3.3.2.3 Analysis of the Second Excitation and Emission Peak

In the course of this project, distinct additional excitation and emission peaks (at 500nm and 508nm respectively) were noted for several mKOκ mutants. Therefore, all variants were probed for the presence of a second peak. To this end, they were excited at 490 nm, which allowed simultaneous recording of both emission peaks (**Figure 51**). Interestingly, almost all mKOκ variants featured a second peak, with mKOκ-WT's being amongst the most significant. A mutant to be referred to as 21_43 and our cp mKO3 (chapter 3.3.1), were the only two not to exhibit a second peak at all.

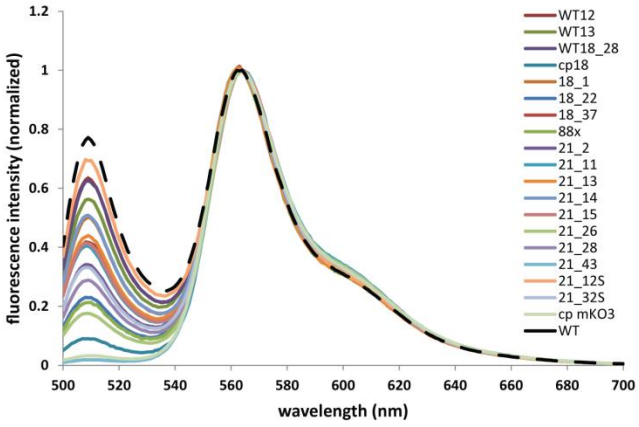

Figure 51: Emission Spectra of New mKOκ Variants Excited at 490 nm
Overlay of emission spectra (excitation at 490 nm) of all mutants of mKOκ in comparison to the parental mKOκ-WT, depicted as a broken black line. Spectra were normalized to their respective maxima.

Figure 52A depicts the shape and position of the two excitation and emission peaks of mKOκ-WT. To compare the intensities of the two emission peaks, mKOκ-WT was excited first at 500 nm and then at 551 nm, under otherwise identical settings (**Figure 52B**). Measurements revealed that the second peak had a fluorescence intensity constituting 16.4 % of the main peak.

As long as mKOκ was excited close to its main excitation maximum (at 551 nm), this second peak would not be problematic. If however, mKOκ was to be used as a FRET acceptor in combination with a green donor (as intended), this second peak would overlap with the donor excitation and emission, distorting FRET. The same would occur if mKOκ was to be used in multicolor imaging experiments.

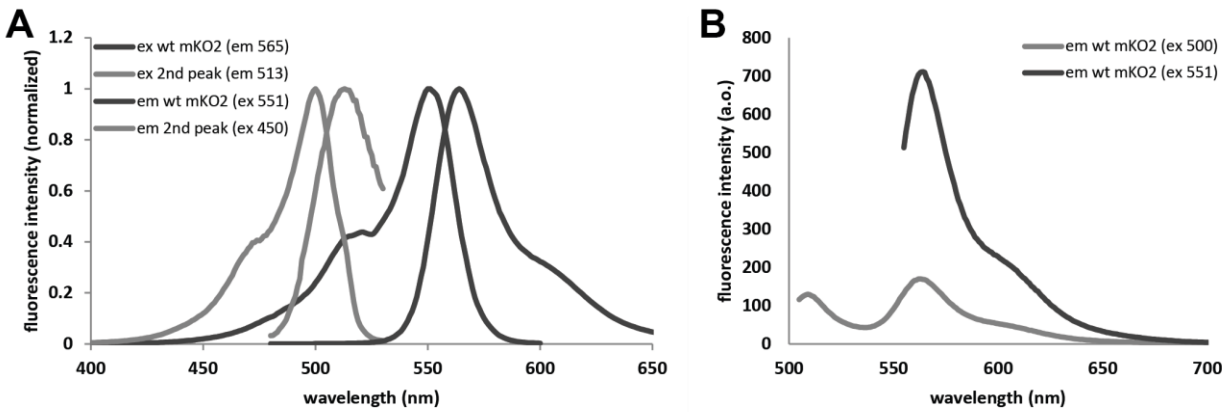

Figure 52: The Two Excitation and Emission Peaks of mKOκ and Green Fluorescent Peak Relative to Orange Fluorescent Peak
The two Excitation and emission peaks of mKOκ-WT are depicted, normalized to their respective maxima **(A)**. mKOκ-WT emission spectra with excitation at 500 nm and 551 nm, under otherwise identical settings **(B)**.

3.3.2.4 Mutations Causing/Eliminating the Second Peak

With the mutants WT-7, 21_43 and 21_34S, we had an entirely green, an entirely orange and an intermediate version of mKOκ available. An attempt was made to pin down the mutations causing this color shift. We assumed that the green version of mKOκ was the green dead-end product, which could potentially develop during chromophore formation (Strack et al., 2010). We therefore assessed mutations in these variants, which were located in close proximity to the chromophore, and could potentially alter the interaction of the maturing chromophore with its environment. Indeed, each of the mutants exhibited one mutation which appeared close enough to allow interaction with the chromophore (**Figure 53**). These positions were; M11T in the orange, M41V in the green and Q210L in the mixed mutant (nomenclature

based on mKOκ-WT). Our assumption was confirmed when the mutation M11T was included in the cp mKO3 construct, resulting in the only mutant besides 21_43 not to exhibit any traces of the green mKOκ dead end product.

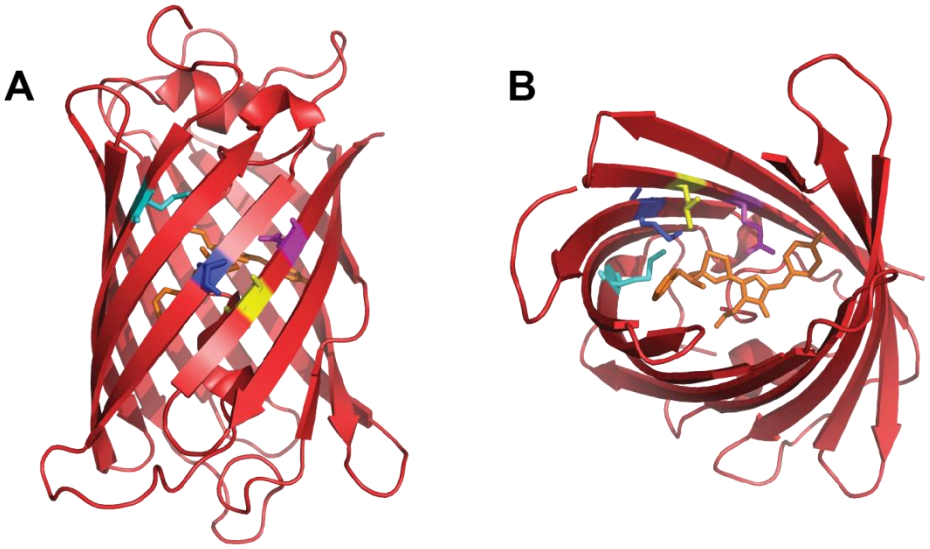

Figure 53: Locations Relevant for the Green and Orange Fluorescent Variants of mKOκ
Protein structure of mKOκ with chromophore depicted in orange, and positions thought to interfere with chromophore formation highlighted in color (pink – E212, known to be important for chromophore formation (Kikuchi et al., 2008), yellow – M11T, found in orange mutant, blue – M41V, found in green mutant, turquoise – Q210L, found in mixed mutant)

3.3.2.5 Quantum Yield, Extinction Coefficient, pH Stability and Oligomeric Structure

For some of the most promising mKOκ variants, the quantum yield was determined, using parental mKOκ-WT as a reference. For those variants exhibiting the highest quantum yields, the extinction coefficient was also determined, and their brightness was calculated (**Table 22**). In measuring protein concentrations to determine the extinction coefficient, proteins were denatured via Guanidin HCl and heat. This process revealed that the mutants 21_43 and cp mKO3 were highly resistant to heat-denaturation compared to mKOκ-WT.

mutant name	quantum yield	extinction coefficient	brightness	additional observations
mKOκ WT	**0.61 literature**	**96872**	**59.1**	
18-22	0.54			
88x	0.55			
21-2	0.54			
21-26	0.65			
21-43	0.66	86396	57.0	heat-resistance
21S-12	0.63			
21S-32	0.57			
21S-34	0.62			
cp mKO3	0.71	70387	50.0	heat-resistance

Table 22: Properties of Promising mKOκ Variants
Quantum yields, extinction coefficients and brightness values of some of the most promising mKOκ mutants.

To determine the pH stability of mutant cp mKO3 in comparison to mKOκ-WT, maximum emission was recorded for both variants in buffers exhibiting pH values ranging from pH 3 to pH 10. A sigmoidal fit was applied to the resulting curves, revealing pK_a values of approximately 5.15 for both variants (**Figure 54**).

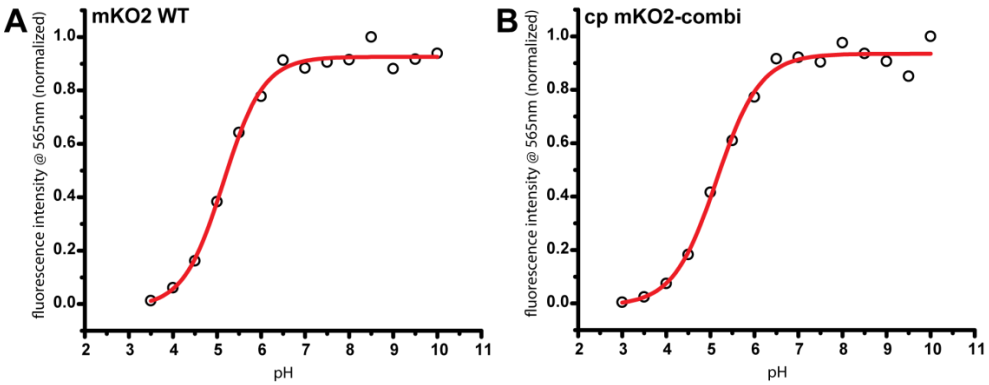

Figure 54: pH Stability of cp mKO3
Fluorescence intensity of mKOκ WT **(A)** and cp mKO3 **(B)** at different pH values, ranging from pH 3 to pH 10. A sigmoidal fit (DoseResp) was applied.

All red fluorescence proteins discovered so far, bear the disadvantage of being obligate dimers or tetramers with a tendency to form aggregates. They must therefore be converted into monomers, requiring numerous tedious steps. The original Kusabira Orange, from which mKOκ and all its progenitors originated, is no exception. To determine if the additional mutations to mKOκ left its monomeric structure intact, we tested some of the new variants in native PAGE, and compared them to the monomer mKOκ-

WT, the dimer HcRed and the tetramer cjBlue (**Figure 55**). Even though both tested mKOκ mutants navigated through the gel matrix slower than the parental monomer mKOκ-WT, they were distinctively faster than the di- and tetramer, confirming that they were still monomeric.

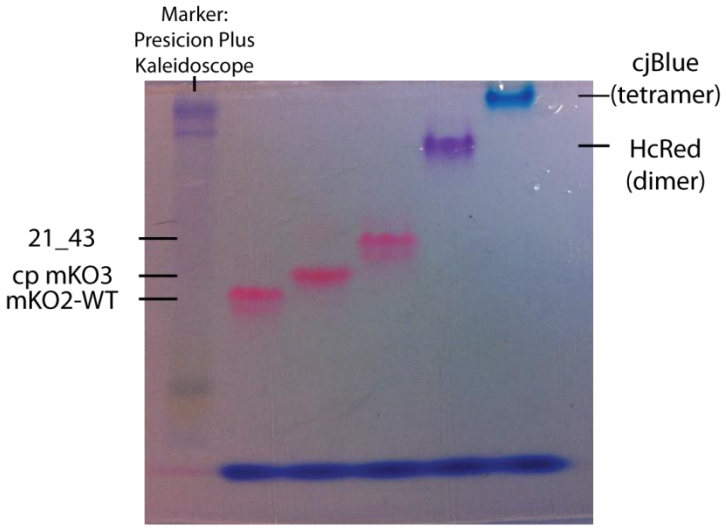

Figure 55: Native PAGE Revealing Oligomeric Structure of mKOκ Variants
Precision plus Kaleidoscope was used as a protein marker. The following samples were applied: mKOκ-WT, cp mKO3, 21_43, HcRed and cjBlue (from left to right).

3.4 Working Towards a Red-shifted Genetically Encoded Ca^{2+} FRET Sensor

3.4.1 Test of Potential FRET Pairs

Eleven red-shifted Ca^{2+} sensor prototypes (based on FRET) were created from:

- ten potential donors with emission maxima in the green, yellow and orange regions of the spectrum
- three potential acceptors with emission maxima in the orange and red regions, and
- Ca^{2+} binding domains based on troponin C from the 'Twitch' sensor series

In addition, cp variants of selected fluorescent proteins, and C-terminal truncations of the donors were tested. In some cases, the conventional order of components (i.e. donor N-terminal and acceptor C-terminal) was reversed (**Figure 56**, **Table 23**).

Donor	Accteptor	R_0	ΔR/R (%)
mAzami Green	mKOκ	**0.39**	**34**
mAzami Green (C-terminal)	mKOκ (N-terminal)	**1.51**	**21**
Clover	mKOκ	**0.54**	**55**
CloverΔ11	mKOκ	**0.62**	**83**
cpCitrine 174	mKOκ	**0.88**	**73**
cpT-Sapphire 174	mKOκ	**0.30**	**108**
Dreiklang	mKOκ	**0.95**	**56**
Dreiklang Δ11	mKOκ	**0.81**	**173**
EGFP	mKOκ	**0.47**	**58**
EGFP (C-terminal)	mKOκ (N-terminal)	**0.52**	**110**
EGFP Δ11	mKOκ	**0.49**	**108**
LSSmOrange	mKate 2	**0.21**	**48**
mNeon Green	mKOκ	**0.76**	**35**
mUKG	mKOκ	**0.72**	**41**
mUKG (C-terminal)	mKOκ (N-terminal)	**0.92**	**50**
SFCitrineΔ11	mKOκ	**0.90**	**86**
T-Sapphire	mKOκ	**0.26**	**64**
T-Sapphire Δ11	mKOκ	**0.32**	**113**
mKOκ WT-7	mKOκ	**0.46**	**9**

Table 23: R_0 and ΔR/R Values of Prototype Sensors Tested *in vitro*
Sensors selected for further experiments are highlighted in green. The term Δ11 indicates a C-terminal truncation of the corresponding protein by 11 amino acids.

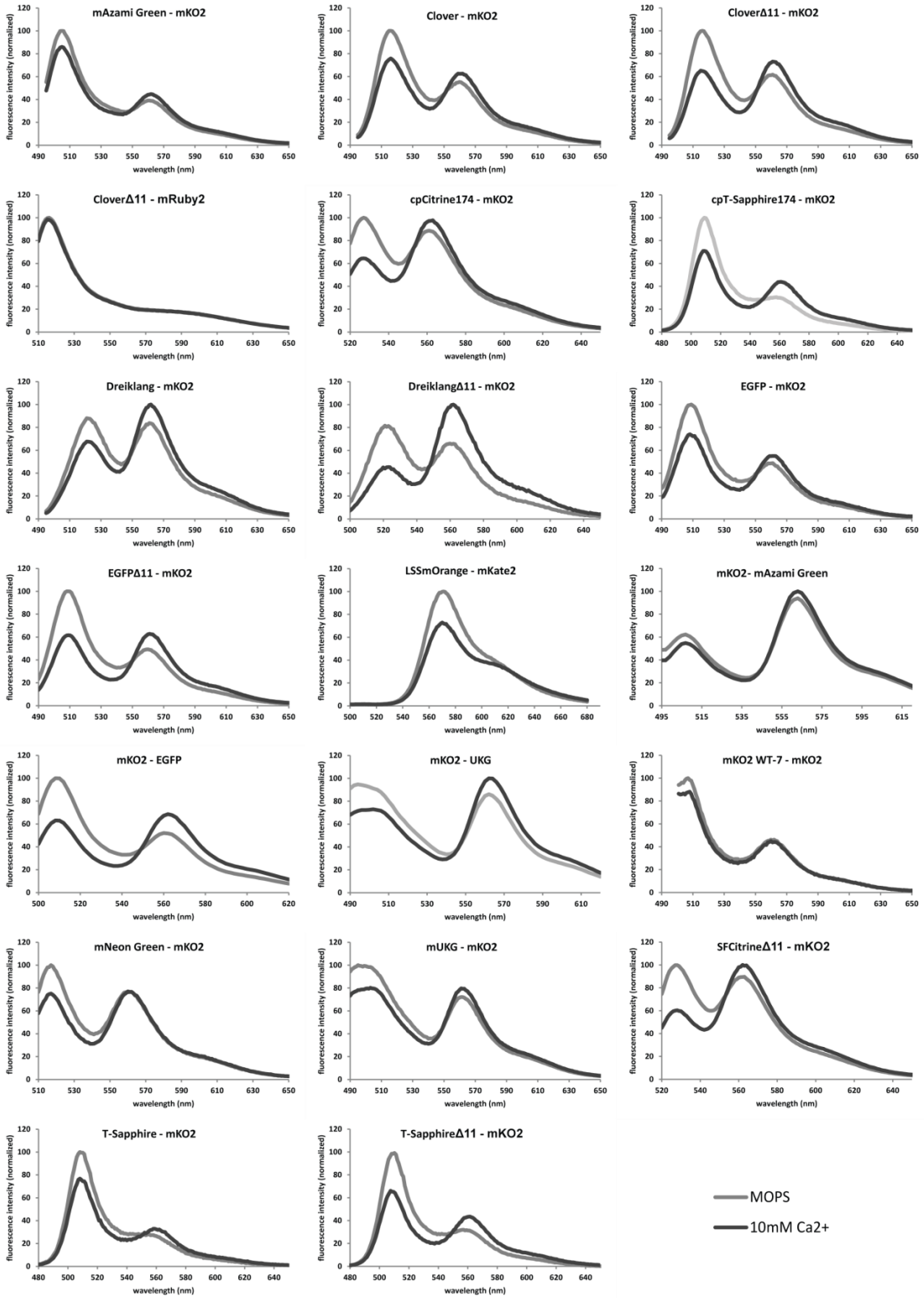

Figure 56: Emission Spectra of Prototype Sensors Tested *in vitro*
Ten different donors were tested with 3 different acceptors and a troponin C-based Ca^{2+} moiety. The term Δ11 indicates a C-terminal truncation of the corresponding protein by 11 amino acids. Spectra were normalized to their respective maxima.

3.4.2 FRET Sensors Comprising Newly Developed cp mKOκ Variants

Since the use of circular permutated versions of given proteins (see chapter 1.1.3) can greatly impact the FRET efficiency of a sensor by changing the orientation of the chromophores, our newly developed cp variants of mKOκ were tested in combination with various donors. Many of the sensors created in this manner however, either failed to function or exhibited ratio changes considerably lower than in the corresponding sensors formed with mKOκ-WT. The most successful sensors consisted of DreiklangΔ11 with a cp variant of mKOκ (exhibiting a ΔR/R value of approximately 95%), and SFCitrineΔ11 with a cp variant of mKOκ (exhibiting a ΔR/R value of approximately 30%).

3.4.3 Screening of the Most Promising FRET Pairs

Due to its superior brightness, sharp emission spectrum, low pH sensitivity and high photostability, mKOκ was chosen as an acceptor for a red-shifted Ca^{2+} FRET sensor. Dreiklang, SFCitrine, T-Sapphire and Clover were chosen as potential donors after appearing promising in the respective prototype sensors (**Figure 56**, **Table 23**). Dreiklang and T-Sapphire both exhibited special features, with the former being photoswitchable and the latter displaying an exceptionally large stokes shift, thereby eliminating any cross-excitation of the acceptor.

3.4.3.1 Library Design

A library of red-shifted Ca^{2+} FRET sensors was designed, building on the success of the extensive random linker library created for the 'Twitch' sensor screening (see chapter 3.2.2.1), and superior cloning efficiency achieved with SLiCE cloning. The idea was to incorporate as many variables as possible using the following components:

- Four donors
- Five troponin C-based Ca^{2+} binding domains, originating from the Twitch sensors 1-5, with either one or two Ca^{2+} binding sites, as well as a range of different linkers and additional mutations, granting them a variety of qualities
- Linkers of one to four amino acids in length

- Multiple acceptors (potentially; dependent upon the results of the mKOκ screening being conducted simultaneously)

DNA fragments of the linearized pRSETB vector, donors, Ca^{2+} binding domains and acceptors were kept separate and only combined into a sensor in a single cloning step prior to the screening. This ensured that the library remained flexible, and allowed the addition or removal of variables at any time (**Figure 57**).

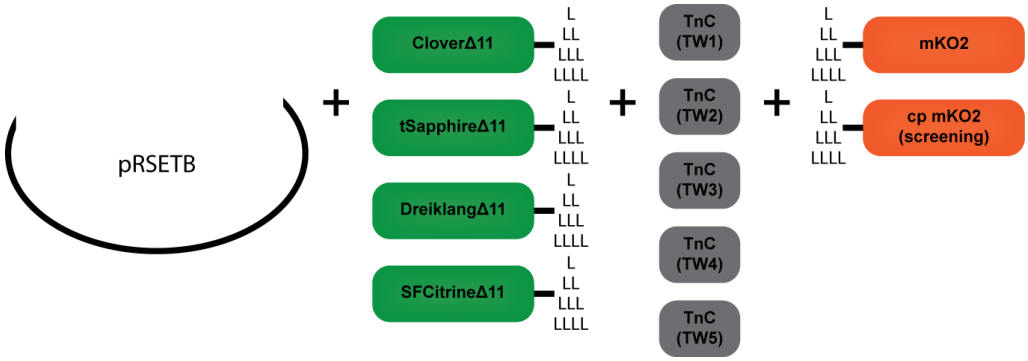

Figure 57: Design of the First Library of Red-shifted Ca^{2+} FRET Sensors
DNA fragments of vector pRSETB, donors with attached random linkers (one to four amino acids), Ca^{2+} binding domains based on troponin C (TnC) (originating from Twitch-1-5), and acceptors with random linkers (one to four amino acids) were combined in a single cloning step immediately prior to screening.

Unfortunately, SLiCE cloning was not effective enough to generate a yield of more than 100 to 300 colonies per plate, greatly decreasing the throughput of the bacterial plate screening. In response, a new library was designed, requiring fewer DNA fragments per cloning step. This increased the number of colonies per plate, but at the expense of the library's flexibility. In the new library, a particular donor and acceptor pair, and random linkers were attached to pRSETB, with the Ca^{2+} binding domain cloned in later (**Figure 58**).

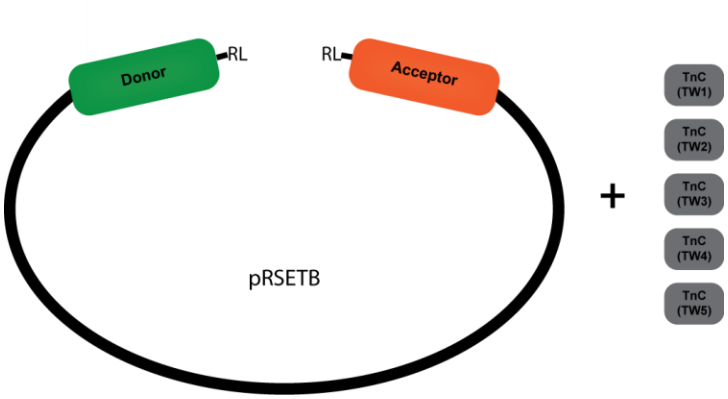

Figure 58: Design of the Second Library of Red-shifted Ca^{2+} FRET Sensors
A particular donor and acceptor pair with random linkers (RL) was already attached to the vector, and only the Ca^{2+} binding domains based on troponin C (TnC) (originating from Twitch-1-5) were added afterwards.

Since the 'Twitch' linker library we designed using the degenerate primer codon NNN proved itself biased towards certain amino acids (see chapter 3.2.2.1), the reduced codon set NNB was tested in its place. NNB encodes for all amino acids, but only 48 of the 64 codons, thereby reducing the number of redundant codons, as well as the probability of stop codons.

To determine if our new library did indeed achieve full coverage whilst reducing bias, 12 sensors with different linkers of one to four amino acids in length were picked at random and sequenced (**Table 24**), revealing that a bias was still existent, but that it had shifted to different amino acids.

F	L	Y	C	W	P	H	Q	I	M	T	N	K	S	R	V	A	D	E	G	Stop
1	7	2	3	1	1	5	1	1	2	2	3	0	6	6	6	4	1	0	1	0

Table 24: Occurrence of Amino Acids with the Codon NNB
Occurrence of single amino acids in random linkers produced with the degenerate codon NNB, encoding for all 20 amino acids, but not for all codons and also not for the stop codon.

3.4.3.2 Bacterial Plate Screening

Approximately 150 000 colonies were screened on a total of 145 plates. In contrast to the 'Twitch' screening, we decided to not pick a certain number of (comparatively well performing) colonies per plate, but to pick only those with outstanding characteristics. Changing the criteria resulted in only ~150 sensor variants being purified and tested *in vitro*. Unfortunately, the majority of them proved greatly inferior to

their parental sensors in terms of their ΔR/R values. **Figure 59** depicts sensor variants, which at least produced a response, with their parental sensors displayed as a reference.

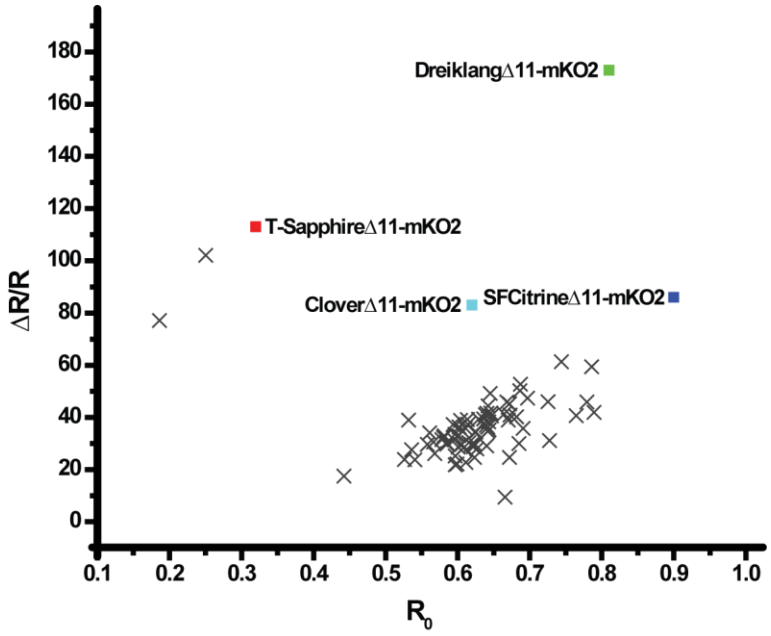

Figure 59: Bacterial Plate Screening for a Red-shifted Indicator
Plot of functional sensor variants picked and measured *in vitro*. The parental sensors are displayed in color as a reference.

3.4.4 *In vitro* Characterization of the Best Red-shifted Sensor

The best red-shifted sensor identified was purified and characterized *in vitro*. It turned out to be one of the prototypes depicted in **Figure 56**, consisting of DreiklangΔ11 as a donor (excitation: 515 nm, emission: 529 nm), mKOκ as an acceptor (excitation: 551 nm, emission: 565 nm), and the troponin C– based Ca^{2+} binding domain of Twitch-3. It exhibited an in vitro R_0 of 0.81 and a ΔR/R upon Ca^{2+} binding of approximately 170 % (**Table 23**). First of all, we verified that Dreiklang was still photoswitchable and could be switched on (365 nm) and off (405 nm) successfully, despite the additional sensor components troponin C and mKOκ (**Figure 60A**). Similarly, we established that the switching characteristics were not affected by the addition of Ca^{2+} and the associated conformational changes in the sensor (**Figure 60B**). A Ca^{2+} titration revealed a K_d value of 365 nM (**Figure 60C**), falling within the physiological range of most cell experiments. Unfortunately, cross-excitation of mKOκ was unavoidable, even if Dreiklang was excited well

below its excitation maximum. Such cross-excitation would not only interfere with FRET, but also lead to constant background in experiments utilizing the switching capability of Dreiklang.

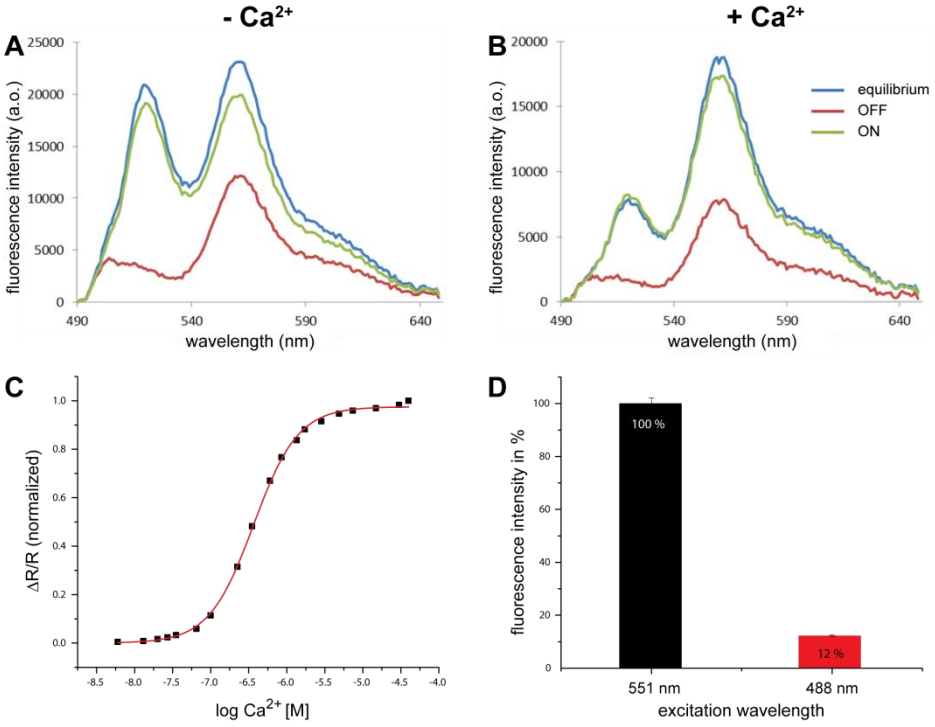

Figure 60: Characterization of Dreiklang – Twitch-3 – mKOκ Sensor
Switching behavior of the sensor without Ca^{2+} **(A)** and in the Ca^{2+}-bound state **(B)**. Ca^{2+} titration with an applied sigmoidal fit (DoseResp), revealing a K_d value of 365 nM **(C)**. Fraction of mKOκ emission potentially elicited through cross-excitation (despite excitation well below Dreiklang's excitation maximum), relative to maximal mKOκ emission **(D)**.

4 Discussion

4.1 Establishment of a New Ca^{2+} Sensor Screening Assay

We developed a cost effective and efficient assay to screen genetically encoded Ca^{2+} indicators on bacterial plates. Designing new indicators used to be a tedious and time-consuming process, involving the expression, purification, and *in vitro* characterization of countless sensor proteins. Improvements were undertaken on the basis of rational design, which was dependent on the availability of structural information on all components. Moreover, each sensor as a whole represented a completely artificial protein construct, assembled from proteins derived from various species, making it difficult to predict its behavior, even with detailed knowledge on all its individual aspects. Finally, it was often observed that findings made for one sensor could not be readily transferred to another sensor, even if the two were very similar. The severe signal loss observed in the optimized FRET sensor Twitch-2A, when its donor ECFP was replaced with Cerulean3 (a fluorescent protein which differs from ECFP by only a few mutations) is an example of such an instance (see chapter 3.2.2.3). Existing screening assays were either considered too inefficient (e.g. (Tian et al., 2009)), or were not compatible with FRET sensors (e.g. (Zhao et al., 2011)).

For our screening assay, we expressed a library of GECIs on the basis of FRET in bacterial cells, which were grown on agar plates, with each bacterial colony expressing a different sensor variant. Bacteria were chosen because they are cheap, easy to propagate, and readily express diverse foreign proteins. While it seemed obvious to choose a bacterial strain for the assay, which has the capacity to produce as much protein as possible, we observed that strains producing little protein actually proved more suitable. This seemed counterintuitive at first, but can be attributed to a reduced likelihood for aggregation and mutual interference of the expressed sensors.

We found that timing was of high importance both for the duration of incubation and the point in time chosen for imaging. Blotting colonies onto blotting paper before imaging proved optimal, not due to the autofluorescence of the agar (as expected), but because applied solutions were able to diffuse better, resulting in larger signal changes. Applied to blotting paper, solutions were able to infiltrate the colonies not only from above, but also from the soaking paper underneath. Furthermore, it is likely that the tight assembly of single cells in a colony, was loosened up after the blotting process.

The uptake of extracellularly applied Ca^{2+} into the cytoplasm proved to be limited in the absence of external assistance, as has been observed previously (e.g. (Gangola & Rosen, 1987)). Since we assumed that the inner membrane of *E.coli* was the barrier for Ca^{2+} (whereby it could freely enter the cell's

periplasm), we used ionomycin to transport Ca^{2+} across the inner membrane. As ionomycin did not seem to be able to cross the outer membrane however, we utilized polylysine in order to further increase outer membrane permeability. The combined application of suitable concentrations of ionomycin and polylysine was able to greatly increase the Ca^{2+} uptake into the cytoplasm, allowing us to detect distinct signal changes within our intracellularly expressed Ca^{2+} indicators. Caution was required regarding the concentration of Ca^{2+}, since the application of too much Ca^{2+} induced a change of the intracellular pH. This had the potential to lead to a disturbance of FRET measurements, as some fluorescent proteins are very pH sensitive and become brighter or dimmer following a change in pH. Such unwanted side-effects bear the risk of being overlooked, leading to an over- or underestimation of the tested indicators. In a single fluorophore sensor, there is no reference allowing the experimenter to distinguish the desired sensor signal from such artifacts. In a FRET sensor on the other hand, a reference can be established by recording traces of the acceptor being directly excited, in addition to the FRET signal.

The reproducibility of our screening method was tested by screening the same sensor or fluorescent protein repeatedly over several days. The R_0 values of the sensors tested remained very consistent in our assay from experiment to experiment and from day to day, and facilitated easy discrimination of different sensors. More variation was observed in the $\Delta R/R$ vales however. The uneven application of solutions was identified as the main cause of these discrepancies, meaning that some colonies were either not as permeable to Ca^{2+} as others, because they had not received the same amount of polylysine and ionomycin, or had simply not received sufficient Ca^{2+}. In response, attempts were made to improve the application of solutions, which was initially conducted using plastic spray bottles. Flooding the blotting paper with solution was not a viable alternative, since entire colonies were washed off and could be observed as fluorescent particles floating in the solution, suggesting that a great amount of invisible contamination also occurred (data not shown). In addition, substantially more solution was required in order to cover the paper (which had a diameter of approximately 8 cm) in solution compared to simply soaking it, making each experiment more expensive.

A nebulizer was then tested, combining the qualities of even distribution of liquid and sparse application. However, the amount of applied solution, even after a minute or more, was too small to induce sensor signal changes comparable to those achieved through alternative methods (data not shown). The most effective method we trialed was the use of a spray gun commonly used for spray painting. This method produced even spray patterns at a radius large enough to cover a whole plate when simply aiming for its center. This reduced human error caused by the experimenter having to move the spray nozzle around whilst spraying, in an attempt to achieve full coverage. The build of the valve however, which all spray

guns have in common, did account for a higher concentration of solution at the center, and a decline towards the edges. Nevertheless, this inconsistency was preferable to the results achieved with the spray bottle, as it was both predictable and reproducible, and could potentially be taken into account in a program used to analyze the screening data.

Data acquired through plate screening was correlated with *in vitro* data, by purifying and measuring all sensors on a screening plate. While the R_0 values of both methods showed rather good correlation, the $\Delta R/R$ values did not match up as well. Nevertheless, since four of the five sensors performing best *in vitro* could have been identified by picking and purifying only 8 % of the total sensors analyzed, the result was still satisfactory. We reasoned that an underestimation of sensors in the plate screening was to be anticipated, due to the uneven application of solutions and non-uniformity of illumination in our screening set-up (see chapter 3.1.8.1), as well as a potential under- or overexpression of protein in *E.coli*. Nevertheless, we wanted to understand why some sensors performed so well in bacteria, yet were barely functional *in vitro*. A transfection of these sensors into mammalian cells revealed that they regained their full function when reintroduced into a cellular environment. The reason that these sensors functioned in cells, but not *in vitro*, could be that they required some sort of integral component contained in the cytoplasm to function. Alternatively, the sensitive structure of these sensors might have been altered during protein purification, either through the rough manual handling, or due to the chemicals and enzymes used, in which case an alternative purification protocol (e.g. French press) might better preserve their function. That the strong performance of these sensors in bacteria can also be reproduced in mammalian cells speaks in favor of our screening assay, proving it even more reliable than previously anticipated. In light of this, sensors performing outstandingly well on bacterial plates, but poorly *in vitro*, should not necessarily be excluded from further testing. That being said, considering such sensors for further experiments would also pose new challenges. Regarding purification for example, an alternative protocol would need to be adopted, which does not affect the sensors. Alternatively, a method would have to be established to fully characterize them *in vivo*, allowing comparison to existing sensors.

In summary, our bacterial plate screening assay greatly reduced the number of sensors to be purified and tested *in vitro*. Moreover, it significantly accelerated the testing process, facilitating the evaluation of up to 1000 different sensor variants within a time span of mere minutes. The utilization of custom-written Matlab and Python programs simplified the testing further by making it automatic, thereby rendering the experimenter's continuous presence unnecessary. Employing a program also ensured that each experiment was carried out consistently, and analyzed in an unbiased way. The automated data analysis

further accelerated screening and made it possible to process large amounts of data, which would have otherwise been difficult to manage.

Numerous universal findings of our assay, such as the optimal bacterial strain, the timing, and the blotting, as well as the penetration of the outer membrane with polylysine, can be easily transferred to other screening assays. Infact, this has already occurred in a second bacterial plate screening assay for a genetically encoded RNA sensor, which was developed in our laboratory (Schifferer & Griesbeck, 2012).

Potential improvements of the assay include the identification of a more appropriate tool that can be used to apply solutions to the plates as evenly as possible. Alternatively, the need to apply solutions could be circumvented altogether by using molecular tools like the recently published light-induced genetically encoded Ca^{2+} releasing protein (Fukuda et al., 2014). Moreover, another means of penetrating the bacterial membrane should be established, for situations where ionomycin cannot be used. Alternatives might include isopropanol, which has been used for this purpose in other laboratories (Oliver Griesbeck, personal communication), or the inducible formation of pores, which could be based on the holin – endolysin system used by bacteriophages (Gao et al., 2013, Young, 2013). Furthermore, the whole screening process could be further automated, to reduce manual labor. To this end, a robot is currently being constructed in our laboratory by Arne Fabritius and David Ng. It will be able to image plates independently, analyze the data acquired, and pick a given number of well-performing colonies into 96 deep well plates, where they can then be cultivated. All that the experimenter will be required to do is manually exchange the plates and apply solutions as necessary.

4.2 Screening for Improved 'Twitch' Ca^{2+} Indicator Variants

Our newly developed screening assay was used to generate a series of genetically encoded Ca^{2+} FRET sensors. Initially, a huge linker library was designed. Two random linkers of one to four amino acids in length were introduced between the Ca^{2+} binding moiety and the fluorescent proteins on either side of it. With the diversification of up to eight amino acid positions, each with the potential to turn into one of 20 amino acids or a stop codon, and 16 possible combinations of linker length, we accepted that it would be impossible to cover the whole library with our screening. Nevertheless, after screening only a small fraction of it, we were able to identify a range of successful linker combinations, indicating that there is no single perfect specimen, but that many linkers have the potential to satisfy the set criteria. If one was inclined to investigate an entire linker library nevertheless, it would be necessary to conduct a number of

pre-tests in order to exclude, for example, certain linker lengths which appear less promising or perhaps even one of the two linkers, should a change in the other one be deemed more likely to give rise to a sensor improvement. Alternatively, one could optimize the linkers one by one, which would greatly reduce the number of possible combinations. Taking such measures early on however, will obviously eliminate many linker options. Assuming that the development of a successful linker pair does not require the identification of the perfect N-terminal and the perfect C-terminal linker individually, but a successful combination of both, this may result in the loss of potentially prosperous linker combinations. It is difficult to say in advance if screening a fraction of a huge random library or fully covering a smaller library will yield better results. In light of this, the best strategy is probably to focus on one of the two options, but be prepared to adapt it along the way if the desired results do not arise.

One refinement of the library which should definitely be implemented however, is the use of an alternative primer set instead of the NNN codon (encoding for all four nucleosides) used in this screening, in order to avoid redundant codons. This topic will be discussed in more detail in chapter 4.4.

Our second library, consisting of sensor variants which were mutated at certain "hot spots" within the Ca^{2+} binding domain, was a prime example of how rational design and screening can interlock. Initially, promising sites were identified based on the structural information available on troponin C, and a small library which was generated by randomly mutating these sites, was screened. Out of the 16 hotspots chosen, 8 gave rise to especially pronounced sensor improvements. They were as follows: K14, G16, G18, F19, I20 and R22, which are all part of the Ca^{2+} binding loop region of EF-hand 3, and; V41 and F58 which are located within the α helices of EF-hand 4, and believed to stabilize troponin C by stretching out into other helices. Surprisingly, while the mutations within the Ca^{2+} binding loop of EF-hand 3 were mostly anticipated to tune the affinity and kinetics regarding Ca^{2+} binding, without causing significant changes in the overall structure of the sensor, some of them actually gave rise to the highest overall signal improvements. This example highlights the importance of screening, since these sites would probably not have been discovered in a rational attempt to increase signal change.

Our third library, again a linker library, was required after we exchanged the original donor ECFP with the brighter Cerulean 3 in a sensor, resulting in a loss of FRET (which came as a surprise, since the two donors differed from one another by only a few mutations). This again emphasized that our knowledge on these sensors is too limited to develop them on a purely rational basis.

The plots summarizing R_0 and $\Delta R/R$ of all sensor variants picked and measured *in vitro*, reveal a significant number of sensors which could be considered mispicks, as they failed to meet any of the screening criteria. We identified a number of reasons for that. Firstly, after observing that some sensors performed well in

cells but were non-functional *in vitro* (chapter 3.1.8.2), it must be assumed that many sensors not even considered for further testing, after failing to perform *in vitro*, would have actually functioned in mammalian cells. Furthermore, some weak *in vitro* performances are likely to have been caused simply by poor protein purification. When up to 96 proteins were purified in parallel, with each purification resulting in a very small amount of protein at best, it is likely that some proteins were not expressed well, or treated carefully enough throughout the purification process, leading to an even smaller yield. Protein expression could be greatly improved however, using auto-inductive medium instead of IPTG for induction. In any case, a limited number of such losses were accepted in favor for the high-throughput of our assay.

In addition to these apparent "mispicks", which may have actually worked in cells or after a second purification, there were certainly many sensors which simply did not function well. The main reason behind this is that we made a number of decisions in the beginning, regarding the execution of the screening, which had to be reconsidered later. An example of such an instance, was our decision to grow as many colonies as possible on each plate to increase throughput. Eventually however, we had to accept, that with more than 800 colonies per plate, the chances of a mispick or picking two colonies into one culture became too high. Initially, we screened for highest $\Delta R/R$ and lowest R_0, as well as sensors ranking high in both categories, and picked 10 colonies per category per plate, regardless of how promising the traces appeared. We later realized though, that sensors with a low R_0 often contained a stop codon or were imaging artifacts, and sensors ranking high in both categories were usually rather average overall. Therefore, the criteria were reassessed and we commenced screening for high $\Delta R/R$, taking the R_0 value into account only to a smaller extend. Regarding the number of picks per plate, an appropriate strategy for the future may be to only pick colonies which perform especially well, as the plate screening seems to be sufficiently reliable.

Overall, the screening for an improved GECI on the basis of FRET can be considered a success, resulting ultimately in an entire family of sensors expressing a variety of desirable features, namely the 'Twitch' sensor series (Thestrup et al., 2014).

Nevertheless, there is still significant room for improvement within the method. The rather imprecise bacterial plate screening, though allowing for a high throughput, requires a number of refining follow-up screening steps to be conducted *in vitro* or in mammalian cells. Especially cumbersome, is the transition from the plate screening to the subsequent protein expression, since the XL1 blue cells necessary for the screening do not express enough protein for *in vitro* measurements. Therefore, sensor DNA needs to be isolated from each colony picked, then a bacterial strain for protein expression (in our case BL21) has to

be transformed and the protein purified from this strain. Conducting the plate screening in BL21 would greatly assist in streamlining the steps outlined above. As mentioned in chapter 3.1.1, BL21 cells are unsuitable for plate screening however, due to their low transformation efficiency and a protein expression level too high for our purpose. While it may be possible to reduce protein expression by using agar plates from a more defined medium (thereby actively suppressing protein expression), there is, to our knowledge, no protein expression strain exhibiting transformation efficiency comparable to that of a cloning strain.

Moreover, a simplification of the protein purification process would be beneficial. This could potentially be realized by using the same inducible pore formation strategy mentioned in chapter 4.1, which would render all measures taken to break the bacterial membranes and release the protein into solution, unnecessary. Measuring the sensors in cell lysate instead of buffer may also be a viable method (despite the sacrifice in the quality of results) since it saves time.

A drawback of the bacterial plate screening is that it only achieves an estimation of R_0 and $\Delta R/R$, while completely neglecting other important sensor properties like Ca^{2+} affinity and kinetics. In our 'Twitch' screening, we still ended up with a series of sensors exhibiting a variety of affinities for different applications, as well as fast kinetics, by factoring these in when designing our library, and not setting the plate screening criteria too stringently. Nevertheless, a screening assay for such essential qualities would be desirable. Although a screen for Ca^{2+} affinity may be difficult in bacteria, a kinetic screen may indeed be possible. The external application of Ca^{2+} used in our current assay would be both too slow and insufficiently uniform for this purpose. It is also likely that the previously mentioned light-induced Ca^{2+} releasing protein would not be fast enough. A valid option however, may be the use of caged Ca^{2+}, which has already been used to determine the kinetics of a number of Ca^{2+} binding proteins, including calmodulin (Faas & Mody, 2012). Caged Ca^{2+}, which essentially, is Ca^{2+} bound to a light sensitive Ca^{2+} chelator, could be applied prior to the experiment. A subsequent short and intense flash of light then leads to a rapid and simultaneous release of Ca^{2+} inside all cells.

4.3 Improvements to mKOκ

mKOκ was chosen as an acceptor for a red-shifted GECI on the basis of FRET, due to its status as a monomer with fast maturation, exhibiting superior brightness over most orange and red fluorescent proteins known to date. However, a disadvantage identified in mKOκ as a potential FRET acceptor was the

"shoulder" in its excitation spectrum. This made mKOκ excitable in the area in which a potential donor would be excited. We intended to decrease this "shoulder" in order to avoid cross-excitation in a future FRET sensor, whilst further increasing the brightness of mKOκ. Furthermore, we planned to improve a number of circularly permutated variants of mKOκ, which had lost considerable brightness during the permutating process. We hoped that a reorientation of mKOκ in a sensor using these cp variants might enhance its FRET efficiency, as has been observed in other sensors in the past (e.g. (Mank et al., 2006)).

We used a custom-written Python program to compare mutants created via error-prone PCR to the parental proteins imaged alongside them, in order to detect even small improvements. In the end, we were able to identify a range of cp variants with improved maturation times and increased brightness. No significant improvements of the (non-cp) mKOκ-WT could be achieved however, and we were not able to combat the aforementioned "shoulder".

An interesting observation however, which has been discussed in the context of other red fluorescent proteins (Kikuchi et al., 2008), was the presence of a green fluorescent fraction, accompanying most of the orange fluorescent mKOκ-based proteins. We reasoned that this must be the green dead-end product, thought to be a byproduct of the red chromophore formation (Strack et al., 2010). This green byproduct would obviously interfere with FRET, as well as multicolor imaging using mKOκ in combination with other fluorescent proteins. In our screening, we found various grades of (more or less) green fluorescence present in the corresponding mutants. Furthermore, we also identified one mutant which was completely green, and two mutants that were completely orange.

The two orange mutants, namely 21_43 and cp mKO3, may be useful in applications requiring multiple fluorophores, as there would not be any interference due to a green byproduct. In addition, both the green and the orange mutants helped us pin down the mutations which gave rise to either the green or the orange chromophore maturation.

A thorough characterization of all new mutants revealed that several cp variants exhibited quantum yields higher than that of mKOκ-WT (QY = 0.61), with mutants 21_43 and cp mKO3 displaying the highest values (0.66 and 0.71 respectively). Both remained monomeric, meaning that none of the new mutations had reversed the previous break of the tetramer. A pH titration of cp mKO3 revealed a pK_a value identical to that of mKOκ-WT. Unfortunately, out of all cp variants tested, none were able to induce the expected increase in FRET efficiency with any of the donors tested so far. A matching donor may still be found however.

4.4 Working Towards a Red-shifted Genetically Encoded Ca^{2+} FRET Sensor

An attempt was made to design a red-shifted genetically encoded Ca^{2+} FRET sensor, as red-shifted FRET sensors are still rare. Essentially, we tested most of the bright green and yellow fluorescent proteins known to date, with a troponin C-based Ca^{2+} domain, and either mKOκ or another recommended red fluorescent protein as an acceptor. Clover for example, was tested in combination with mRuby2, but while this FRET pair was reported to improve the dynamic range of a number of sensors previously based on CFP and YFP (Lam et al., 2012), our Clover-mRuby2 Ca^{2+} sensor proved non-functional. Two of the donors chosen, namely T-Sapphire and LSSmOrange, exhibited distinctively large stokes shifts. This would have been an attractive characteristic in a FRET sensor, preventing cross-excitation with the acceptor. LSSmOrange would have been even more appealing, as the resulting sensor would have been shifted further into the red than any of the other pairs. One of the other donors tested, Dreiklang, was a very bright photoswitchable protein with the potential to repeatedly light up cells of interest, whilst switching off their surroundings.

After initial prototyping of all pairs, four prosperous donors were selected for a library of red-shifted Ca^{2+} sensors with random linkers between fluorescent proteins and the Ca^{2+} binding domain. As previously mentioned, the degenerate codon NNN, with N encoding all four nucleosides, had been used to create the 'Twitch' library. This time, we decided to utilize the codon NNB instead. B only encodes C, G and T, meaning NNB is still able to encode all amino acids, but only 48 of the 64 codons. This measure decreased the occurrence of redundant codons and stop codons, thereby reducing the size of our library. It did still exhibit a strong bias towards certain amino acids however, which should ideally be avoided. A further refinement of the library in the future would save time and money, as fewer variants would require screening in order to capture each amino acid. Moreover, this would ensure that selected variants were actually the best performers, and that no better performer was missed, due solely to its rarity.

After extensive screening of the linker library, the best sensor was still one of the original prototypes, namely DreiklangΔ11-mKOκ, meaning that our screening was unsuccessful. DreiklangΔ11-mKOκ exhibited a ΔR/R value of approximately 170%, a Ca^{2+} affinity suitable for experiments in many cell types, with the photoswitching characteristic of Dreiklang remaining intact. The switching would be of limited use in an experiment however, as the excitation of Dreiklang would always lead to a cross-excitation of mKOκ, causing a constant orange background even with Dreiklang switched off.

There are a number of potential improvements which could be incorporated into a new library and its subsequent screening. Firstly, since the anticipated changes in these sensors would be more subtle than

those in the 'Twitch' screening, it would be advantageous to screen a sample of the parental sensors along with each plate, to ensure that only mutants that exhibited a better performance were picked.

It has also been observed in the past that no other fluorescent protein FRET pair exhibits FRET efficiencies comparable to those of CFP and YFP. A reason for that may be that CFP and YFP are not only derived from the same species, but based on the same fluorescent protein, GFP, thereby ehhibiting great similarity. More importantly, GFP has a well-known tendency to dimerize, which could potentially facilitate the occurrence of FRET. Other fluorescent proteins may either lack this intrinsic attraction, or even repel one another. If that was indeed the case, the best way to improve FRET between these proteins would be to enhance their mutual attraction. This could be achieved in various ways.

One obvious measure was taken by Lindenburg and colleagues. Since many of the red fluorescent proteins are based on the obligate tetramer DsRed, and contain mutations which transform them into monomers, they reasoned that reversing some of the mutations that broke the tetramer, may in turn promote FRET. This strategy was indeed successful and resulted in a FRET sensor based on mOrange and mCherry, with a markedly improved dynamic range (Lindenburg et al., 2013). A similar approach should be compatible with all red-shifted fluorescent proteins that are former tatramers derived from the same species. This method would be an effective way to turn the inconvenient tetramerization of these proteins into an advantage.

A similar approach could be attempted with the green and orange dead-end products of mKOκ which, like mOrange and mCherry, are derived from the same species. They too originated from an obligate tetramer, but have the additional benefit of being brighter than most proteins in that spectral region.

Gruenberg and colleagues pursued two slightly more complicated strategies in order to increase the interaction between two non-interacting proteins. In one approach, they introduced complementary electrostatic charges around the putative interface of the fluorescent proteins Citrine and mCherry. The increased interaction did indeed contribute to an increase in FRET, but unfortunately not without side-effects. Moreover, this method requires substantial structural knowledge on a given FRET pair, including the location of their interface.

In an alternative approach, they attached a domain to one fluorescent protein, and the peptide it recognized to the other fluorescent protein. The interaction between this domain-peptide module was able to facilitate FRET. The sensing moiety used in the proof of principle experiment, namely a caspase recognition site, was very short (5 amino acids), which is probably the reason why the introduction of the same module into one of our Ca^{2+} FRET sensors, featuring a much larger sensing domain, failed to have an effect on the sensor (data not shown). The utilization of a similar module, with a stronger interaction

to account for the greater distance between donor and acceptor, might give rise to a similar improvement in our sensors (Grünberg et al., 2013).

5 Conclusion

The research presented in this thesis led to the development of a highly efficient screening assay for GECIs. The use of bacteria makes our assay faster and more cost effective than existing screening assays in mammalian cells (e.g. (Wardill et al., 2013)). In contrast to another bacterial based screening assay for Ca^{2+} sensors developed previously (Zhao et al., 2011), our assay is also applicable to FRET sensors. While our particular assay is designed especially for genetically encoded Ca^{2+} sensors, it can easily be adapted to suit other applications.

Our screening assay contributed to the development of a new series of genetically encoded Ca^{2+} FRET sensors, recently published as the 'Twitch' series (Thestrup et al., 2014). The 'Twitch' sensors utilize either one or two EF-hands of the high affinity C-lobe of troponin C as their Ca^{2+} binding moiety. This reduction in Ca^{2+} binding sites (from the previous four) reduces buffering, and results in more linear response properties. The sensors are very bright and exhibit a large dynamic range of up to 1000 % *in vitro*. Furthermore, they possess a high affinity for Ca^{2+} and display fast kinetics (with higher affinities resulting in slower kinetics and vice versa). Their signal strength is high enough to match synthetic dyes.

In a similar approach, we attempted to develop a red-shifted genetically encoded Ca^{2+} FRET sensor, allowing for multi-parameter imaging experiments, as well as deep tissue imaging. Four potential donors were chosen, which possessed interesting features such as increased brightness (Clover), photoswitchability (Dreiklang), and a large stokes shift (T-Sapphire). The orange fluorescent protein mKOκ, was chosen as an acceptor due to its superior brightness in that particular spectral region.

A second screening was conducted in parallel, to further improve mKOκ, as well as two of its cp variants, as potential acceptors. The mKOκ screening produced no significant advantages over the original mKOκ in terms of brightness, however numerous improvements to the cp variants were identified, which, introduced into mKOκ may lead to a further improvement. We were also able to identify mutations which produced either entirely green, or entirely orange versions of mKOκ and may be useful in multi-color experiments and FRET sensors. The most successful red-shifted sensor we developed consisted of Dreiklang, mKOκ and the C-lobe of troponin C.

In summary, our newly established screening assay can greatly accelerate the optimization of genetically encoded indicators. Its suitability for Ca^{2+} sensors on the basis of FRET has been proven by the development of the successful new 'Twitch' sensor series, as well as a similar red-shifted sensor. The assay can also be easily adapted to screen other types of sensors, making it a valuable tool in the development of multiple sensor types.

6 Appendix

6.1 Python Script Plate Screening (David Ng)

''' This script controls the hardware for the Bacterial Colony Screening Apparatus. It controls the camera and illumination system and via the µManager software package (www.micro-manager.org), and processes the results with Numpy and generates plots with Matplotlib. It is run via iPython, as this is our preferred scripting environment.

The hardware used in the setup was a CoolSNAP ES2 CCD camera (Photometrics). The excitation and emission filter wheels and shutters were controlled by a Lambda 10-2 optical filter changer (Sutter Instrument), and the illumination system was a Lambda LS/30 Stand-Alone Xenon Arc Lamp (Sutter Instruments).

ng (at) neuro (dot) mpg (dot) de

'''

''' **Initalization Codeblock**

This section of code imports the needed modules, defines constants, and sets up the camera, shutter and filter system.

'''

```
import PIL
import time
import sys
import scipy.ndimage
import numpy
import MMCorePy # Note: add the installation directory of µManager to the system path, so that Python can access the needed files.
import tkMessageBox
import tkFileDialog
import tkSimpleDialog
import Tkinter as tk

# Selection of fluorophores used for this experiment. Change as required.

donor = 'Cerulean'
acceptor = 'mCitrine'

# Shutterwheel postions dictionary. This is a list of the various filters we have installed at each postion. The bandpass filters are described by the spectra of the fluorescent protein they are most often used with. The donor and acceptor variables are taken
```

from the dictionary, using the keys selected above.

```
ShutterWheel = {'Closed': 0, 'DsRed': 1, 'mOrange': 2, 'mCitrine': 3, 'eGFP': 4, 'Cerulean': 5, 'tSapphire': 6}
donorEx = ShutterWheel[donor]
donorEm = ShutterWheel[donor]
acceptorEx = ShutterWheel[acceptor]
acceptorEm = ShutterWheel[acceptor]

# Imports the modules for the filterwheel, camera and shutters

core = MMCorePy.CMMCore();
core.unloadAllDevices(); # makes sure there isn't anything previously loaded

# Loads Camera

core.loadDevice("Camera", "PrincetonInstruments", "Camera-1");

# Loads Serial interface the Sutter Controlbox

core.loadDevice("P1", "SerialManager", "COM1");
core.setProperty("P1", "StopBits", "1");

# setup filter wheels

core.loadDevice("Em", "SutterLambda", "Wheel-A");
core.setProperty("Em", "Port", "P1");
core.loadDevice("Ex", "SutterLambda", "Wheel-B");
core.setProperty("Ex", "Port", "P1");
core.loadDevice("SHUT", "SutterLambda", "Shutter-A 10-2");
core.setProperty("SHUT", "Port", "P1");
core.initializeAllDevices();

# Sets the filters to closed, which is Position 0. Also sets the shutters wheel to fastest speed

core.setState("Ex", 0);
core.setProperty("Ex", "Speed", 4);
core.setState("Em", 0);
core.setProperty("Em", "Speed", 4);

# Final setup for camera

core.setCameraDevice("Camera");

# This trick hides the empty TK window that is generated when TK is started

root = tk.Tk()
root.withdraw()
def snapImage(ExPos, EmPos, Exposure):

    """ This function takes a picture with a given excitation/emission filter and exposure time, and returns an image.

    """

    core.setAutoShutter(0)
    core.setState("Ex", ExPos);
    core.setState("Em", EmPos);
    core.setExposure(Exposure)
    core.setShutterOpen(1)
```

```
    core.snapImage()
    pic = core.getImage()
    core.setShutterOpen(0)
    core.setState("Ex", 0)
    core.setState("Em", 0)
    return pic

def newMask():

    """ This function generates a mask, that sets the area outside the plate to black. Its an array of zeros the size of the picture, with a filled circle of 1's in the location of the petri dish. This is done to make the colony-detection algorithm work more accurately.

    """

    # these are the parameters for the mask, i.e. its height and width, and radius and center of the circle as measured in pixels. The circle parameters are determined by measuring a picture taken of a plate.

    h,w = 1040, 1392
    a,b = 480, 720
    r = 300
    y,x = numpy.ogrid[-a:h-a, -b:w-b]

            # Thanks, Mr. Pythagorus!

    mask = x*x + y*y <= r*r
    array = numpy.zeros((h, w))
    array[mask] = 1
    return array

def segmentImage(picture):

    """ This function takes a picture, and tries to isolate the colonies

    """

            # creates a new mask, from the function above

    mask = newMask()

            #uses the mask to get rid of the background

    masked = mask*picture

            # only takes pixels 3 times greater than the standard deviation of the pixel intensity. This has been found to reliably find only fluorecent colonies in our system.

    binaryImage = where(masked>mean(picture)+3*std(picture),1,0)

            # This function eroded the binary image, getting rid of tiny specs, and removing the edges of blobs.

    binaryImage = scipy.ndimage.binary_erosion(binaryImage)

            # This function fill in any gaps in blobs.

    binaryImage = scipy.ndimage.binary_opening(binaryImage,structure=ones((2,2)))
```

```
        # This function identifies the colonies, and gives them labels and a total.

    labeled,nr_objects = scipy.ndimage.label(binaryImage)

    return labeled,nr_objects

def getRatiometric(ex1, em1, em2, colonies, exposure):

    """ This is takes the location of previously found colonies, and the takes two images, one of the donor and one of FRET.

    It then uses the generated images to get the ratiometric responce for all the colony, using the colony locations.

        It returns an array, of Donor fluorence, FRET fluorescence, and FRET Ratios.

    """

    core.setAutoShutter(0)

        # Gets Donor Imaging

    core.setState("Ex", ex1);
    core.setState("Em", em1);
    core.setExposure(exposure)
    core.snapImage()
    donorIMG = core.getImage()

        # Gets FRET Imaging

    core.setState("Em", em2);
    core.snapImage()
    fretIMG = core.getImage()

        # closes filter wheel

    core.setState("Ex", 0)
    core.setState("Em", 0)

        # Calculates Donor,Acceptor and FRET values

    donorValues = scipy.ndimage.mean(donorIMG, colonies[0], np.unique(colonies[0]))
    fretValues = scipy.ndimage.mean(fretIMG, colonies[0], np.unique(colonies[0]))
    ratioValues = fretValues/donorValues

        # puts the values together in a 2D array

    data_slice = vstack([donorValues, fretValues, ratioValues])
    return data_slice
```

''' **Measurement Codeblock**

This section of code allows the user to select the file location, records images and calculated FRET ratios, and prompts the user to spray the plates.

'''

```
# Gets the directory location for saving the files
```

```
directory = tkFileDialog.askdirectory()
plate_name = tkSimpleDialog.askstring('File', 'Plate Name:')

# Gets the date in the nice string format, to add to the graphs at the end

datestr = time.strftime("%d %b %Y %H:%M:%S", time.localtime())

# Checks to see if the plate name is actually there, exit if nothing has been entered in the popup box

if len(plate_name) == 0:
   sys.exit()
if not directory:
   sys.exit()

# takes a picture, finds the colonies

picture = snapImage(acceptorEx,acceptorEm,500)
colonies = segmentImage(picture)

# generates plots for the user to decide if they want to continue, e.g. have the correct filters and exposure time been chosen to generate good images? Have enough colonies been found? If not, exit gracefully.

figure(0, (6,10))
subplot(2,1,1)
imshow(picture[150:820,370:1060]*100, cmap = 'gray')
plt.axis("off")
subplot(2,1,2)
imshow(colonies[0][150:820,370:1060], cmap = 'jet')
plt.annotate("Colonies found: %d" %int(colonies[1]-1), xy = (50,50),bbox = dict(boxstyle = 'round,pad=0.2', fc = 'yellow'))
plt.axis("off")
show()
imageOK = tkMessageBox.askyesno('Option','Continue?') # Dialog box: Do you want to continue?
print "here"
print imageOK
if not(imageOK):
   sys.exit()

# The user is satisfied, so go on to record the baseline ratiometric values and plot them in realtime. It records 5 data points for each colony, at 15 second intervals

plt.close()
core.setShutterOpen(1)
core.setAutoShutter(0)
init = time.time()
data = getRatiometric(donorEx, donorEm, acceptorEm, colonies, 100)[newaxis,...]
t = time.time() - init
figure(1)
plot(data[:,2,:])
draw()
show()
ion()
if t <= 15:
   delay = 15-t
   time.sleep(delay)
for i in range(5):
   init2 = time.time()
   data = numpy.vstack([data, getRatiometric(donorEx, donorEm, acceptorEm, colonies, 100)[newaxis,...]])
   clf()
```

```
    plot(data[:,2,:])
    draw()

    # This code account for the variable delay in recording an image.

    t = time.time() - init2
    if t <= 15.0:
        delay = 15.0-t
        time.sleep(delay)
    print "Recording %d of 5" %(i+1)

# Prompts the user to add Ionomycin, then records 25 data points for each colony, at 15 second intervals.

tkMessageBox.showinfo("Command", "Add Ionomycin")
print "continuing after ionomycin addition"
init = time.time()
t = time.time() - init
for i in range(25):
    init2 = time.time()
    data = numpy.vstack([data, getRatiometric(donorEx, donorEm, acceptorEm, colonies, 100)[newaxis,...]])
    clf()
    plot(data[:,2,:])
    draw()

    # This code account for the variable delay in recording an imaage.

    t = time.time() - init2
    if t <= 15.0:
        delay = 15.0-t
        time.sleep(delay)
    print "Recording %d of 25" %(i+1)

# Prompts the user to add Calcium, then records 25 data points for each colony, at 15 second intervals.

tkMessageBox.showinfo("Command", "Add Calcium")
print "continuing after calcium addition"
init = time.time()
t = time.time() - init
for i in range(25):
    init2 = time.time()
    data = numpy.vstack([data, getRatiometric(donorEx, donorEm, acceptorEm, colonies, 100)[newaxis,...]])
    clf()
    plot(data[:,2,:])
    draw()

    # This code account for the variable delay in recording an imaage.

    t = time.time() - init2
    if t <= 15.0:
        delay = 15.0-t
        time.sleep(delay)
    print "Recording %d of 25" %(i+1)
print "Finished aquisition"

# last image update
```

```
figure(0)
show()

''' Analysis Codeblock

This section of code analyses the recorded data, and selects the best responding colonies. It generates plots, highlighting the
best responders, and generates an image the shows the best responding colonies locations, to make picking easier.

'''

# Find starting and ending FRET ratios, from 10 reading just before calcium addition, to the last 10 readings.

start = numpy.mean(data[20:30,2,:], axis = 0)
end = numpy.mean(data[-10:,2,:], axis = 0)

# Sort the selection to find those colonies with the greatest response, as defined by change-in-FRET-ratio divided by the square
of the starting FRET ratio. Squaring the starting ratio adds to its weight as a negative selection criteria.

selection = (end-start)/(start)**2
sel = numpy.argsort(selection)

# Generate a picture of colonies with best locations marked

figure(figsize=(8, 8))
imshow(picture[150:820,370:1060], cmap = 'gist_yarg')
xs = []
ys = []
for i in range(10):
   xpos = scipy.ndimage.center_of_mass(picture, colonies[0], sel[-1-i])[0]-151
   ypos = scipy.ndimage.center_of_mass(picture, colonies[0], sel[-1-i])[1]-370
   xs.append(xpos)
   ys.append(ypos)
   plt.annotate(
      i+1,
      alpha=0.5,
      color = 'b',
      xy = (ypos,xpos), xytext = (-5, 5),
      textcoords = 'offset points', ha = 'right', va = 'bottom',
      arrowprops = dict(arrowstyle = '->', connectionstyle = 'arc3,rad=0'))
c = scatter(ys,xs, color = 'r')
c.set_alpha(0.25)
plt.axis("off")
plt.title('Colony Selection from Plate: ' + plate_name + ', at ' + datestr)
plt.savefig(directory + '/' + plate_name + '_Colonies', papertype='A4')
plt.close()

# Scatter plot of Calcium response, with the best ten colonies marked in red

figure(figsize=(9, 6))
scatter(start[sel[-10:]], (end[sel[-10:]]-start[sel[-10:]])/start[sel[-10:]], c = 'r')
scatter(start[sel[0:-10]], (end[sel[0:-10]]-start[sel[0:-10]])/start[sel[0:-10]], c = 'b')
plt.title('Colony Selection from Plate: ' + plate_name + ', at ' + datestr)
plt.xlabel(r'$\o Ca^{2+}\frac{Acceptor}{Donor}$')
plt.ylabel(r'$\frac{(\o Ca^{2+}\frac{Acceptor}{Donor})-(+Ca^{2+}\frac{Acceptor}{Donor})}{\o Ca^{2+}\frac{Acceptor}{Donor}}$')
for i in range(10):
   plt.annotate(i+1, xy = (start[sel[-1-i]],(end[sel[-1-i]]-start[sel[-1-i]])/start[sel[-1-i]]), xytext = (-10, 10),
      textcoords = 'offset points', ha = 'right', va = 'bottom',
      bbox = dict(boxstyle = 'round,pad=0.2', fc = 'yellow', alpha = 0.5),
```

```
        arrowprops = dict(arrowstyle = '->', connectionstyle = 'arc3,rad=0'))
plt.savefig(directory + '/' + plate_name + '_Selection', papertype='A4')
plt.close()

# Traces of Calcium response for the best ten colonies

figure()
plot(array([numpy.arange(0,shape(data)[0],1),]*7).T,data[:,2,sel[-1:-8:-1]] );
plot(array([numpy.arange(0,shape(data)[0],1),]*3).T,data[:,2,sel[-8:-11:-1]], linestyle='--' );
plt.legend( ('1', '2', '3', '4', '5','6','7','8','9','10'))
plt.title('Colony Traces from Plate: ' + plate_name + ', at ' + datestr)
plt.xlabel(r'Time (second)')
plt.ylabel(r'$\frac{YFP}{Donor}$')
show()
plt.savefig(directory + '/' + plate_name + '_Traces', papertype='A4')

# saves raw data and images, for further analysis

numpy.save(directory + '/' + plate_name, data)
numpy.save(directory + '/' + plate_name + '_Image', picture)

# Offer exit dialog

imageOK = tkMessageBox.askyesno('Finished','Close?')
if (imageOK):
   sys.exit()
```

6.2 Matlab Script Analysis of Protein Spectra (Christopher Zarbock)

```
set(0,'DefaultFigureVisible', 'off'); %makes figures invisible during analysis
process_date = input('Enter date on which proteins were processed: ', 's');
cd(strcat('C:\Documents and Settings\folder name', process_date)); %accesses folder containing csv files of spectral data
FileList = dir('*.csv');
N = size(FileList,1);
for k = 1:N
   filename = regexprep(FileList(k).name,'.csv','');
   string_of_interest = strcat('C:\Documents and Settings\folder name', process_date,...
      '\',FileList(k).name); %creates string to be used by import data.
   csv_data = importdata(string_of_interest);

  if k == 1

%file containing all data
      file_id4 = fopen(strcat('C:\Documents and Settings\folder name',...
      process_date,'\masterfile', process_date, '.csv'), 'a');
      fprintf(file_id4, '%s %s, %s, %s, %s, \r\n', 'masterfile',...
         process_date, 'Starting Ratio',...
         'Mg^2+ DeltaR\R [%]', 'Ca^2+ DeltaR\R [%]');
      fclose(file_id4);

%file containing sensors not meeting the requirements
      file_id1 = fopen(strcat('C:\Documents and Settings\folder name',...
      process_date,'\badones.csv'), 'a');
      fprintf(file_id1, '%s %s,\r\n', 'Bad Ones', process_date);
      fclose(file_id1);
```

```
%file containing sensors exhibiting high ΔR/R values
      file_id2 = fopen(strcat('C:\Documents and Settings\folder name',...
      process_date,'\more than 500.csv'), 'a');
      fprintf(file_id2, '%s %s,\r\n', 'More than 500', process_date);
      fclose(file_id2);

%file containing functional sensors exhibiting low R0 values
      file_id3 = fopen(strcat('C:\Documents and Settings\folder name',...
      process_date,'\small starting ratio and more than 250.csv'), 'a');
      fprintf(file_id3, '%s %s,\r\n', 'Small Starting Ratio and More than 250', process_date);
      fclose(file_id3);

   end

   if size(csv_data.data,2) < 6
      disp([filename, ' - bad one']);
      file_id1 = fopen(strcat('C:\Documents and Settings\folder name',...
      process_date,'\badones.csv'), 'a');
      fprintf(file_id1, '%s,\r\n', filename);
      fclose(file_id1);
      continue
   end

%regexprep takes out the .csv ending
   string_for_saving = strcat('C:\Documents and Settings\folder name',...
      process_date,'\',regexprep(FileList(k).name,'.csv',''),'.txt');
   file_id = fopen(string_for_saving, 'w');

   four_seventy_five = [csv_data.data(14,2) csv_data.data(14,4) csv_data.data(14,6)]; %CFP data
   four_seventy_five = [four_seventy_five(1) / csv_data.data(33,2),...
      four_seventy_five(2) / csv_data.data(33,4), ...
      four_seventy_five(3) / csv_data.data(33,6)]; %normalizes
   five_twenty_seven = [csv_data.data(39,2) csv_data.data(39,4) csv_data.data(39,6)]; %YFP data
   five_twenty_seven = [five_twenty_seven(1) / csv_data.data(33,2),...
      five_twenty_seven(2) / csv_data.data(33,4), ...
      five_twenty_seven(3) / csv_data.data(33,6)]; %normalizes
   five_over_four = five_twenty_seven ./ four_seventy_five; %first calculation (FRET/ CFP)
   final = ((five_over_four - five_over_four(1,1)) ./ (five_over_four(1,1))...
      .* 100; %second calculation (R-R0/R0)

%Output file
   output = [four_seventy_five' five_twenty_seven' five_over_four' final'];

   if final(1,3) > 500
      disp([filename, ' - more than 500']);
      file_id2 = fopen(strcat('C:\Documents and Settings\folder name',...
      process_date,'\more than 500.csv'), 'a');
      fprintf(file_id2, '%s,\r\n', filename);
      fclose(file_id2);
   end

   if (five_over_four(1,1) < 1) && (final(1,3) > 250)
      disp([filename, ' - small starting ratio and more than 250']);
      file_id3 = fopen(strcat('C:\Documents and Settings\folder name',...
      process_date,'\small starting ratio and more than 250.csv'), 'a');
      fprintf(file_id3, '%s,\r\n', filename);
      fclose(file_id3);
   end
```

```
   file_id4 = fopen(strcat('C:\Documents and Settings\folder name',...
      process_date,'\masterfile', process_date, '.csv'), 'a');
   fprintf(file_id4, '%s, %f, %f, %f,\r\n', filename, five_over_four(1,1),...
      final(1,2), final(1,3));
   fclose(file_id4);

   for count = 1:3
      if count == 1
         fprintf(file_id, '%s %s %s %s\r\n', '475', '     527',...
            '     527/475', ' DeltaR/R [%]');
      end
      fprintf(file_id, '%f %f %f %f\r\n\r\n',output(count,1),...
         output(count,2),output(count,3),output(count,4));
   end

   fclose(file_id);
   plot(csv_data.data(:,1),(csv_data.data(:,2) ./ csv_data.data(33,2)),csv_data.data(:,1),...
      (csv_data.data(:,4) ./ csv_data.data(33,4)),...
      csv_data.data(:,1),(csv_data.data(:,6) ./ csv_data.data(33,6)));
   xlabel('Wavelength (nm)');
   ylabel('\DeltaR/R [normalized]');
   legend('EGTA','Mg^2^+','Ca^2^+');
   title([regexprep(regexprep(FileList(k).name,'.csv',''), '_','.'), ' ', process_date]);
   text(500,.25, [num2str(five_over_four(1,1)), ' - Starting Ratio [YFP/CFP]']);
   text(500,.15, [num2str(final(1,2)), ' - Mg^2^+ \DeltaR/R [%]']);
   text(500,.05, [num2str(final(1,3)), ' - Ca^2^+ \DeltaR/R [%]']);
   print(1,'-djpeg','-r600',regexprep(FileList(k).name,'.csv',''));
   close(1);

   x(k) = five_over_four(1,1);
   y(k) = final(1,3);
end
plot(x,y,'x');
xlabel('YFP/CFP');
ylabel('\DeltaR/R [%]');
print(1,'-djpeg','-r600',process_date);
```

6.3 Python Script Fluorescent Protein Screening (Christopher Zarbock, David Ng)

```
# imports information needed for image processing

import PIL
import time
import sys
import scipy.ndimage
import numpy
import pylab
import matplotlib
from matplotlib.widgets import  RectangleSelector
from skimage.filter import threshold_adaptive

# imports GUI modules
```

```
import tkMessageBox
import tkFileDialog
import tkSimpleDialog
import Tkinter as tk

# hides empty TK window

root = tk.Tk()
root.withdraw()

# gets directory location for saving the files

directory = tkFileDialog.askdirectory()
plate_name = tkSimpleDialog.askstring('File', 'Plate Name:')

# gets date in a string format, to add to the graphs at the end

datestr = time.strftime("%d %b %Y %H:%M:%S", time.localtime())

# imports modules for filter wheels, camera and shutters

import MMCorePy
core = MMCorePy.CMMCore();
core.unloadAllDevices(); # makes sure there isn't anything previously loaded

# FRET PAIR FILTERS USED:

ShutterWheel = {'Closed': 0, 'DsRed': 1, 'mKO': 2, 'mCitrine': 3, 'eGFP': 4, 'Cerulean': 5, 'tSapphire': 6}
name_ex1 = 'mKO'
name_em1 = 'mKO'
name_ex2 = 'eGFP'
name_em2 = 'mKO'
name_ex3 = 'mCitrine'
name_em3 = 'mCitrine'
ex1 = ShutterWheel[name_ex1]
em1 = ShutterWheel[name_em1]
ex2 = ShutterWheel[name_ex2]
em2 = ShutterWheel[name_em2]
ex3 = ShutterWheel[name_ex3]
em3 = ShutterWheel[name_em3]

# loads camera

core.loadDevice("Camera", "PrincetonInstruments", "Camera-1");

# loads serial interface sutter controlbox

core.loadDevice("P1", "SerialManager", "COM1");
core.setProperty("P1", "StopBits", "1");

# setup filter wheels

core.loadDevice("Em", "SutterLambda", "Wheel-A");
core.setProperty("Em", "Port", "P1");
core.loadDevice("Ex", "SutterLambda", "Wheel-B");
core.setProperty("Ex", "Port", "P1");
core.loadDevice("SHUT", "SutterLambda", "Shutter-A 10-2");
```

```
core.setProperty("SHUT", "Port", "P1");
core.initializeAllDevices();

# sets the filters to closed and wheel to fastest speed

core.setState("Ex", 0);
core.setProperty("Ex", "Speed", 0);
core.setState("Em", 0);
core.setProperty("Em", "Speed", 0);

# final setup for camera

core.setCameraDevice("Camera");

# functions used in the program!

def snapImage(ExPos, EmPos, Exposure):
   """ This function takes a picture with a given excitation, emission and exposure time, and returns an image """
   core.setAutoShutter(0)
   core.setState("Ex", ExPos);
   core.setState("Em", EmPos);
   core.setExposure(Exposure)
   core.setShutterOpen(1)
   core.snapImage()
   pic = core.getImage()
   core.setShutterOpen(0)
   core.setState("Ex", 0)
   core.setState("Em", 0)
   return pic

def newMask():
   """ This function generates a mask that sets the area outside the plate to black. """

  # parameters for the mask (height, width, diameter of the circle)

   h,w = 1040, 1392
   a,b = 536, 709
   r = 300
   y,x = numpy.ogrid[-a:h-a, -b:w-b]
   mask = x*x + y*y <= r*r
   array = numpy.zeros((h, w))
   array[mask] = 1
   return array
def segmentImage(picture, lower_cutoff, upper_cutoff, block_size):
   """ This function takes a picture, and tries to isolate the colonies"""
            # creates a new mask, from the function above
   mask = newMask()
            #uses the mask to get rid of the background
   bool_mask = (mask > 0)
   masked = mask*picture
            # only takes pixels 3 times greater than the standard deviation of the pixel intensity.
   #binaryImage = (masked > picture[bool_mask].mean()+ (colony_standard_deviation) * picture[bool_mask].std())
   binaryImage = threshold_adaptive(masked, block_size, offset = 0)
            # gets rid of tiny specs, and removes the edges of blobs
   binaryImage = scipy.ndimage.binary_erosion(binaryImage)
            # fills in any gaps in blobs
   binaryImage = scipy.ndimage.binary_opening(binaryImage,structure=numpy.ones((2,2)))
            # identifies the colonies, and gives a number of how many it found
```

```
    labeled,nr_objects = scipy.ndimage.label(binaryImage)
    non_colonies = ((lower_cutoff > scipy.ndimage.sum(binaryImage, labeled, pylab.arange(0,nr_objects + 1))) ^ (upper_cutoff <
scipy.ndimage.sum(binaryImage, labeled, pylab.arange(0,nr_objects + 1))))
    for count, boolean in enumerate(non_colonies):
        if (boolean == 1):
            labeled[labeled == count] = 0
    labeled_new, nr_objects_new = scipy.ndimage.label(labeled)
    return labeled_new,nr_objects_new
def annotate_picture(picnum, picture, colonies_of_interest, num_of_interest, plate_name, datestr):
            # picture of bright colonies with locations marked
    pylab.figure(num = picnum, figsize = (6.9,6.9))
    pylab.imshow(picture[255:855, 420:1020], cmap = 'gist_yarg')
    xs = []
    ys = []
    for i in range(num_of_interest):
        xpos = scipy.ndimage.center_of_mass(picture, colonies_of_interest[0], i + 1)[0] - 255
        ypos = scipy.ndimage.center_of_mass(picture, colonies_of_interest[0], i + 1)[1] - 420
        xs.append(xpos)
        ys.append(ypos)
        pylab.annotate(
            i+1,
            alpha=0.5,
            color = 'b',
            xy = (ypos,xpos), xytext = (-5, 5),
            textcoords = 'offset points', ha = 'right', va = 'bottom',
            arrowprops = dict(arrowstyle = '->', connectionstyle = 'arc3,rad=0'))
    c = pylab.scatter(ys,xs, color = 'r')
    c.set_alpha(0.25)
    if picnum == 1:
        pylab.title('Bright Colonies Selection from Plate: ' + plate_name + ', at ' + datestr)
    if picnum == 2:
        pylab.title('488 Dim Colony Selection from Plate: ' + plate_name + ', at ' + datestr)
    if picnum == 1:
        pylab.savefig(directory + '/' + plate_name + '_Bright_Colonies', papertype='A4')
    if picnum == 2:
        pylab.savefig(directory + '/' + plate_name + '_Somewhat_Bright_and_Dim_Colonies', papertype='A4')

################################################################################
#The code to draw the rectangle#
################################################################################

def onselect(eclick, erelease):
  'eclick and erelease are matplotlib events at press and release'
  print ' startposition : (%f, %f)' % (eclick.xdata, eclick.ydata)
  print ' endposition   : (%f, %f)' % (erelease.xdata, erelease.ydata)
def toggle_selector(event):
    print ' Key pressed.'
    if event.key in ['Q', 'q'] and toggle_selector.RS.active:
        print ' RectangleSelector deactivated.'
        toggle_selector.RS.set_active(False)
    if event.key in ['A', 'a'] and not toggle_selector.RS.active:
        print ' RectangleSelector activated.'
        toggle_selector.RS.set_active(True)
class Annotate(object):
    def __init__(self):
        self.ax = pylab.plt.gca()
        self.rect = matplotlib.patches.Rectangle((0,0), 1, 1, fill = False, color = 'yellow')
        self.x0 = None
```

```
        self.y0 = None
        self.x1 = None
        self.y1 = None
        self.ax.add_patch(self.rect)
        self.ax.figure.canvas.mpl_connect('button_press_event', self.on_press)
        self.ax.figure.canvas.mpl_connect('button_release_event', self.on_release)
    def on_press(self, event):
        print 'press'
        self.x0 = event.xdata
        self.y0 = event.ydata
    def on_release(self, event):
        print 'release'
        self.x1 = event.xdata
        self.y1 = event.ydata
        self.rect.set_width(self.x1 - self.x0)
        self.rect.set_height(self.y1 - self.y0)
        self.rect.set_xy((self.x0, self.y0))
        self.ax.figure.canvas.draw()
        global firstx
        global secondx
        global firsty
        global secondy
        firstx = self.x0
        secondx = self.x1
        firsty = self.y0
        secondy = self.y1

################################################################################

# First codeblock!
# takes a picture, finds the colonies

ImageOk = 0
while not(ImageOk):
    picture1 = snapImage(ex1,em1,800)
    picture2 = snapImage(ex2,em2,1000)
    picture3 = snapImage(ex3,em3,3000)
    pylab.figure(0)
    pylab.imshow(picture3[255:855, 420:1020] * 100, cmap = 'gray')
    pylab.ion()
    pylab.show()
    ImageOk = tkMessageBox.askyesno('Option', 'Good plate position?')
    if not(ImageOk):

        #pylab.close()
        repositionedOK = 0
        while not(repositionedOK):
            repositionedOK = tkMessageBox.askyesno('Reposition','Have you repositioned the plate?')
pylab.close(0)
pylab.figure(0)
ax = pylab.subplot(1,1,1)
pylab.imshow(picture3[255:855, 420:1020] * 100, cmap = 'gray')
toggle_selector.RS = RectangleSelector(ax, onselect, drawtype='box', rectprops = dict(facecolor = 'red', edgecolor= 'red', alpha =
0.5, fill = False))
pylab.connect('key_press_event', toggle_selector)
a = Annotate()
pylab.ion()
pylab.show()
```

```
ImageOk = tkMessageBox.askyesno('Option', 'Click \' Yes \' when done drawing control rectangle.')
pylab.close()

ColoniesOk = 0
while not(ColoniesOk):
   lower_colony_limit = input('Please enter the lower colony size limit: ')
   upper_colony_limit = input('Please enter the upper colony size limit: ')
   block_size = input('Please enter the block size for adaptive thresholding: ')
   pylab.figure(num = 5)
   colonies1 = segmentImage(picture1, lower_colony_limit, upper_colony_limit, block_size)
   colonies2 = segmentImage(picture2, lower_colony_limit, upper_colony_limit, block_size)
   colonies3 = segmentImage(picture3, lower_colony_limit, upper_colony_limit, block_size)
   pylab.subplot(2,3,1)
   pylab.imshow(picture1[255:855, 420:1020] * 100, cmap = 'gray')

   rect1 = matplotlib.patches.Rectangle((firstx, firsty), (secondx - firstx), (secondy - firsty), fill = False, color = 'yellow')
   pylab.subplot(2,3,1).add_patch(rect1)
   #pylab.axis("off")

   pylab.subplot(2,3,4)
   pylab.imshow(colonies1[0][255:855, 420:1020], cmap = 'jet')
   pylab.annotate("MKO2 Excitation/Emission \n Colonies found: %d" %int(colonies1[1]), xy = (50,50),bbox = dict(boxstyle =
'round,pad=0.2', fc = 'yellow'))
   pylab.axis("off")

   #Second set of images

   pylab.subplot(2,3,2)
   pylab.imshow(picture2[255:855, 420:1020] * 100, cmap = 'gray')
   rect2 = matplotlib.patches.Rectangle((firstx, firsty), (secondx - firstx), (secondy - firsty), fill = False, color = 'yellow')
   pylab.subplot(2,3,2).add_patch(rect2)

   #pylab.axis("off")

   pylab.subplot(2,3,5)
   pylab.imshow(colonies2[0][255:855, 420:1020], cmap = 'jet')
   pylab.annotate("eGFP Excitation / mKO2 Emission \n Colonies found: %d" %int(colonies2[1]), xy = (50,50),bbox =
dict(boxstyle = 'round,pad=0.2', fc = 'yellow'))
   pylab.axis("off")

   #Third set of images

   pylab.subplot(2,3,3)

   #imshow(((picture3[150:820,370:1060] - picture3.min()) / (picture3.max()-picture3.min())) * 1000000, cmap = 'gray')

   pylab.imshow(picture3[255:855, 420:1020] * 100, cmap = 'gray')
   rect3 = matplotlib.patches.Rectangle((firstx, firsty), (secondx - firstx), (secondy - firsty), fill = False, color = 'yellow')
   pylab.subplot(2,3,3).add_patch(rect3)

   #pylab.axis("off")

   pylab.subplot(2,3,6)
   pylab.imshow(colonies3[0][255:855, 420:1020], cmap = 'jet')
   pylab.annotate("mCitrine Excitation/Emission \n Colonies found: %d" %int(colonies3[1]), xy = (50,50),bbox = dict(boxstyle =
'round,pad=0.2', fc = 'yellow'))
   pylab.axis("off")
```

```
    pylab.ion()
    pylab.show()
    ColoniesOk = tkMessageBox.askyesno('Option', 'Continue?')

# Dialog box: Do you want to continue?

pylab.savefig(directory + '/' + plate_name + 'Overview')
CalculationsOK = 0
while not(CalculationsOK):
    bright_colony_standard_deviation_upper = input('Please enter the bright colony standard deviation upper: ')
    dim_colony_standard_deviation_lower = input('Please enter the dim colony standard deviation lower: ')

    #Pull the colonies out of the initial labeling step (trying to relabel after pulling a part of the image gave strange colony
results).

    control_colonies1 = scipy.ndimage.label(colonies1[0][(firsty + 255):(secondy + 255), (firstx + 420):(secondx + 420)])
    control_colonies_array1 = numpy.zeros((1040,1392))
    control_colonies_array1[(firsty + 255):(secondy + 255), (firstx + 420):(secondx + 420)] = control_colonies1[0]
    control_colonies1 = scipy.ndimage.label(control_colonies_array1)
    control_colonies2 = scipy.ndimage.label(colonies2[0][(firsty + 255):(secondy + 255), (firstx + 420):(secondx + 420)])
    control_colonies_array2 = numpy.zeros((1040,1392))
    control_colonies_array2[(firsty + 255):(secondy + 255), (firstx + 420):(secondx + 420)] = control_colonies2[0]
    control_colonies2 = scipy.ndimage.label(control_colonies_array2)
    control_colonies3 = scipy.ndimage.label(colonies3[0][(firsty + 255):(secondy + 255), (firstx + 420):(secondx + 420)])
    control_colonies_array3 = numpy.zeros((1040,1392))
    control_colonies_array3[(firsty + 255):(secondy + 255), (firstx + 420):(secondx + 420)] = control_colonies3[0]
    control_colonies3 = scipy.ndimage.label(control_colonies_array3)
    control_colonies_logical1 = (control_colonies1[0] > 0)
    control_colonies_logical2 = (control_colonies2[0] > 0)
    control_colonies_logical3 = (control_colonies3[0] > 0)
    avg_control_brightness1 = picture1[control_colonies_logical1].mean()
    avg_control_brightness2 = picture2[control_colonies_logical2].mean()
    avg_control_brightness3 = picture3[control_colonies_logical3].mean()
    i = 1
    num_bright = 0
    bright_colonies = numpy.zeros((1040,1392))
    while i <= colonies1[1]:
        current_colony = (colonies1[0] == i)
        if (control_colonies1[1] == 0):
            bright_colonies = colonies1[0]
            num_bright = colonies1[1]
        else:
            if (picture1[current_colony].mean() > (picture1[control_colonies_logical1].mean() +
((bright_colony_standard_deviation_upper) * picture1[control_colonies_logical1].std()))):
                bright_colonies[current_colony] = 1
                num_bright = num_bright + 1
        i = i + 1
    bright_colonies = scipy.ndimage.label(bright_colonies)
    i = 1
    num_somewhat_bright_and_dim_colonies = 0
    somewhat_bright_and_dim_colonies = numpy.zeros((1040,1392))
    while i <= colonies1[1]:
        current_colony = (colonies1[0] == i)
        if (control_colonies1[1] == 0):
            somewhat_bright_and_dim_colonies = colonies1[0]
            num_somewhat_bright_and_dim_colonies = colonies1[1]
        else:
```

```
        if ((picture1[current_colony].mean() >= picture1[control_colonies_logical1].mean()) and
(picture2[current_colony].mean() < (picture2[control_colonies_logical2].mean() - ((dim_colony_standard_deviation_lower) *
picture2[control_colonies_logical2].std())))):
            somewhat_bright_and_dim_colonies[current_colony] = 1
            num_somewhat_bright_and_dim_colonies = num_somewhat_bright_and_dim_colonies + 1
      i = i + 1
   somewhat_bright_and_dim_colonies = scipy.ndimage.label(somewhat_bright_and_dim_colonies)
   annotate_picture(1, picture1, bright_colonies, num_bright, plate_name, datestr)
   annotate_picture(2, picture2, somewhat_bright_and_dim_colonies, num_somewhat_bright_and_dim_colonies, plate_name,
datestr)
   pylab.show()

   # saves raw data and images

   numpy.save(directory + '/' + plate_name + '_Image1', picture1)
   numpy.save(directory + '/' + plate_name + '_Image2', picture2)
   numpy.save(directory + '/' + plate_name + '_Image3', picture3)
   CalculationsOK = tkMessageBox.askyesno('Option', 'Continue?')
   pylab.close(1)
   pylab.close(2)

#Offer exit dialog

imageOK = tkMessageBox.askyesno('Finished','Close?')
if (imageOK):
   pylab.close('all')
   exit
```

7 Bibliography

Adam V, Berardozzi R, Byrdin M, Bourgeois D (2014). Phototransformable fluorescent proteins: Future challenges. *Curr Opin Chem Biol* **20**:92–102.

Ai H, Baird MA, Shen Y, Davidson MW, Campbell RE (2014). Engineering and characterizing monomeric fluorescent proteins for live-cell imaging applications. *Nat Protoc* **9**(4):910–928.

Ai H, Henderson J, Remington S, Campbell R (2006). Directed evolution of a monomeric, bright and photostable version of Clavularia cyan fluorescent protein: structural characterization and applications in fluorescence imaging. *Biochem J* **400**(3):531–540.

Akerboom J, Carreras Calderón N, Tian L, Wabnig S, Prigge M, Tolö J, Gordus A, Orger MB, Severi KE, Macklin JJ, Patel R, Pulver SR, Wardill TJ, Fischer E, Schüler C, Chen TW, Sarkisyan KS, Marvin JS, Bargmann CI, Kim DS, Kügler S, Lagnado L, Hegemann P, Gottschalk A, Schreiter ER, Looger LL (2013). Genetically encoded calcium indicators for multi-color neural activity imaging and combination with optogenetics. *Front Mol Neurosci* ***6***:2.

Akerboom J, Rivera JD, Guilbe MM, Malavé EC, Hernandez HH, Tian L, Hires SA, Marvin JS, Looger LL, Schreiter ER (2009). Crystal structures of the GCaMP calcium sensor reveal the mechanism of fluorescence signal change and aid rational design. *J Biol Chem* **284**(10):6455–6464.

Baird GS, Zacharias DA, Tsien RY (1999). Circular permutation and receptor insertion within green fluorescent proteins. *Proc Natl Acad Sci U S A* **96**(20):11241–11246.

Baird GS, Zacharias DA, Tsien RY (2000). Biochemistry, mutagenesis, and oligomerization of DsRed, a red fluorescent protein from coral. *Proc Natl Acad Sci U S A* **97**(22):11984–11989.

Bean BP (2007). The action potential in mammalian central neurons. *Nat Rev Neurosci* **8**(6):451–465.

Belal AS, Sell BR, Hoi H, Davidson MW, Campbell RE (2014). Optimization of a genetically encoded biosensor for cyclin B1-cyclin dependent kinase 1. *Mol Biosyst* **10**(2):191–195.

Berridge MJ (1998). Neuronal calcium signaling. *Neuron* **21**(1):13–26.

Berridge MJ, Lipp P, Bootman MD (2000). The versatility and universality of calcium signalling. *Nat Rev Mol Cell Biol* **1**(1):11–21.

Brakemann T, Stiel AC, Weber G, Andresen M, Testa I, Grotjohann T, Leutenegger M, Plessmann U, Urlaub H, Eggeling C, Wahl MC, Hell SW, Jakobs S (2011). A reversibly photoswitchable GFP-like protein with fluorescence excitation decoupled from switching. *Nat Biotechnol* **29**(10):942–947.

Brini M, Calì T, Ottolini D, Carafoli E (2014). Neuronal calcium signaling: function and dysfunction. *Cell Mol Life Sci* **71**(15):2787-2814.

Campbell AK, Naseem R, Holland IB, Matthews SB, Wann KT (2007). Methylglyoxal and other carbohydrate metabolites induce lanthanum-sensitive Ca^{2+} transients and inhibit growth in *E. coli*. *Arch Biochem Biophys* **468**(1):107–113.

Campbell RE, Tour O, Palmer AE, Steinbach PA, Baird GS, Zacharias DA, Tsien RY. (2002). A monomeric red fluorescent protein. *Proc Natl Acad Sci U S A* **99**(12):7877–7882.

Chalfie M, Tu Y, Euskirchen G, Ward WW, Prasher DC (1994). Green fluorescent protein as a marker for gene expression. *Science* **263**(5148):802–805.

Chen TW, Wardill TJ, Sun Y, Pulver SR, Renninger SL, Baohan A, Schreiter ER, Kerr RA, Orger MB, Jayaraman V, Looger LL, Svoboda K, Kim DS (2013). Ultrasensitive fluorescent proteins for imaging neuronal activity. *Nature* **499**(7458):295–300.

Cheung WY (1970). Cyclic 3′, 5′-nucleotide phosphodiesterase. Demonstration of an activator. *Biochem Biophys Res Commun* **38**(3):533–538.

Chin D, Means AR (2000). Calmodulin: a prototypical calcium sensor. *Trends Cell Biol* **10**(8):322–328.

Chou CP (2007). Engineering cell physiology to enhance recombinant protein production in Escherichia coli. *Appl Microbiol Biotechnol* **76**(3):521–532.

Chu J, Haynes RD, Corbel SY, Li P, González-González E, Burg JS, Ataie NJ, Lam AJ, Cranfill PJ, Baird MA, Davidson MW, Ng HL, Garcia KC, Contag CH, Shen K, Blau HM, Lin MZ (2014). Non-invasive intravital imaging of cellular differentiation with a bright red-excitable fluorescent protein. *Nat Methods* **11**(5):572-578.

Cubitt AB, Heim R, Adams SR, Boyd AE, Gross LA, Tsien RY (1995). Understanding, improving and using green fluorescent proteins. *Trends Biochem Sci* **20**(11):448–455.

Day RN, Davidson MW (2009). The fluorescent protein palette: tools for cellular imaging. *Chem Soc Rev* **38**(10):2887–2921.

Direnberger S, Mues M, Micale V, Wotjak CT, Dietzel S, Schubert M, Scharr A, Hassan S, Wahl-Schott C, Biel M, Krishnamoorthy G, Griesbeck O (2012). Biocompatibility of a genetically encoded calcium indicator in a transgenic mouse model. *Nat Commun* **3**:1031.

Ebashi S, Kodama A (1965). A new protein factor promoting aggregation of tropomyosin. *J Biochem* **58**(1):107–108.

Escherich T (1988). The intestinal bacteria of the neonate and breast-fed infant. 1884. *Rev Infect Dis* **10**(6):1220–1225.

Faas GC, Mody I (2012). Measuring the kinetics of calcium binding proteins with flash photolysis. *Biochim Biophys Acta* **1820**(8):1195–1204.

Fukuda N, Matsuda T, Nagai T (2014). Optical Control of the Ca^{2+} Concentration in a Live Specimen with a Genetically Encoded Ca^{2+}-Releasing Molecular Tool. *ACS Chem Biol* **9**(5):1197-1203.

Förster T (1948). Zwischenmolekulare Energiewanderung und Fluoreszenz. *Ann Phys* **437**(1-2):55–75.

Gangola P, Rosen B (1987). Maintenance of intracellular calcium in Escherichia coli. *J Biol Chem* **262**(26):12570–12574.

Gao Y, Feng X, Xian M, Wang Q, Zhao G (2013). Inducible cell lysis systems in microbial production of bio-based chemicals. *Appl Microbiol Biotechnol* **97**(16):7121–7129.

Geiger A, Russo L, Gensch T, Thestrup T, Becker S, Hopfner KP, Griesinger C, Witte G, Griesbeck O (2012). Correlating calcium binding, Förster resonance energy transfer, and conformational change in the biosensor TN-XXL. *Biophys J* **102**(10):2401–2410.

Gifford JL, Walsh MP, Vogel HJ (2007). Structures and metal-ion-binding properties of the Ca^{2+}-binding helix-loop-helix EF-hand motifs. *Biochem J* **405**(2):199–221.

Goedhart J, van Weeren L, Hink MA, Vischer NO, Jalink K, Gadella TW Jr (2010). Bright cyan fluorescent protein variants identified by fluorescence lifetime screening. *Nat Methods* **7**(2):137–139.

Goemans C, Denoncin K, Collet JF (2013). Folding mechanisms of periplasmic proteins. *Biochim Biophys Acta* **1843**(8):1517-28.

Goryshin IY, Reznikoff WS (1998). Tn5 *in Vitro* Transposition. *J Biol Chem.* **273**(13):7367–7374.

Graham FL, van der Eb AJ (1973). A new technique for the assay of infectivity of human adenovirus 5 DNA. *Virology* **52**(2):456–467.

Grünberg R, Burnier JV, Ferrar T, Beltran-Sastre V, Stricher F, van der Sloot AM, Garcia-Olivas R, Mallabiabarrena A, Sanjuan X, Zimmermann T, Serrano L (2013). Engineering of weak helper interactions for high-efficiency FRET probes. *Nat Methods* **10**(10):1021–1027.

Heim N, Griesbeck O (2004). Genetically encoded indicators of cellular calcium dynamics based on troponin C and green fluorescent protein. *J Biol Chem* **279**(14):14280–14286.

Heim R, Cubitt AB, Tsien RY (1995). Improved green fluorescence. *Nature* **373**(6516):663-4.

Heim R, Prasher DC, Tsien RY (1994). Wavelength mutations and posttranslational autoxidation of green fluorescent protein. *Proc Natl Acad Sci U S A* **91**(26):12501–12504.

Heim R, Tsien RY (1996). Engineering green fluorescent protein for improved brightness, longer wavelengths and fluorescence resonance energy transfer. *Curr Biol* **6**(2):178–182.

Helmchen F, Imoto K, Sakmann B (1996). Ca2+ buffering and action potential-evoked Ca2+ signaling in dendrites of pyramidal neurons. *Biophys J* **70**(2):1069–1081.

Herzberg O, James MN (1985). Structure of the calcium regulatory muscle protein troponin-C at 2.8 Å resolution. *Nature* **313**(6004):653-659.

Hires SA, Zhu Y, Tsien RY (2008). Optical measurement of synaptic glutamate spillover and reuptake by linker optimized glutamate-sensitive fluorescent reporters. *Proc Natl Acad Sci U S A* **105**(11):4411–4416.

Horikawa K, Yamada Y, Matsuda T, Kobayashi K, Hashimoto M, Matsu-ura T, Miyawaki A, Michikawa T, Mikoshiba K, Nagai T (2010). Spontaneous network activity visualized by ultrasensitive Ca^{2+} indicators, yellow Cameleon-Nano. *Nat Methods* **7**(9):729–732.

Huang CJ, Lin H, Yang X (2012). Industrial production of recombinant therapeutics in *Escherichia coli* and its recent advancements. *J Ind Microbiol Biotechnol* **39**(3):383–399.

Ibraheem A, Yap H, Ding Y, Campbell R (2011). A bacteria colony-based screen for optimal linker combinations in genetically encoded biosensors. *BMC Biotechnol* **11**:105.

Jones H, Holland I, Campbell A (2002). Direct measurement of free Ca^{2+} shows different regulation of Ca^{2+} between the periplasm and the cytosol of *Escherichia coli*. *Cell Calcium* **32**(4):183–192.

Kakiuchi S, Yamazaki R (1970). Calcium dependent phosphodiesterase activity and its activating factor (PAF) from brain: studies on cyclic 3′, 5′-nucleotide phosphodiesterase (III). *Biochem Biophys Res Commun* **41**(5):1104–1110.

Kaper JB, Nataro JP, Mobley HL (2004). Pathogenic *Escherichia coli*. *Nat Rev Microbiol* **2**(2):123–140.

Karasawa S, Araki T, Nagai T, Mizuno H, Miyawaki A (2004). Cyan-emitting and orange-emitting fluorescent proteins as a donor/acceptor pair for fluorescence resonance energy

transfer. *Biochem J* **381**(Pt 1):307–312.

Katsu T, Yoshimura S, Fujita Y (1984). Increases in permeability of *Escherichia coli* outer membrane induced by polycations. *FEBS Lett* **166**(1):175–178.

Kikuchi A, Fukumura E, Karasawa S, Mizuno H, Miyawaki A, Shiro Y (2008). Structural Characterization of a Thiazoline-Containing Chromophore in an Orange Fluorescent Protein, Monomeric Kusabira Orange. *Biochemistry* **47**(44):11573–11580.

Kogure T, Karasawa S, Araki T, Saito K, Kinjo M, Miyawaki A (2006). A fluorescent variant of a protein from the stony coral *Montipora* facilitates dual-color single-laser fluorescence cross-correlation spectroscopy. *Nat Biotechnol* **24**(5):577–581.

Komatsu N, Aoki K, Yamada M, Yukinaga H, Fujita Y, Kamioka Y, Matsuda M (2011). Development of an optimized backbone of FRET biosensors for kinases and GTPases. *Mol Biol Cell* **22**(23):4647–4656.

Kremers GJ, Gilbert SG, Cranfill PJ, Davidson MW, Piston DW (2011). Fluorescent proteins at a glance. *J Cell Sci* **124**(2):157–160.

Kretsinger RH, Nockolds CE (1973). Carp muscle calcium-binding protein. II. Structure determination and general description. *J Biol Chem* **248**(9):3313–3326.

Lakowicz JR (2006). *Principles of fluorescence spectroscopy*. 3rd ed Springer Berlin.

Lam AJ, St-Pierre F, Gong Y, Marshall JD, Cranfill PJ, Baird MA., McKeown MR, Wiedenmann J, Davidson MW, Schnitzer MJ, Tsien RY, Lin MZ (2012). Improving FRET dynamic range with bright green and red fluorescent proteins. *Nat Methods* **9**(10):1005–1012.

Leive L (1965). A nonspecific increase in permeability in Escherichia coli produced by EDTA. *Proc Natl Acad Sci U S A* **53**(4):745-750.

Lewit-Bentley A, Réty S (2000). EF-hand calcium-binding proteins. *Curr Opin Struct Biol* **10**(6):637–643.

Lindenburg LH, Hessels AM, Ebberink EH, Arts R, Merkx M (2013). Robust red FRET sensors using self-associating fluorescent domains. *ACS Chem Biol* **8**(10):2133–2139.

Mank M, Griesbeck O (2008). Genetically encoded calcium indicators. *Chem Rev* **108**(5):1550–1564.

Mank M, Reiff DF, Heim N, Friedrich MW, Borst A, Griesbeck O (2006). A FRET-based calcium biosensor with fast signal kinetics and high fluorescence change. *Biophys J* **90**(5):1790–1796.

Mank M, Santos AF, Direnberger S, Mrsic-Flogel TD, Hofer SB, Stein V, Hendel T, Reiff DF, Levelt C, Borst A, Bonhoeffer T, Hübener M, Griesbeck O (2008). A genetically encoded calcium indicator for chronic *in vivo* two-photon imaging. *Nat Methods* **5**(9):805–811.

Matz MV, Fradkov AF, Labas YA, Savitsky AP, Zaraisky AG, Markelov ML, Lukyanov SA (1999). Fluorescent proteins from nonbioluminescent Anthozoa species. *Nat Biotechnol* **17**(10):969–973.

Miyawaki A, Llopis J, Heim R, McCaffery JM, Adams JA, Ikura M, Tsien RY (1997). Fluorescent indicators for Ca^{2+} based on green fluorescent proteins and calmodulin. *Nature* **388**(6645):882–887.

Monici M. (2005). Cell and tissue autofluorescence research and diagnostic applications. *Biotechnol Annu Rev* **11**:227–256.

Moore MM, Oteng-Pabi SK, Pandelieva AT, Mayo SL, Chica RA (2012). Recovery of Red Fluorescent Protein Chromophore Maturation Deficiency through Rational Design. *PloS One* **7**(12):e52463.

Müller B, Grossniklaus U (2010). Model organisms - A historical perspective. *J Proteomics* **73**(11):2054–2063.

Nagai T, Sawano A, Park ES, Miyawaki A (2001). Circularly permuted green fluorescent proteins engineered to sense Ca^{2+}. *Proc Natl Acad Sci U S A* ***98***(6):3197–3202.

Nakai J, Ohkura M, Imoto K (2001). A high signal-to-noise Ca2+ probe composed of a single green fluorescent protein. *Nat Biotechnol* **19**(2):137–141.

Nguyen AW, Daugherty PS (2005). Evolutionary optimization of fluorescent proteins for intracellular FRET. *Nat Biotechnol* **23**(3):355–360.

Nikaido H, Vaara M (1985). Molecular basis of bacterial outer membrane permeability. *Microbiol Rev* **49**(1):1-32.

Ohtsuki I (2007). Troponin: structure, function and dysfunction. *Adv Exp Med Biol* **592**:21-36.

Ormö M, Cubitt AB, Kallio K, Gross LA, Tsien RY, Remington SJ (1996). Crystal structure of the *Aequorea victoria* green fluorescent protein. *Science **273***(5280):1392–1395.

Piatkevich KD, Hulit J, Subach OM, Wu B, Abdulla A, Segall JE, Verkhusha VV (2010). Monomeric red fluorescent proteins with a large Stokes shift. *Proc Natl Acad Sci U S A* **107**(12):5369–5374.

Piljic A, de Diego I, Wilmanns M, Schultz C (2011). Rapid development of genetically encoded FRET reporters. *ACS Chem Biol* **6**(7):685–691.

Pletnev S, Subach FV, Dauter Z, Wlodawer A, Verkhusha VV (2010). Understanding blue-to-red conversion in monomeric fluorescent timers and hydrolytic degradation of their chromophores. *J Am Chem Soc* **132**(7):2243–2253.

Prasher DC, Eckenrode VK, Ward WW, Prendergast FG, Cormier MJ (1992). Primary structure of the *Aequorea victoria* green-fluorescent protein. *Gene* **111**(2):229–233.

Pray L (2008). Restriction enzymes. *Nature Education*. Retrieved 8, 2014, from http://www.nature.com/scitable/topicpage/restriction-enzymes-545.

Reid BG, Flynn GC (1997). Chromophore formation in green fluorescent protein. *Biochemistry* **36**(22):6786–6791.

Romoser VA, Hinkle PM, Persechini A (1997). Detection in Living Cells of Ca^{2+}-dependent Changes in the Fluorescence Emission of an Indicator Composed of Two Green Fluorescent Protein Variants Linked by a Calmodulin-binding Sequence. A New Class of Fluorescent Indicators. *J Biol Chem* **272**(20):13270–13274.

Ruiz N, Kahne D, Silhavy TJ (2006). Advances in understanding bacterial outer-membrane biogenesis. *Nat Rev Microbiol* **4**(1):57–66.

Sakaue-Sawano A, Kurokawa H, Morimura T, Hanyu A, Hama H, Osawa H, Kashiwagi S, Fukami K, Miyata T, Miyoshi H, Imamura T, Ogawa M, Masai H, Miyawaki A (2008). Visualizing spatiotemporal dynamics of multicellular cell-cycle progression. *Cell **132***(3):487–498.

Salih A, Larkum A, Cox G, Kühl M, Hoegh-Guldberg O (2000). Fluorescent pigments in corals are photoprotective. *Nature* **408**(6814):850–853.

Schifferer M, Griesbeck O (2012). A Dynamic FRET Reporter of Gene Expression Improved by Functional Screening. *J Am Chem Soc* **134**(37):15185–15188.

Schindelin J, Arganda-Carreras I, Frise E, Kaynig V, Longair M, Pietzsch T, Preibisch S, Rueden C, Saalfeld S, Schmid B, Tinevez JY, White DJ, Hartenstein V, Eliceiri K, Tomancak P, Cardona A (2012). Fiji: an open-source platform for biological-image analysis. *Nat Methods*, **9**(7):676–682.

Schnitzler CE, Keenan RJ, McCord R, Matysik A, Christianson LM, Haddock SH (2008). Spectral diversity of fluorescent proteins from the anthozoan *Corynactis californica*. *Mar Biotechnol* **10**(3):328–342.

Shaner NC, Campbell RE, Steinbach PA, Giepmans BN, Palmer AE, Tsien RY (2004). Improved monomeric red, orange and yellow fluorescent proteins derived from *Discosoma* sp. red fluorescent protein. *Nat Biotechnol* **22**(12):1567–1572.

Shcherbakova DM, Hink MA, Joosen L, Gadella TW, Verkhusha VV (2012). An orange fluorescent protein with a large Stokes shift for single-excitation multicolor FCCS and FRET imaging. J *Am Chem Soc* **134**(18):7913–7923.

Shcherbakova DM, Verkhusha VV (2013). Near-infrared fluorescent proteins for multicolor *in vivo* imaging. *Nat Methods* **10**(8):751–754.

Shimomura O, Johnson FH, Saiga Y (1962). Extraction, purification and properties of aequorin, a bioluminescent protein from the luminous hydromedusan, Aequorea. *J Cell Comp Physiol.* **59**(3):223–239.

Stokes, G. G. (1852). On the change of refrangibility of light. *Philos Trans R Soc Lond* **142**:463–562.

Strack RL, Strongin DE, Mets L, Glick BS, Keenan RJ (2010). Chromophore formation in DsRed occurs by a branched pathway. *J Am Chem Soc* **132**(24):8496–8505.

Studier FW (2005). Protein production by auto-induction in high-density shaking cultures. *Protein Expr Purif* **41**(1):207–234.

Subach FV, Verkhusha VV (2012). Chromophore transformations in red fluorescent proteins. *Chem Rev* **112**(7):4308–4327.

Tallini YN, Ohkura M, Choi BR, Ji G, Imoto K, Doran R, Lee J, Plan P, Wilson J, Xin HB, Sanbe A, Gulick J, Mathai J, Robbins J, Salama G, Nakai J, Kotlikoff MI (2006). Imaging cellular signals in the heart *in vivo*: Cardiac expression of the high-signal Ca^{2+} indicator GCaMP2. *Proc Natl Acad Sci U S A* **103**(12):4753–4758.

Tang S, Wong HC, Wang ZM, Huang Y, Zou J, Zhuo Y, Pennati A, Gadda G, Delbono O, Yang JJ (2011). Design and application of a class of sensors to monitor Ca^{2+} dynamics in high Ca^{2+} concentration cellular compartments. *Proc Natl Acad Sci U S A* **108**(39):16265–16270.

Terai T, Nagano T (2013). Small-molecule fluorophores and fluorescent probes for bioimaging. *Pflugers Arch* **465**(3):347–359.

Thestrup T, Litzlbauer J, Bartholomäus I, Mues M, Russo L, Dana H, Kovalchuk Y, Liang Y, Kalamakis G, Laukat Y, Becker S, Witte G, Geiger A, Allen T, Rome LC, Chen TW, Kim DS, Garaschuk O, Griesinger C, Griesbeck O (2014). Optimized ratiometric calcium sensors for functional *in vivo* imaging of neurons and T lymphocytes. *Nat Methods* **11**(2):175–182.

Tian L, Hires SA, Mao T, Huber D, Chiappe ME, Chalasani SH, Petreanu L, Akerboom J, McKinney SA, Schreiter ER, Bargmann CI, Jayaraman V, Svoboda K, Looger LL (2009). Imaging neural activity in worms, flies and mice with improved GCaMP calcium indicators. *Nat Methods* 6(12):875–881.

Tsien R, Pozzan T (1989). Measurement of cytosolic free Ca^{2+} with quin2. *Methods Enzymol* 172:230–262.

Tsutsui H, Karasawa S, Okamura Y, Miyawaki A (2008). Improving membrane voltage measurements using FRET with new fluorescent proteins. *Nat Methods* 5(8):683–685.

Vassylyev DG, Takeda S, Wakatsuki S, Maeda K, Maéda Y (1998). Crystal structure of troponin C in complex with troponin I fragment at 2.3-Å resolution. *Proc Natl Acad Sci U S A* 95(9):4847–4852.

Wang L, Jackson WC, Steinbach PA, Tsien RY (2004). Evolution of new nonantibody proteins via iterative somatic hypermutation. *Proc Natl Acad Sci U S A* 101(48):16745–16749.

Wang L, Tsien RY (2006). Evolving proteins in mammalian cells using somatic hypermutation. *Nat Protoc* 1(3):1346–1350.

Wang S, Hazelrigg T (1994). Implications for *bcd* mRNA localization from spatial distribution of exu protein in *Drosophila* oogenesis. *Nature* 369(6479):400-403.

Wardill TJ, Chen TW, Schreiter ER, Hasseman JP, Tsegaye G, Fosque BF, Behnam R, Shields BC, Ramirez M, Kimmel BE, Kerr RA, Jayaraman V, Looger LL, Svoboda K, Kim DS (2013). A Neuron-Based Screening Platform for Optimizing Genetically-Encoded Calcium Indicators. *PloS One* 8(10):e77728.

Wiedenmann J, Oswald F, Nienhaus GU (2009). Fluorescent proteins for live cell imaging: opportunities, limitations, and challenges. *IUBMB Life* 61(11):1029–1042.

Yáñez M, Gil-Longo J, Campos-Toimil M (2012). Calcium binding proteins. *Adv Exp Med Biol* 740:461-82.

Yang F, Moss LG, Phillips GN Jr (1996). The molecular structure of green fluorescent protein. *Nat Biotechnol* 14(10):1246-51.

Young R (2013). Phage lysis: do we have the hole story yet? *Curr Opin Microbiol* 16(6):790–797.

Zapata-Hommer O, Griesbeck O (2003). Efficiently folding and circularly permuted variants of the Sapphire mutant of GFP. *BMC Biotechnol* 3(1):5.

Zhang Y, Werling U, Edelmann W (2012). SLiCE: a novel bacterial cell extract-based DNA cloning method. *Nucleic Acids Res* 40(8):e55.

Zhao Y, Araki S, Wu J, Teramoto T, ChangYF, Nakano M, Abdelfattah AS, Fujiwara M, Ishihara T, Nagai T, Campbell RE (2011). An expanded palette of genetically encoded Ca^{2+} indicators. *Science* 333(6051):1888–1891.

Acknowledgements

First, and foremost, I would like to thank my 'Doktorvater' Oliver Griesbeck for giving me the opportunity to undertake my PhD in his lab. His constant inspiration, guidance and support were highly appreciated. Furthermore, I would like to thank the additional members of my thesis committee, Carsten Grashoff and Kamyar Hadian, for their input, allowing me to see my research from another perspective, and for the interesting discussions we had.

I would like to thank all 'Griesbecks', former and present, for being such an amazing group. Mr. 'knowseverysinglepersonintheworld' Anselm for his clever ideas and endless motivation, Gayane for all the re-energyzing chocolate/ cake/ coffee breaks (Giovanni still misses you!) and optimizing my style, Thomas aka the Dane for helping me survive endless picking sessions with 'Schmarrn' talking and too many energy drinks, Steph the Chef for knowing just about everything about imaging, Jonny aka Scottish for quietly taking care of everything and everybody (and Friday doughnuts!!), and Martina for being an inspiration at work and a great friend. Thanks to Arne for making us better molecular biologists, his readiness to help and our cake breaks, David for the great programming that made my life much easier, and our entertaining discussions featuring totally random topics over lunch. Furthermore, I would like to thank Birgit for her amazing technical support, taking care of even more things than we realized at the time, and especially for her help with the sreening project, I hope none of us will ever have to do so many mini preps again. Also a big thank you to Chris, Maja and Anja for their support throughout the screening project.

I would like to thank the Borst group for creating such a bright atmosphere in the department, as well as some of the best parties and retreats over the years. All the Baier girls for being such great friends, and their moral support and motivation, especially throughout the last months of my thesis, and a special thanks to Alison for our endless conversations, and even longer runs at all day and night times. I was almost able to prove that running a marathon is easier than writing a thesis (but in the end, the thesis won I guess).

Thank you to my family, for their constant support, their belief in me, my ideas and my potential. And for sending me Brittany and all sorts of goodies, at times when belief was not enough. And most importantly, I would like to express my deepest thanks to Matt for making it possible for me to study in Germany for four years, for his endless support throughout that time, and for not forgetting me, as well as for the delicious meals, and all the proofreading sessions during the last few months of writing. He is the best in every way, and as an Austrian to-be, he truly deserves to share this title with me, Dr. Matey!

Versicherung

Eidesstattliche Erklärung

Ich versichere hiermit an Eides statt, dass die vorgelegte Dissertation von mir selbständig und ohne unerlaubte Hilfe angefertigt ist.

München, den

.....

Julia Litzlbauer

Erklärung

Hiermit erkläre ich, dass die Dissertation nicht ganz oder in wesentlichen Teilen einer anderen Prüfungskommission vorgelegt worden ist und dass ich mich anderweitig einer Doktorprüfung ohne Erfolg nicht unterzogen habe.

München, den

.....

Julia Litzlbauer